Università degli Studi di Catania
Scuola Superiore di Catania

International PhD

in

Energy

XXV cycle

Expert Control Strategies for Solar Cooling Systems

Chiara Dipasquale

Coordinator and Tutor
Prof. Luigi Marletta

Supervisor
Roberto Fedrizzi

Index

List of Figures

Nomenclature

a_0, a_1, a_2	collector efficiency coefficients, [-], [W/m^{2}K], [W/m^{2}K^2]
A	Area, [m^2]
c_p	specific heat, [J/(kg K)]
C	capacity rate of fluid, [kJ/(s K)]
CED	Cumulative Energy Demand, [kWh$_{PE}$/kWh$_{FE}$]
fc	Shading coefficient of external shading, [kJ/hr]
f_{sky}	view sky factor
FSS	Fraction of solar shading (Type 34 output), [-]
n	infiltration rate, [h^{-1}]
g	g-value, SHGC of external window, [kJ/hr]
GSY	Gross Solar Yield, [kWh/m^2]
I	Solar radiation from weather station, [kJ/(h m^2)]
$\dot{m}$	mass flow rate, [kg/h]
n_{50}	infiltration rate measured at 50 Pa pressure difference, [h^{-1}]
PER	Primary Energy Ratio, [kWh$_{PE}$/kWh$_{UE}$]
q	specific energy, [kWh/m^2]
$\dot{q}$	specific heat flow rate, [kW/m^2]
Q	yearly specific energy, [kWh/m^2 a]
$\dot{Q}$	heat flow rate, [kW]
SF	Solar Fraction, [%]
SPF	Seasonal Performance Factor, [kWh$_{UE}$/ kWh$_{PE}$]
T	temperature, [°C]
T*	Reduced temperature, [(m^{2}K)/W]
v	air velocity, [m/s]
UA	overall heat exchange coefficient, [W/K]

Subscripts

amb	ambient air
b	beam
c	cold
coll	collector
COOL	cooling
d	diffuse
ESHADE	External Shading Factor

FE	Final Energy
frame	window frame
glass	glass of an external window
GINT	internal gains
h	heat side
HEAT	heating
hx	heat exchanger
in	input
INF	infiltration
ISHADE	Internal Shading Factor
j	*j*-th parameter
Long	longitudinal
m	mean
max	maximum
min	minimum
NRE	non-renewable
out	output
PE	Primary Energy
real	real
set	set-point
SH	shaded
SHD	shading
SOL	absorbed solar gains on all inside surfaces of zone
SP	generator side of sorption chiller
sky	sky-vault
sim	simulated
STAR	"star" node
surf	surface
Transv	transversal
tot	total
TRANS	transmission into the wall from inner surface node
UE	Useful Energy
VENT	ventilation
w	water

Greek letters

ρ	density, [kg/m^3]

Abbreviation

AHU	Air Handling Unit
BMA	Bin Method Analysis
BS	Basement
DHW	Domestic Hot Water
EB	Energy Box
F1	First floor
F2	Second floor
GF	Ground floor
IAM	Incident Angle Modifier
IPES	Istituto Per l'Ediliza Sociale, institute for social housing
ISM	InSolation Matrix of a zone
PC	Performance Comparison
PI	Parameter Identification
REF	Reference
Sc	operating scheme
SERC	Swedish Energy Research Center
SHC	Solar Heating and Cooling
SHM	SHading Matrix

Background

Between 1990 and 2009, household final energy consumption in EU-27 increased by 8%, caused by rising standards of living, an increase in comfort levels and broader ownership of domestic appliances. In 2009, the total electrical consumption due to residential sector amounted at 36% (Fig. 0.1) [1].

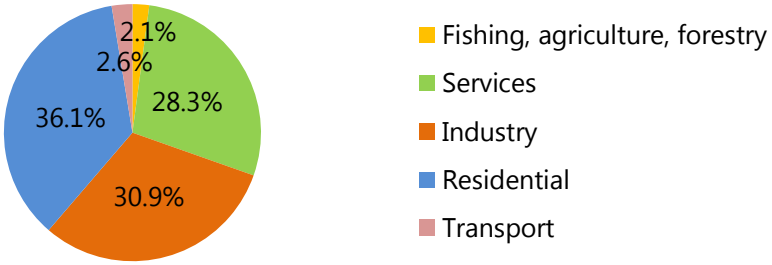

Fig. 0.1 Final energy consumption of electricity by sector in the EU-27, 2009 [1]

Space heating and cooling is the most significant component of household energy demand. The European Directive to promote renewable heating and cooling requires that 25% of EU heating and cooling to be supplied by renewables in 2020. In the building sector, a high energy saving potentials can be realized by energy efficient building design. The energy efficiency of buildings is significantly influenced by architectural design aspects, such as orientation, shape of the building structure, envelope.

Building design should look at the site where it is located in order to take into account the climatic conditions, too. Today, some modern architectures neglect these aspects and compensate inefficient building design with enormous effort concerning the energy supply for heating, cooling and lighting. A strong reduction of energy consumption may be achieved minimizing losses (i.e. appropriate insulation, reduction of thermal bridge, airtight façade components), minimizing solar gains in low latitudes or maximizing solar gains in high latitudes.

In addition to passive solutions, a reduction of energy consumption may be achieved with active parts of a building, as space heating and cooling and Domestic Hot Water (DHW) production. In this sense, solar thermal technologies offer a great potential for providing a carbon-free response to residential energy demand [2].

In accordance with these matters, the work here presented describes a SHC system installed in a low energy building located in the north Italy where cold winters and warm summers occur. The aim of the work is the reduction of energy consumption, with regard to the level of thermal comfort. The improvement of a system performances requires a reliable model and the individuation of relevant parameters to be optimized. The modelling of the whole system, the calibration of its parts (building model and supply energy plant), the individuation of the most relevant parameters on the energetic performances and quality level and the selection of best configurations have been here investigated.

1. Introduction

1.1. Solar heating and cooling systems

Solar technologies can supply the energy for all of a building's needs, heating, cooling, hot water, light and electricity, with a reduced effect on the greenhouse gas emissions created by fossil fuels. Moreover, solar heating and cooling (SHC) technologies are compatible with main sources for heat back-ups and they can be applied to several systems due to their capability in deliver hot water, hot and cold air. Solar thermal energy, in fact, is appropriate for those applications that require low heat temperature such as domestic hot water preparation and space heating. Solar applications can also meet cooling needs, with the advantage that the supply (sunny summer days) and the demand (desire for a cool indoor environment) are well matched. Furthermore, solar cooling systems have low electrical power rating, durability and environmental compatibility [2].

Nevertheless, solar cooling systems are often not yet economically viable. Even if the operating and maintenance costs of the sorption chillers are lower than conventional systems, the investment costs, due to the small numbers of installation and standardization, are even higher.

The reason of the slow entry of solar technologies on the market can be found in three main categories of barriers: technical barriers, economic barriers and other barriers including legal, cultural or behavioural barriers [4].

The main technical challenge for solar cooling today lies in small scale system level. Many systems have difficulties in achieving the planned energy savings because of lack of competence and knowledge of planning. Energy management of systems may result in a high overall electricity consumption of auxiliary components due to the heat rejection sub-system and the hot and cold backups for covering the hours of not sufficient solar radiation. Moreover, no standardized components or layout are usually available and systems result too complex. An optimal control should be identified for each specific installations and large maintenance efforts is often required.

Economic barriers can be individuated in capital costs that may be several times those of conventional electric vapour-compression systems. In case of only space heating systems, the investment cost is lower, but the solar resource is greater in summer when the demand is null and lower in winter when the demand is the greatest. This problem can be solved with summer solar air conditioning, but in this case, the cost significantly increases. Costs per unit of energy are reduced if a solar thermal collector is designed to be used for both summer cooling and winter heating. For covering the cooling demand during no sunny hours, it is also necessary to foresee a hot or cold back up for replacing the lower solar energy. The problem of high costs might be resolved with incentives, but in most European cities, incentives for thermal technologies are no widespread and, especially in small scale installations, the investment cost becomes not bearable.

Finally, some barriers are related to user's culture and behaviour and include the lack of awareness of the current status of the technology and its possibilities.

1.2. Control of solar heating and cooling plant

1.1.1. Control strategies of solar heating and cooling systems

The control of a solar cooling system concerns simultaneously the control of the single devices and all parts of the system. The main aim of the system control is an efficient functioning of the system, a minimization of the purchased energy consumption, a maximization of renewable cooling and heating to the user. Even if high-quality components are involved in the energy plant, the combination of such devices cannot lead an optimal working without an appropriate control. The control of a SHC system is challenging due to the fact that the energy source is not controllable (the solar radiation) and the dynamics of the process vary depending on the environmental conditions. As a consequence, the operating modes become part of the control strategy and the control design have to be adapted to the given characteristics of the system layout a location.

1.1.2. Literature review

The control of solar heating and cooling system has been investigated in multiple publications, focusing on the control of the single devices or parts of the system. The focus of research in this area lies on the control of absorption chillers, cooling tower or primary circuit. Another investigated field is the control of large solar thermal systems and their performance with regard to solar fraction and power consumption. However, a scarce research on control strategies for small scale solar cooling systems is nowadays offered. One possible reason for the lack of research on this subject could be the small number of existing solar cooling installations that are suitable for experimental testing. In addition, the number of available simulation models for absorption chiller simulation is low, which limits a theoretical approach to the subject. Here following a short literature review on the research on the control of solar cooling systems is reported.

Studies on the single components have been widely made focusing both on simulations or laboratory tests in steady state conditions.

In 1979, Alizadeh et al. [10] proposed a control for maximizing the absorption chiller performances based on the generator temperature. This control could become too complex if the entire system is considered. At the end of seventies and beginning of eighties, different studies focalized on the absorption chiller performances have been carried out [11], [12], [13]. The results of the tests show lower COP values than expected due to the energy used to heat up the hydraulic system.

More publications restricted to purely theoretical simulation have been presented by several authors in which the cooling power of air-conditioning absorption machine have been investigated under different conditions. As examples, Liao et al. [17] studied the crystallization issues and control strategies in LiBr–H_2O air-cooled absorption chillers suggesting the integration of absorption chillers into cooling, heating and power (CHP) systems. Izquierdo et al. [16] obtained operating conditions of the double-stage absorption machine, integrated in the solar plant, without crystallization problems for low-temperature solar heat.

In the seventies, first simulations of only energy plant control appeared. Butz et al. [7] used a simple system model with water heating collector, a water storage unit, a service hot water facility, a lithium bromide-water air conditioner (with cooling tower), an auxiliary energy source to find out

the dependence of thermal performances on collector area. In the same years, Winn at al. , [8] and [9] suggested optimal control based on the mass flow rate control to maximize the integral of the difference between the useful energy and the pumping costs incurred in collecting the solar energy. Bong et al. [18] suggest a division of the system control in three main circuits: one circuit from solar collectors to storage tank, another one from storage tank to absorption chiller and one from chiller to fan-coil units. The first circuit is controlled with two-point control via the temperature difference between collector field and the bottom of the storage tank; the absorption chiller is controlled with a real-time control and the distribution circuit is regulated by the level of the chilled water tank and the monitored room temperature. The system performance has been compared to two other solar cooling systems and the authors report lower collector efficiencies and higher power consumption for their system. Yeung et al. [19] use in a solar air-conditioning system a differential controller in on-off mode for regulating the charging of the chiller and the wet cooling tower starting. These control strategies result in a fluctuating operation of the chiller with increased thermal losses due to a higher number of start-up and shut-down procedures. Wolkenhauer and Albers [20] used an insolation-based control strategy for the solar pump in combination with a temperature-difference (hysteresis) two-point control strategy and a combination of temperature and mass flow based control strategy for the generator pump. The cooling water temperature is recommended to be kept as low as possible in order to allow the most effective chiller. Li and Sumathy [21] use an active control of the hot water feed-in position into the storage tank, depending on available solar and tank temperatures. The total solar cooling COP can be increased up to 15% compared to the traditional whole-tank mode. Klein at al.[22] suggest to relate the regulation of the solar plant with the available radiation, in particular they control the pumps of the primary solar circuit with relation to the critical radiation.

In 2005, improved control strategies for solar cooling systems are presented by Zambrano and Camacho [23] with a predictive control algorithm based in a model of the plant and by Glaser [24] who proposed the control of the pumps via a mass flow control using a PI-controller. In 2003 and 2004, investigations on operational performance of solar cooling systems reported by Kaelke et al. [26] and Albers [27], [28] show technical difficulties during the operation of the system and lower chiller performances than expected.

These last examples show that the control of a solar cooling system has to be carefully designed in order to include all components that can be controlled actively in the system control.

The lower performances of installed solar cooling systems can be due to insufficient planning and system design, incompatible system components, inexperienced operation, wrong hydraulic setup or technical defects. However, an insufficient control strategy may play an important role in the system performances.

Due to the difficulty in solar system control and the variety of existing cases, an accurate analysis on system features, including site, weather conditions, user's behaviour, devices involved in the plant layout, size of the components and operating mode of the whole system, is needed. The development of an accurate model, the optimization of parameters sets and simulations of the control applied to the whole system, supply energy plant and building, may come out the weaknesses and complexities of the system and implement adequate control strategies for the specific system.

1.3. Research objectives and approach

Following this considerations, in this work, the optimization of the performance of a solar heating and cooling system and the improvement of internal comfort in a passive house have been investigated.

A case study has been taken has a reference to develop a structured methodology to reliably and effectively tackle the problem of the integrated planning of the system established by the building and the solar heating and cooling plant.

The demo case has been modelled and the model has been verified with monitored data. Firstly the building and the energy plant have been developed and calibrated separately, then the integrated system, building + supply energy system, has been investigated.

In Chapter 2, an accurate model of the building has been developed. A calibration of supply air flow rate and infiltration rate has been made with regard to the monitored data. A study aimed to the reduction of computational efforts has been carried out. The influence of some parameters on the simulation runtime relative to the building energy performance has been investigated and a simplified building energy model has been developed.

In Chapter 3, a model of the entire supply energy system has been created. Each system component has been modelled and then validated with monitored data. Sensitivity and parametric analysis of the most influencing parameters on the system performance have been carried out.

In Chapter 4, the whole system, building + supply energy plant, has been simulated. The influence on the Primary Energy Ratio and internal comfort of set values has been investigated. An optimal control of the whole system have been individuated and a final configuration, trade-off of the reduction of energy consumption and satisfactory level of thermal comfort, has been chosen.

For each configuration, figures of merit referred to the energy consumption and level of thermal comfort, have been calculated. Here following, performance figures referred to the entire system (SPF, PER), solar field efficiency (η_{coll}, GSY), cooling, heating and DHW solar production ($SF_{cooling}$, $SF_{heating}$, SF_{DHW}) and state of the comfort (PPD) are described.

1.4. Performance figures

Seasonal Performance Factor (SPF)[80].

The Seasonal Performance Factor gives the efficiency of the whole system or a defined subsystem for given operating conditions – heat source temperature, solar irradiation, supply temperature profile etc. It is calculated as the overall useful energy output to the overall driving final energy input:

$$SPF = \frac{\int (\dot{Q}_{HEAT,user} + \dot{Q}_{COOL,user} + \dot{Q}_{DHW}) \cdot dt}{\int \Sigma FE \cdot dt} \qquad \textit{Eq. 1.1}$$

Besides an overall SPF which provides the efficiency of the system in all operation modes, separate SPFs for single operation modes (e.g. heating only, heating and DHW, cooling and DHW) can be defined. The SPF does not take into consideration the "quality" of the driving energy, e.g. in terms of the use of non-renewable resources or greenhouse emissions caused during the lifetime of a system. For such an environmental performance of the system, has been taken into account, the Primary Energy Ratio (PER).

In case of non-mono-energetic systems (only one fossil energy purchased), the consumption of any additional fuels should be given separately and the overall system performance expressed through the Primary Energy Ratio (PER). In this work, the SPF referred only to electrical consumption (mainly pumps and dry cooler) has been considered.

Primary Energy Ratio (PER) [80]

This performance figure represents the overall system performances and take into account the solar energy use as well as heating backup energy use. The PER is the ratio of primary energy demand in relation to the useful heat, cold or DHW ($PER = \frac{\int \sum_i \left(\dot{Q}_{FE,i} \cdot CED_{NRE,i} \right) \cdot dt}{\int \left(\dot{Q}_{HEAT,user} + \dot{Q}_{COOL,user} + \dot{Q}_{DHW} \right) \cdot dt}$ *Eq. 1.2*).

$$PER = \frac{\int \sum_i \left(\dot{Q}_{FE,i} \cdot CED_{NRE,i} \right) \cdot dt}{\int \left(\dot{Q}_{HEAT,user} + \dot{Q}_{COOL,user} + \dot{Q}_{DHW} \right) \cdot dt} \qquad \textit{Eq. 1.2}$$

Where i is referred to the *i*-th energy source and CED_{NRE} quantifies the non-renewable primary energy used to provide the final energy, including the energy used for the construction of the electric grid and power plants.

The CED_{NRE} values of energy sources used in this work are reported in Table 1.1. For the PER calculation, the auxiliary heater has be supposed to be a gas boiler.

Table 1.1 European average values for CED_{NRE} for different energy carrier [80]

Energy carrier	CED_{NRE} [kWh_{PE}/kWh_{FE}]
Electricity	3.13
Gas	1.21
Pellets	0.24

Gross Solar Yield

The Gross Solar Yield (GSY) of the collector can be defined as the overall energy output from the collector per collector area for defined operating conditions [5].

This performance figure take into account the overall energy provided by the collector to the system, including sensible or latent heat from the surrounding moist air or any other phenomena and it is defined as:

$$GSY = \frac{Q_{coll}}{A_{coll}} \qquad \textit{Eq. 1.3}$$

Collector thermal efficiency [5]

Collector thermal efficiency η_{coll} is defined both in ISO and EN standards as "the ratio of the energy removed by the heat transfer fluid over a specified time period, to the product of a defined collector gross area and the solar irradiation incident on the collector for the same period, under steady-state or transient conditions". This definition can be used for solar collector types which are designed to transform solely solar radiation into usable heat and can be defined as follows:

$$\eta_{coll} = \frac{Q_{coll}}{I} \qquad \textit{Eq. 1.4}$$

Solar Fraction

The cooling solar fraction accounts for the percentage of cooling load covered through the solar energy utilization.
According to the EN 12976 and EN12977, the Solar Fraction is the energy supplied by the solar part of a system divided by the total system load. The solar part of a system and any associated losses need to be specified, otherwise the solar fraction is not uniquely defined (according to ISO 9488).

The solar fraction can be referred to the fraction of the total DHW, heating and cooling needs covered through the solar energy utilization and can be defined as follows:

$$SF = \frac{Q_{user,solar}}{Q_{user,tot}} \qquad \textit{Eq. 1.5}$$

Predicted mean vote

The Predicted Mean Vote (PMV) is an index that predicts the mean value of the votes of a large group of persons on the 7-point thermal sensation scale (see Table 1.2), based on the heat balance of the human body. Thermal balance is obtained when the internal heat production in the body is

equal to the loss of heat to the environment. In a moderate environment, the human thermoregulatory system will automatically attempt to modify skin temperature and sweat secretion to maintain heat balance. The PMV is a function of activity, clothing, air temperature, mean radiant temperature, relative air velocity and air humidity [29].

Table 1.2 Seven-point thermal sensation scale [29]

+3	Hot
+2	Warm
+1	Slightly warm
0	neutral
-1	Slightly cool
-2	Cool
-3	Cold

Instead of giving the predicted mean vote as an expression for the thermal environment, the percentage of persons can be expected to be decidedly dissatisfied is commonly used. The percentage of dissatisfied is simply an expression for the number of "potential complainers".

The relation between the PMV and the PPD is shown in Fig. 1.1. The curve is symmetric and it has a minimum of 5% dissatisfied for a mean vote equal to zero. This point correspond to the optimal comfort condition should be sought. As Fig. 1.1 shows, it is impossible to satisfy all persons in a large group sharing a collective climate. Even with a perfect environmental system, which creates absolutely uniform conditions in the occupied zone, one cannot attain a PPD value lower than 5% for similarly clothed people in the same activity.

The PPD may be considered a "figure of merit" for the quality of the actual measured thermal environment.

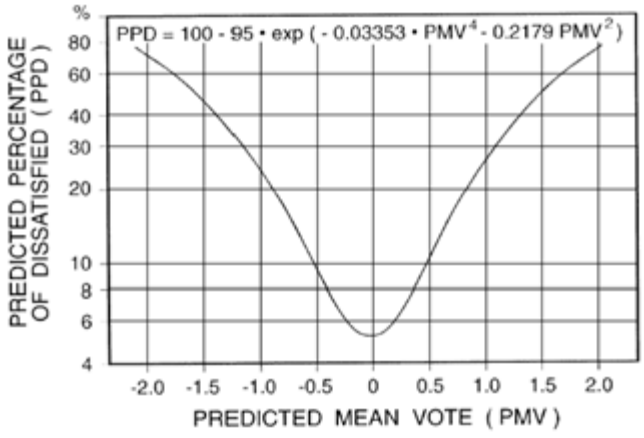

Fig. 1.1 Relation between PMV and PPD

The PPD predicts the number of thermally dissatisfied persons among a large group of people. The rest of the group will feel thermally neutral, slightly warm or slightly cool. The predicted distribution of votes is given in Table 1.3.

Table 1.3 Distribution of individual thermal sensation votes for different values of mean vote [30]

PMV	PPD	Persons predicted to vote [a] %		
		0	–1, 0 or +1	–2, –1, 0, +1 or +2
+2	75	5	25	70
+1	25	30	75	95
+0,5	10	55	90	98
0	5	60	95	100
–0,5	10	55	90	98
–1	25	30	75	95
–2	75	5	25	70

[a] Based on experiments involving 1 300 subjects.

Bibliography

[1] CSI 027/ENER 016. Final energy consumption by sector. (2012)

[2] Balaras A. C., Grossman G., Henning H.M., Infante C.A., Podesser E., Wang L., Wiemken E. Solar air conditioning in Europe – an overview. Renewable Sustainable Energy Review 11 (2007)

[3] IEA. Technology Roadmap, Solar heating and cooling. OECD/IEA, Paris (2012)

[4] Philibert C. Barriers to technology diffusion: the case of solar thermal technologies. International Energy Agency (2006)

[5] Malenkovic I. Definition of performance figures for solar and heat pump systems. Technical Report 5.1.3, QAiST, Austrian Institute of Technology (2012)

[6] Malenkovic I, Eicher S., Bony J. Definition of main system boundaries and performance figures for reporting on SHP systems- A technical report of Subtask B- Deliverable B1.1. IEA SHC Task 44, HPP Annex 38 (2012)

[7] Butz, L.W., Beckman, W.A., Duffie, J.A. Simulation of a solar heating and cooling system. Solar Energy 16 (1974)

[8] Winn, C.B., Johnson, G.R., Moore, J.B. Optimal Utilization of Solar Energy in Heating and Cooling of Buildings. International Solar Society U.S. Section Annual Meeting Colorado State University For Colorado (1974)

[9] Winn, C.B., Hull, D.E., Optimal controllers of the second kind. Solar Energy, Vol. 23, (1979)

[10] Alizadeh, S., Bahar, F., Geoola, F. Design and optimization of an absorption refrigeration system operated by solar energy. Solar Energy, Vol. 22 (1979)

[11] Ward, D.S., Weiss, T.A., Löf G.,. Preliminary performance of CSU Solar House I heating and cooling system. Solar Energy, Vol. 18(1976)

[12] Blinn, J.C., 1979. Simulation of solar absorption air conditioning. Master of Science on Chemical Engineering. University Wisconsin-Madison

[13] Lazzarin, R.. Steady and transient behaviour of LiBr absorption chillers of low capacity. Revue Internationle du Froid 3–4(1980)

[14] Bujedo, L.A., Rodríguez, J., Martínez, P.J. Experimental results of different control strategies in a solar air conditioning system at part load. Solar Energy, Vol. 85 (2011)

[15] Salim, M., Simulation of automotive LiBr/H2O absorption A/C machine, ASME IMECE (2001)

[16] Alva, L., González, J. Simulation of an air-cooled solar-assisted absorption air conditioning system. ASHRAE Transactions (2002)

[17] Izquierdo, M., Venegas, M., Rodriguez, P., Lecuona, A. Crystallization as a limit to develop solar air-cooled LiBr–H2O absorption systems using low-grade heat. Solar Energy Materials and Solar Cells, Vol. 81 (2004)

[18] Bong, T. Y., Ng, K. C., and Tay, O. A. Performance study of a solar-powered air-conditioning system. Solar Energy, Vol. 39(3) (1987)

[19] Yeung, M. R., Yuen, P. K., Dunn, A., and Cornish, L. S.. Performance of a solar-powered air conditioning system in Hong Kong. Solar Energy, Vol. 48(5) (1992)

[20] Wolkenhauer, H., Albers, J.. Systemlösungen und Regelungskonzepte von solarunterstützten Klimatisierungssystemen. HLH-Lüftung/Klima-Heizung/Sanitär-Gebäudetechnik, 52(12) (2001)

[21] Li, Z. F., Sumathy, K. Experimental Studies on a Solar Powered Air Conditioning System with Partitioned Hot Water Storage Tank. Solar Energy, Vol. 71(5) (2001)

[22] Klein, S.A., Beckman, W.A. Review of solar radiation utilizability. Journal of Solar Engineering. Transaction of the ASME 106 (1984)

[23] Zambrano, D., Camacho, E.F. Application of MPC with multiple objective for a solar refrigeration plant. In: Proceedings of the 2002 IEEE International Conference on Control Applications. Glasgow Scotland, UK (2002)

[24] Glaser, H. Beiträge zur Betriebsoptimierung solarthermisch betriebener Adsorptionskälteanlagen. PhD-Thesis, Faculty III - Process Engineering, Technical University of Berlin (2005)

[25] Núñez-Reyes, A., Normey-Rico, J.E., Bordons, C., Camacho, E.F. A smith predictive based MPC in a solar conditioning plant. Journal of Process Control 15 (2005)

[26] Kaelke, M., Keil, C., Kren, C., Schweigler, C. Querschnittsauswertung Solarunterstützte Klimatisierungsanlagen in Deutschland (QASUK). FIA-Projekt Nr. 88, Fachinstitut Gebäude-Klima e.V., Bietigheim-Bissingen (2003)

[27] Albers, J. Solar gestützte Sorptionskältesysteme bei den umzugsbedingten Bundesbaumassnahmen. Teil 1: Systemdarstellung. KI Luft- und Kältetechnik, (2003).

[28] Albers, J. Planungs- und Betriebserfahrungen bei solaren Kühlsystemen mit geschlosssenen Sorptionskälteanlagen. AAE-Tagungsband: Solares Kühlen, Ergebnisse aus dem IEA-Forschungsprogramm, SHC TASK25, Arbeitsgemeinschaft Erneuerbare Energie, Wien (2004)

[29] Fanger, P. O. Thermal comfort analysis and application in environmental design. McGraw Hill (1972)

[30] ISO 7730. Ergonomics of the thermal environment – Analytical determination and interpretation of thermal comfort using calculation of the PMV and PPD indices and local thermal criteria (2005)

2. Building

2.1. Building energy modeling

Accurate building models are more and more used for the definition of design parameters and for the evaluation of building demand and indoor comfort conditions. Building modeling can be time consuming, it needs of expertise and it might require computational effort during simulations. The developing of a good building model requires to focus on most important building's features (weather file, building size, energy loads…), to minimize the number of thermal zones, to properly characterize HVAC and controls [31]. Building models are commonly referred to predict the energy consumption, and their accuracy is related to the phase of the design process [32]. Less importance is given to the design and operation of integrated building energy and control systems model. When the interaction between the energy plant and building model is investigated, a strong. Several modeling approaches exist, but there is a lack of agreement on which building modeling is most suitable. The model needs to be as complex as needed to achieve its purpose. A good work is made when a balance between accuracy and model complexity is found. For this reason, it is important to define priorities and to individuate the features which have greater impact on performances.

Starting from a detailed model and arriving to a simplified model, a process has been individuated (see Table 2.1). This process consists of three steps that analyze the main issues which influence energy balance and simulation runtime in a building model. Monitored data have been used to verify the detailed model assumed as "Reference" case; the impact of radiation mode, geometry mode and shadings devices on building performance and simulation runtime have been analyzed; a model, with reduced computational effort which maintains a satisfying approximation of the heating demand, has been created.

Table 2.1. Simplification process from a detailed to a simplified building energy model

	INITIAL →	STEP 1 →	STEP 2 →	STEP 3 →	FINAL
CASE	**Reference case**	Radiation mode	Geometry mode	Shadings	**8 zones case**
RAD_1	**Detailed**	Detailed			
RAD_2		Standard	Standard	Standard	**Standard**
SHD_1	**Shad group**	Shad group	1-fcEshade		
SHD_2			Type 34	Type 34	**Type 34**
GEO_1	**3D data**	3D data	3D data	3D data	
GEO_2				Manual	**Manual**

2.2. Detailed building model

2.2.1. Building description

The detailed building model reproduces a real building with high accuracy. The analysed building was built by IPES (a local social housing institution), in 2006 [33], according to the "CasaClima A Plus" standard [34]. It is a residential building with 8 apartments for a total of 577 m^2 of conditioned living area distributed on three storeys. The building is oriented along the direction North South-East; a façade is oriented to the South (Fig. 2.1 and Fig. 2.2).

Fig. 2.1. Picture of the building (south side)

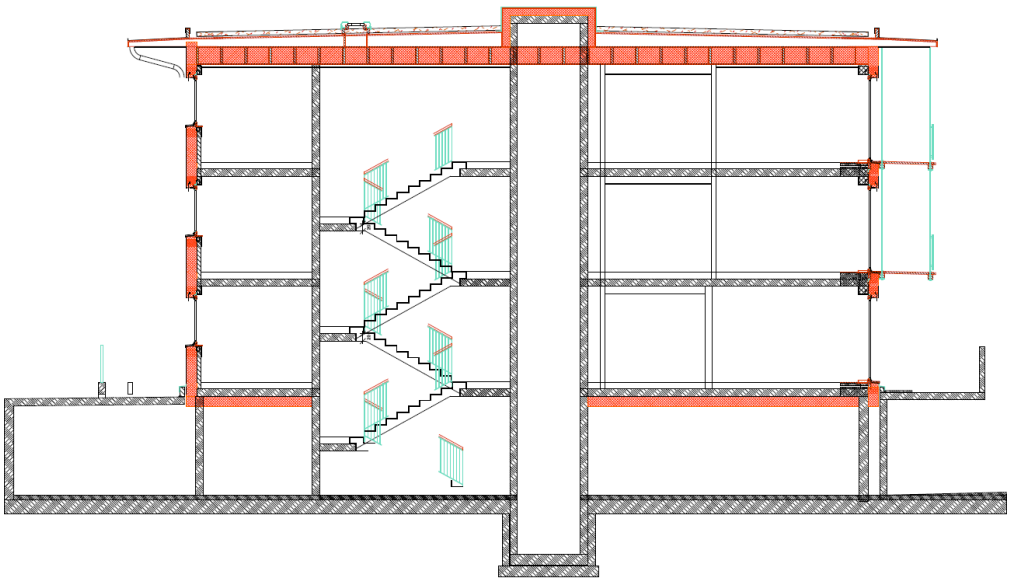

Fig. 2.2. Section of the building

The energy concept of the building includes passive and active solutions [35]. A very insulated building envelope allows to achieve low U-values. The heavy-weight construction flattens heating and cooling peaks. With overhangs (the cantilever roof and the balconies) and windows with sun-blinds, the solar gains can be used in winter, avoiding undesired overheating periods in summer. Architectural details are defined in the design phase in order to avoid thermal-bridges (Fig. 2.3).

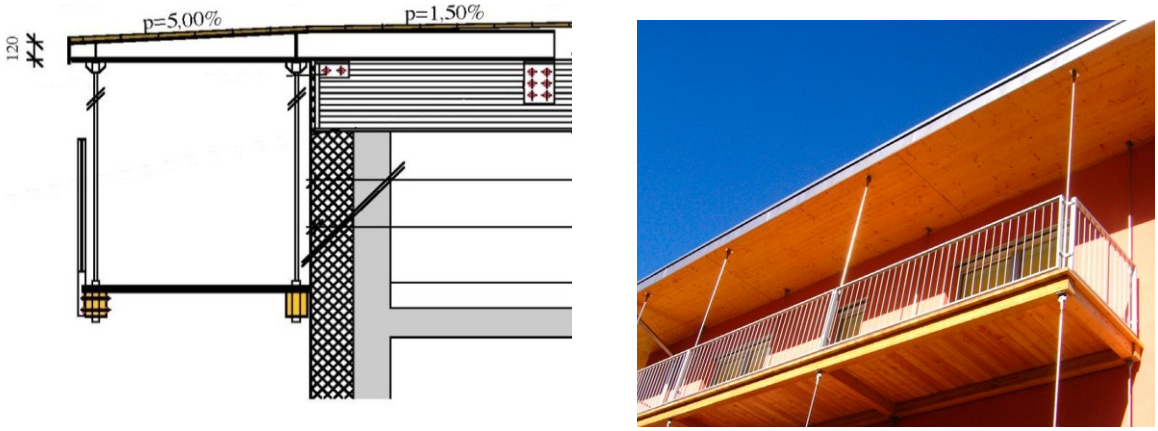

Fig. 2.3. Architectural detail and picture of hooked balcony [33]

Domestic Hot Water (DHW) and heating demand are covered by a 12 kW pellet boiler. The hot water is stored in a tank-in-tank puffer of 800 L and then distributed to each apartment.

A recirculation water system is also used in order to provide DHW during peak hours. For the supply air, a forced ventilation system is used. External air is pre-heated by geothermal probes, to avoid the freezing of the ventilation fan; an Air Handling Unit (AHU) acts as a heat recovery from the exhaust air to the fresh air and the supply air is then divided in three ducts, for the distribution on the three floors. A post-heating in each apartment is then provided through coils fed by a pellet boiler.

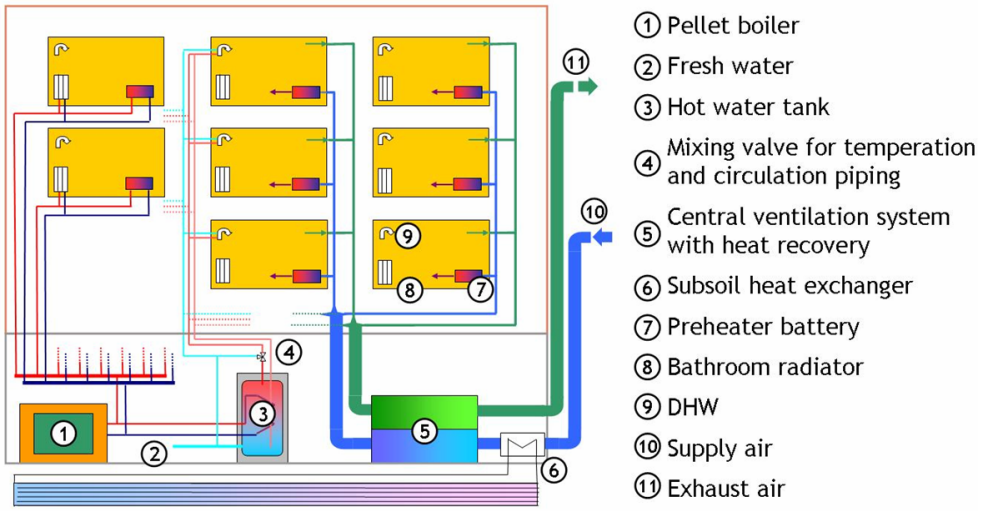

Fig. 2.4. Ventilation and Domestic Hot Water (DHW) system [35]

The detailed model of the building has been made in a previous work [36] using Google SketchUp [37] and Trnsys 3D plugin [38]. Walls and floors have been defined according to the real geometry and orientation and they have been described in TRNBuild in the "Wall Type" manager. Three wall categories have been individuated depending on their boundary conditions: external, boundary, adjacent. Table 2.2 shows the U-values for the building envelope. For windows, a predefined window has been used, whose characteristics reproduce to the original one.

Table 2.2 U-values of the building envelope (design values) [36]

Wall type	**U-value [W/m^{2}K]**
Exterior walls	0.14
Roof	0.08
Cellar ceiling	0.15
Entrance door	0.7
Windows	0.86

Due to calculation modes used to run the detailed model (see also Par. 2.3 and 2.5), only convex zones have been accepted (see also Par. 2.3.1). Apartments 1, 2, 3, 5, 6 and 8 have a L-shape, so they have been divided in two zones. Fig. 2.5 shows the result of zone partitioning and the labels used to indicate the zones. Staircase has been modeled as a single zone with 4 stacked air-node, one for each storey. This is the only zone not conditioned.

Fig. 2.5 Zone partitioning of basement (BS), ground floor (GF), first (F1) and second (F2) floor

In the 3D building model, self-building shadings and shadings due to the surrounding have been modeled with several shading groups. In Fig. 2.6, a picture of the real case and a view of the SketchUp model are shown. The colors indicate different wall types, e.g. yellow refers to exterior walls, brown to the roof and violet to shading elements. In the middle of the roof two shading elements represent the outer volume of the elevator shaft.

Fig. 2.6. Picture of the real case (above) and view of the SketchUp model (below)

2.2.2. Building model calibration

2.2.2.1. Definition ventilation rate

In order to reduce energy losses in passive houses, a forced ventilation is usually required. In the case study, external air crosses a coil which exchanges heat with geothermal probes installed below the building; then, air enters into an Air Handling Unit (AHU) to recover thermal energy from exhaust air. The AHU includes two fans, an air-to-air heat exchanger and filters to clean the outside air from dust and to protect the heat exchanger. The air-to-air heat exchanger transfers heat from the exhaust air coming from the building to the supply air. The two air flows are separated, only sensible and no latent heat is exchanged.

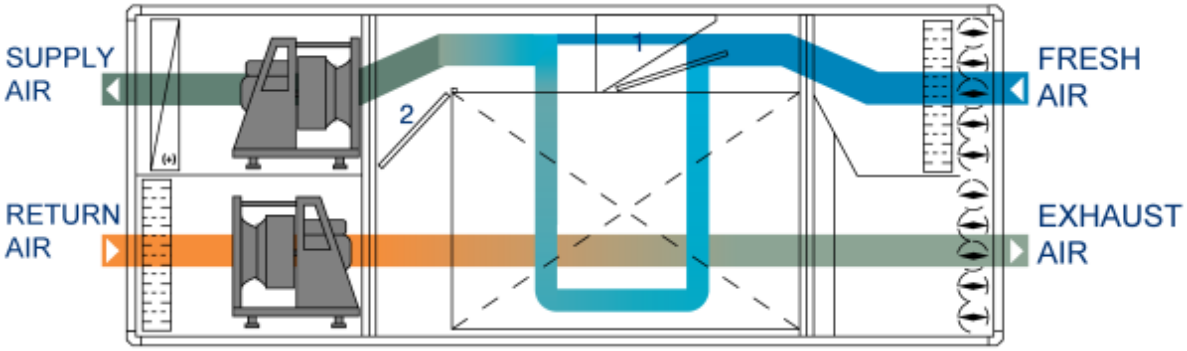

Fig. 2.7 Scheme of the Air Handling Unit

After the pre-conditioning through the AHU, the supply air is divided in three ducts, for the distribution on the three floors. A post-heating in each apartment is provided by coils fed by a pellet boiler. In the apartments, a thermostat can regulate the inlet air temperature according with users' needs.

In the 8 apartments, two different models of coils have been installed: the model 125-2R for the apartments number 2, 3, 4, 6, 7 and the model 160-2R for the apartments 1, 5, 8. The rated values are shown in Table 2.3.

Table 2.3 Datasheet characteristics of the coils

Model	**Air Volume Flow**	**Air Volume Flow**	**Connections - Φ**		**Dimensions**	**Heating at input temperature**	
	V_1 [m^3/h]	V_2 [l/h]	Air [mm]	Water [mm]	L x B x H [mm]	50 °C [kW]	70°C [kW]
125-2R	72 125 145	180	125	15	500 x 360 x 230	0,76 1,16 1,26	1,22 1,86 2,03
160-2R	72 125 145	180	160	15	500 x 410 x 230	1,32 1,71 2,00	2,12 2,74 3,21

air inlet temperature = 17°C

Monitored data have been used for calibrating the model. From monitoring, the following measurements were:

- supply air temperature and relative humidity;
- air speed in the ducts (v_1, v_2, v_3),
- water flow rate ($\dot{m}_w$),
- inlet temperature ($T_{w,in}$) and outlet temperature of water ($T_{w,out}$) in each coil.

In operation, inlet water temperature and inlet air temperature are very close to design conditions; the air flow slightly fluctuates, while the water flow is almost the double of the design value. As both air and water flow influences the UA value, it has been fixed a coefficient which takes into account the two contributions. Here following, the procedure for one coil (model 160-2R) is presented; same procedure has been made for model 125-2R.

The UA has been defined [40] for each model for the three air flows indicated ($UA = \frac{q}{\Delta T_{ml}}$ Eq. 2.3). It has been calculated for fixed inlet air temperature (17°C) and water flow (180 m^3/h) and for inlet water temperature at 70°C. Each UA value is referred to a specific air flow rate and the relation between air flow and UA value is expressed in Fig. 2.8.

$$q = UA \cdot \Delta T_{ml} \qquad \textit{Eq. 2.1}$$

$$\textit{Where } \Delta T_{ml} = \frac{(T_{h,out} - T_{c,in}) - (T_{h,in} - T_{c,out})}{\ln\left(\frac{T_{h,out} - T_{c,in}}{T_{h,in} - T_{c,out}}\right)} \qquad \textit{Eq. 2.2}$$

$$UA = \frac{q}{\Delta T_{ml}} \qquad \textit{Eq. 2.3}$$

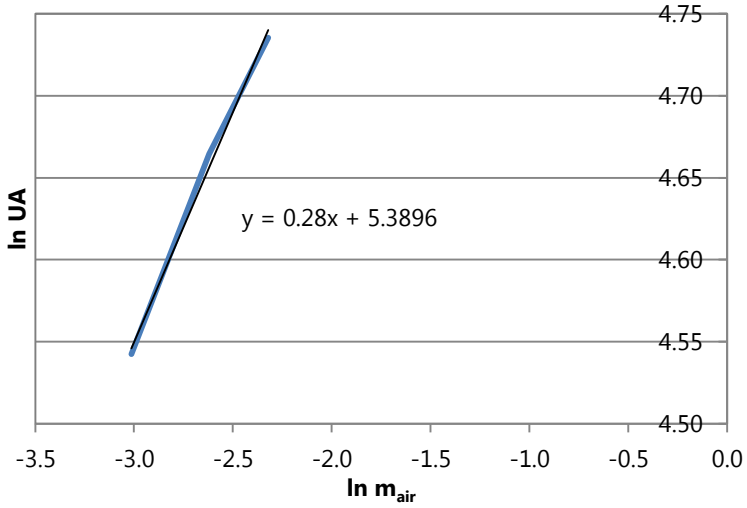

Fig. 2.8. Relation between UA and air flow rate (expressed in natural logarithm)

Starting from this relation, the UA value is so expressed:

$$\ln UA_{air} = 0.28 \cdot \ln m_{air} + 5.3896 \rightarrow UA_{air} = e^{5.3896} \cdot m_{air}^{\ 0.28} \qquad \textit{Eq. 2.4}$$

From "Dittus-Boelter" equation [40], the Nusselt number for fully developed turbulent flow in a smooth circular tube is defined as:

$$Nu_D = 0.023 \mathrm{Re}_D^{0.8} \mathrm{Pr}^n \qquad \textit{Eq. 2.5}$$

where *n=0.4* for heating and *n=0.3* for cooling; *Re* is the Reynolds number and *Pr* is the Prandtl number. The relation between UA in operating conditions and the variable water flow can be expressed as:

$$UA_{water} \propto m_{water}^{0.8} \qquad \textit{Eq. 2.6}$$

The final expression to calculate the UA for each coil is the UA rated multiplied by a coefficient which takes into account the variation of the water flow rate:

$$UA_{coil} = UA_{160} \cdot \left(1 + \left(\frac{m_{water}}{m_{design}} \right)^{0.8} \right) \qquad \textit{Eq. 2.7}$$

Simulations have been run with the TRNSYS simulation tool [42], where coils have been modeled as a counter-flow heat exchanger (Type 5) with water in the source side and air in the load side [43]. To verify the coil model, monitored data have been used. The heat exchanged in the water side has been calculated from monitored data as follows:

$$\dot{Q}_{water} = \dot{m}_{water} c_{p\,water} (T_{w,in} - T_{w,out}) \qquad \textit{Eq. 2.8}$$

In the air side, inlet air temperature is known ($T_{air,AHU}$) and the total air flow is calculated using the air velocity in the channels:

$$\dot{m}_{air} = \rho \cdot v_m \cdot A_c \qquad \textit{Eq. 2.9}$$

where $\dot{m}_{air}$ is the air mass flow, ρ is the air density, v_m is the mean air velocity and A_c is the channel area.

The air flow rate of each apartment has been defined multiplying the total air flow rate for two different fractions. The first fraction calculates the flow rate proportioned to the area of each apartment (VEN_1), the second considers the design values (VEN_2). To verify the appropriate calibration of coils, monitored heat transfer has been compared with the simulated one. A coil for each apartment has been set: monitored temperature and flow rate have been used for water and air, UA value has been defined as specified above.

Fig. 2.9 shows the heat exchanged in each coil. A comparison between monitored and simulated results is made.

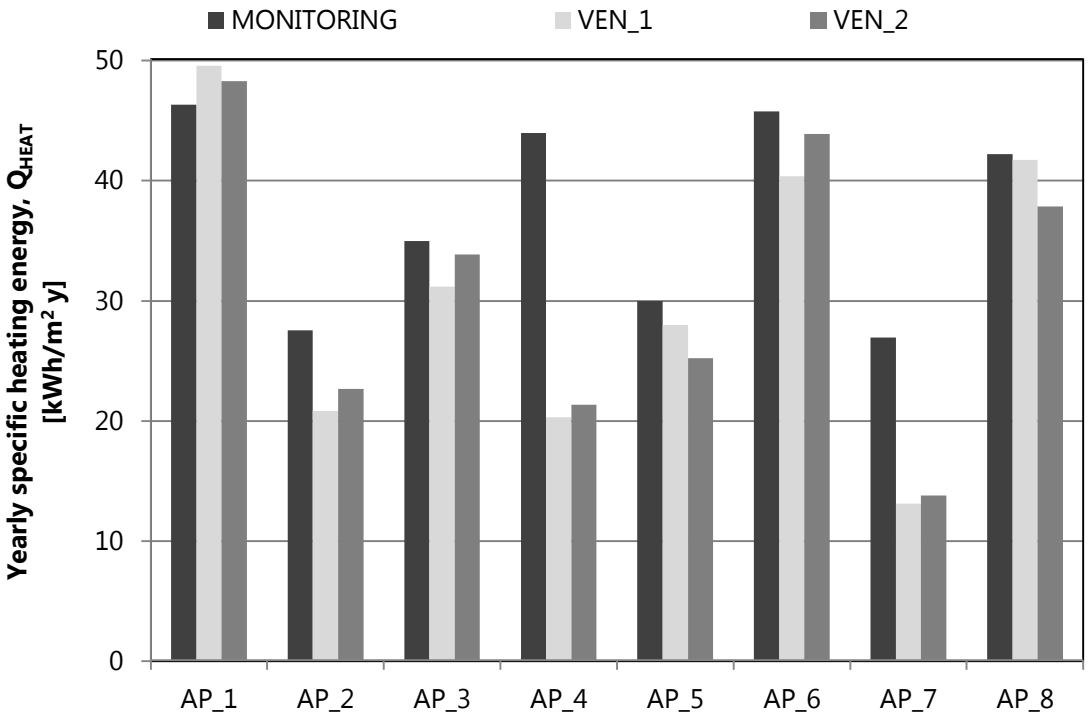

Fig. 2.9 Specific heating energy for apartment with different air flow fraction.

The discrepancy of specific heating energy between VEN_1, VEN_2 and the monitored heating consumption is quite high in some apartments rather than in others. In apartments 1, 3, 6 and 8 the difference is less than 10%; whereas in apartments 4 and 7, the smaller ones, the difference can achieve the 50%. This discrepancy is due to a wrongly position of the sensor for the measurement of the air velocity. To solve such a discrepancy, an optimization of the air flow rate has been made.

An iterative feedback controller has been used to calculate the exact coefficient that, multiplying the air flow rate obtained with design coefficients, makes the design flow rate being equal to the measured one. The iterative feedback controller is modeled in the TRNSYS deck with Type 22 [43]. It calculates the control signal (u) required to maintain the controlled variable (y) at the set-point (y_{Set}). In this case, the controlled variable (y) is the simulated heat exchange, the set-point (y_{Set}) is the difference between monitored and simulated heat exchange, fixed at 0.05, control signal (u) is the fraction (Y) for multiplying the design air flow rate. A fraction for each apartment has been calculated.

$$\dot{m}_{air,exact} = \dot{m}_{air,design} \cdot (1 + Y) \qquad \textit{Eq. 2.10}$$

The relation between $\dot{m}_{air,exact}$ and $\dot{m}_{air,calc}$ has been observed plotting the instantaneous values for both cases. For apartments 4 and 7 the optimized rate is almost double than the design rate, whereas for apartments 1, 3, 6 and 8, the optimized flow rate almost fits the designed one (Fig. 2.10).

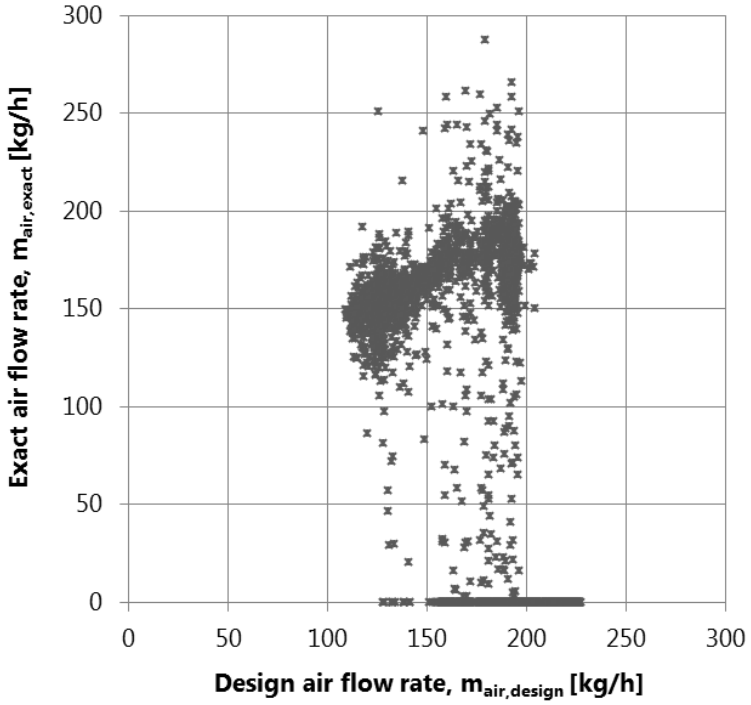

Fig. 2.10 Comparison between design and exact air flow rate for the apartment 8

In order to individuate a fixed coefficient for each coil, the frequency of Y index has been plotted (Fig. 2.11). Afterwards, the value with the highest frequency most frequent has been used as corrective factor for defining the optimized air flow rate.

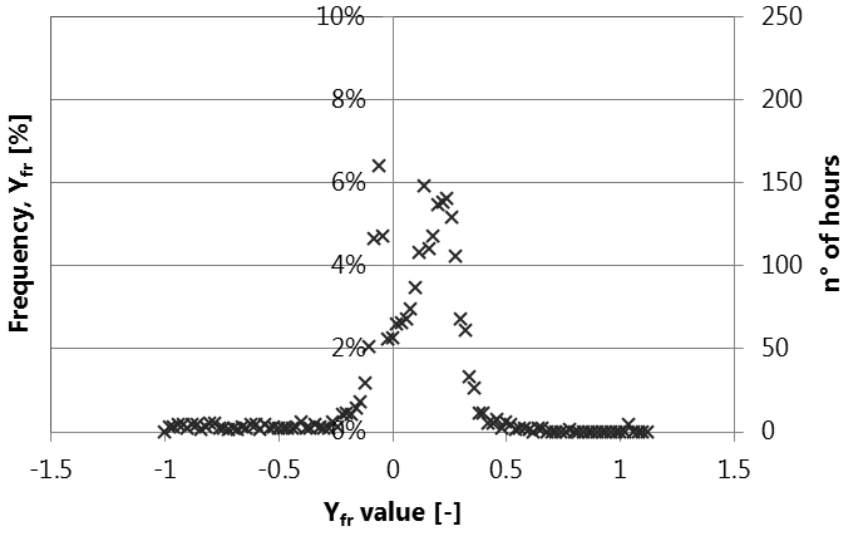

Fig. 2.11 Frequency of Y value for the air flow rate in apartment 4

Once the Y value for each coil has been identified, the air flow rate has been corrected and new simulations have been run. Table 2.4 shows the yearly heating demand from monitoring (MONIT) and calculated in each coil on the water side with fractions obtained from design air flow rate (VEN_2) and optimized air flow rate (VEN_3). The row above the heating energy represents the fraction of air flow for the correspondent apartment; the row below is the difference between

monitored and simulated heating energy.

Table 2.4 Heating energy consumption in monitoring (MONIT), with fractions from design (VEN_2) and with optimized air flow rate (VEN_3).

		AP_1	AP_2	AP_3	AP_4	AP_5	AP_6	AP_7	AP_8
MONIT	Q_{HEAT} [kWh/m^2 y]	**46.23**	**27.46**	**34.89**	**43.87**	**29.87**	**45.65**	**26.83**	**42.09**
VEN_2	air fraction	0.18	0.12	0.12	0.08	0.15	0.12	0.08	0.15
	Q_{HEAT} [kWh/m^2 y]	**48.18**	**22.55**	**33.76**	**21.24**	**25.14**	**43.76**	**13.72**	**37.76**
	ΔQ_{HEAT}	-4.2%	17.9%	3.2%	51.6%	15.8%	4.1%	48.9%	10.3%
VEN_3	Y value	-0.06	0.20	0.04	1.10	0.16	0.00	0.94	0.14
	air fraction	0.169	0.144	0.125	0.17	0.174	0.120	0.155	0.171
	Q_{HEAT} [kWh/m^2 y]	**45.44**	**26.82**	**34.96**	**43.29**	**29.05**	**44.53**	**25.98**	**42.81**
	ΔQ_{HEAT}	1.7%	2.4%	-0.2%	1.3%	2.7%	2.5%	3.2%	-1.7%

The sum of the fractions, for each apartment in the "optimized" case, is 1.22. This means that the real air flow should be the 22% more than the measured flow. In Fig. 2.12, the air flow before and after the optimization is plotted.

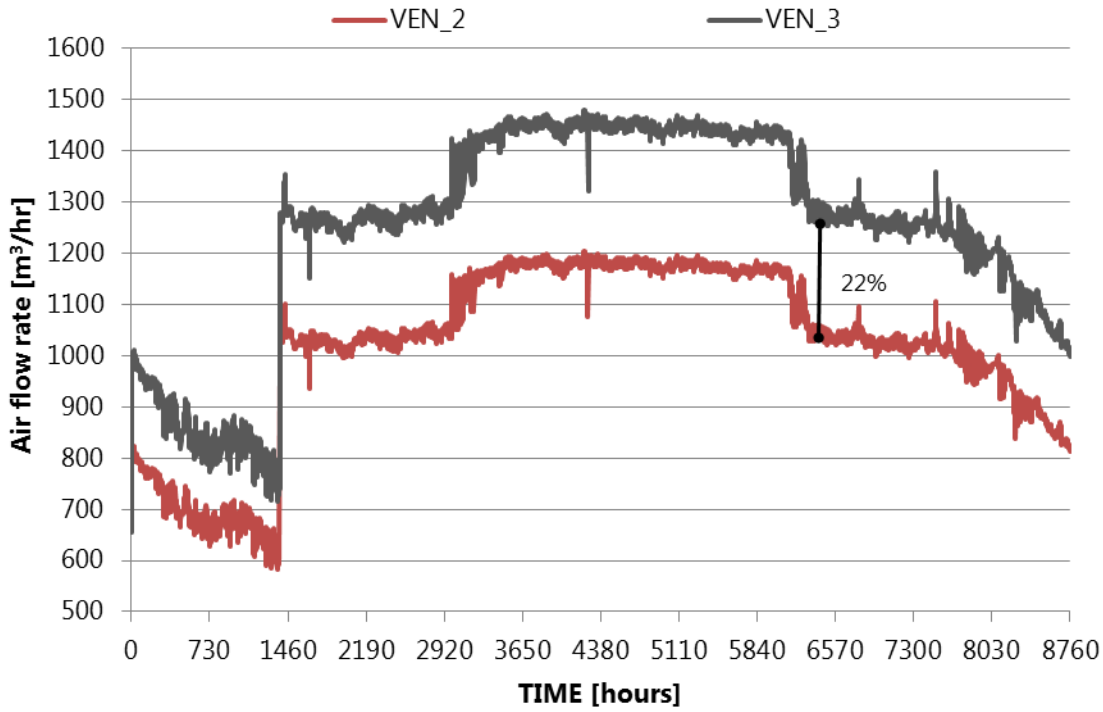

Fig. 2.12 Total air flow rate from measurements (VEN_2) and optimized (VEN_3) [1]

[1] The gap around hour 1100 is due to a change of the filter in the AHU, for this reason before that point the flow rate decreases and after, it suddenly increases.

2.2.2.2. Definition of infiltration rate

From monitoring, measurements on infiltration rate were not available, so the measured value of the total leakage through the building envelope (INFIL_1) has been assumed as first attempt [44]. The parameter which describes the level of airtightness of a Passive House, when the air velocity is less than 2 m/s, is called n_{50} value and it is calculated by an air pressure test, known as Blower Door Test. The air pressure test describes the air changes at a differential pressure of 50 Pa in the building with all doors and windows normally closed. In this specifically case, the n_{50} value is equal to 0.8 h^{-1}[33]. Commonly, to calculate the infiltration rate from the n_{50} value, the Sherman equation is used [45]:

$$n = \frac{n_{50}}{20} = 0.04 \qquad \textit{Eq. 2.11}$$

where n is the infiltration rate.

The calculated airtightness value gives an idea of the infiltration rate, but it only considers measurements of the building structures and not the building exposure to the wind direction, ventilation strategy, internal to external temperatures, occupant's behaviour. For this reason, a survey on the infiltration rate has been done and, for simplification, a yearly fixed value for each apartment has been individuated.

In the staircase, infiltration rate has been fixed with a value of 0.35 h^{-1} [46] to consider the opening of the doors in the basement, in the ground floor and an air intake on the third floor. No optimization for the staircase infiltration rate has been done, because monitored data are not available.

The infiltration rate in each zone has been studied running the detailed building model and comparing monitored and simulated heating demand. Real data have been used for the weather file and electrical internal gains; the occupancy has been specified with a schedule [36]; the supply air flow has been fixed according to Par. 2.2.2.1 and the supply temperature and relative humidity have been defined as the external air warmed up in a heat recovery with an efficiency of the 85% (see also Par. 2.2.3). As in the real case, no cooling system has been foreseen, while an ideal heating has been supposed to exist. Elaborating monitored data, the thermostat temperature in each apartment has been individuated and then used as heating set temperature. With this assumption, the simulation has been run and heating demand values have been plotted with the monitored heating consumption (Fig. 2.13). An important discrepancy, around 38% for the whole building heating demand is shown between monitoring and simulation.

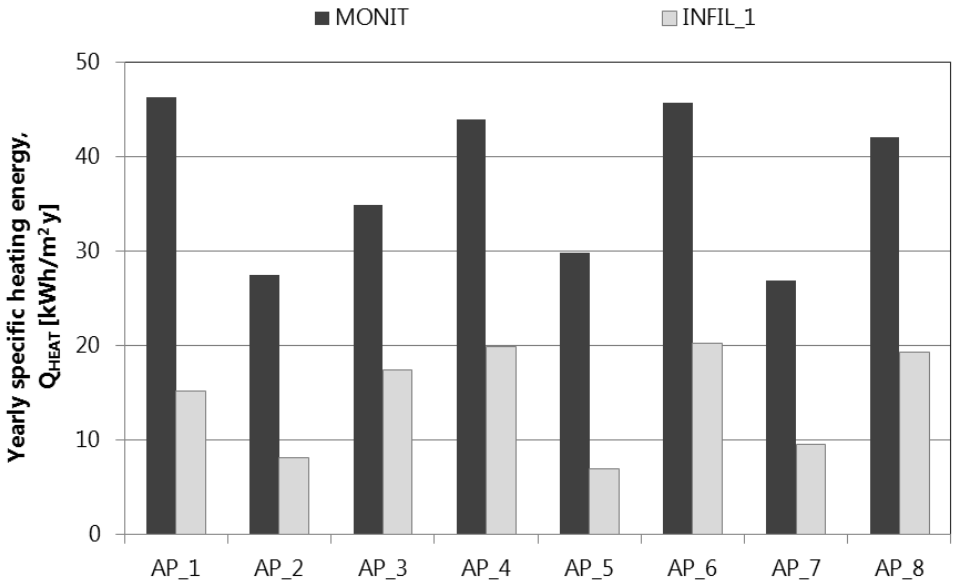

Fig. 2.13 Specific heating energy calculated from monitoring (MONIT) and with infiltration design value (INFIL_1)

To individuate the yearly fixed infiltration rate, a parametric analysis has been performed, as already specified in Par. 2.2.2.1. The control signal (u) represents the infiltration rate, the controlled variable is the simulated internal temperature and the set point is the monitored internal temperature.

In Fig. 2.14, the frequency of the values which occur during one year in each apartment is presented.

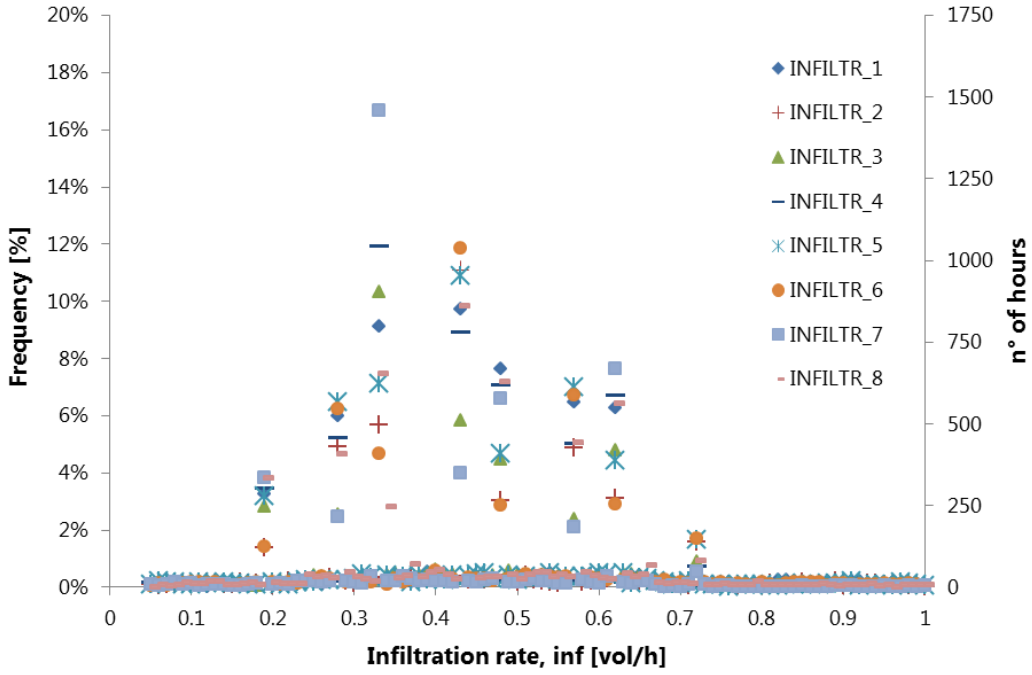

Fig. 2.14 Frequency of optimized infiltration rate's values in each apartment.

According to the results shown in Fig. 2.14, the Y value with the highest frequency has been chosen. In particular, for apartments 3, 4 and 7, an infiltration rate of 0.34 h^{-1} has been individuated,

while 0.44 h^{-1} has been taken for apartments 1, 2, 5, 6 and 8. These values are related to the apartment size or to the monitored CO_2 level inside the apartments.

New infiltration rate values have been set in the detailed model and the yearly simulation has been run (INFIL_2). Fig. 2.15 shows the heating demand calculated from monitoring (MONIT) and from simulations using both design infiltration rate (INFIL_1) and optimized infiltration rate (INFIL_2).

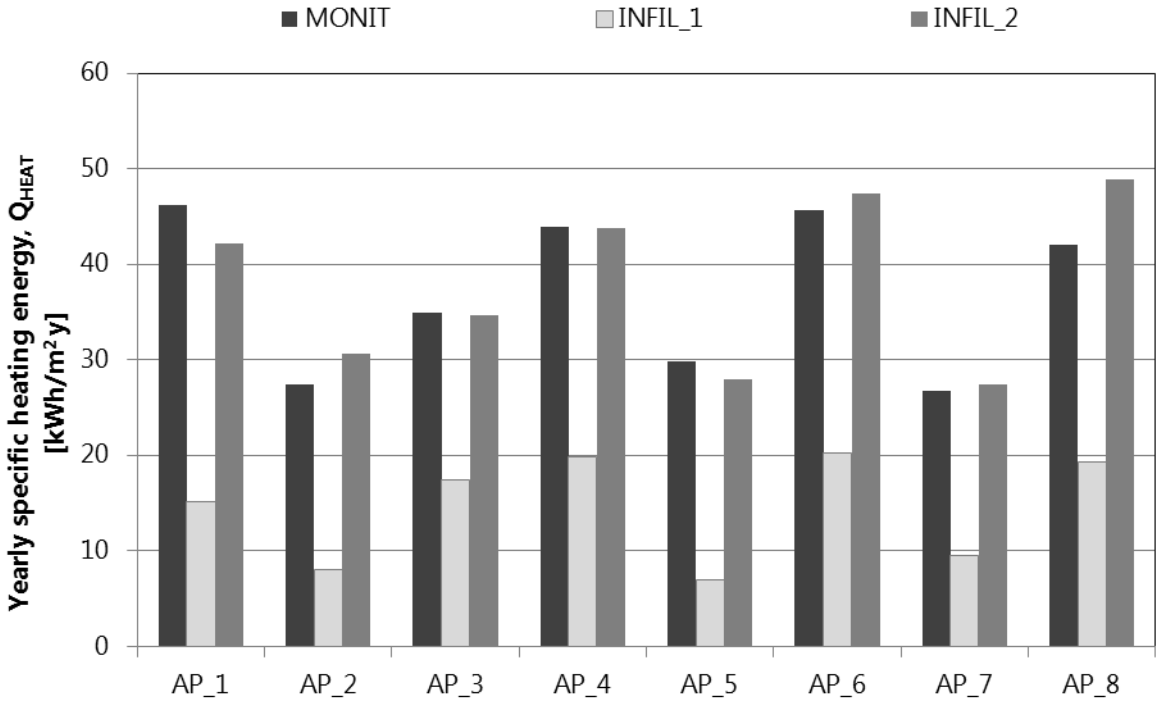

Fig. 2.15 Specific heating demand calculated from monitoring (MONIT), with design infiltration value (INFIL_1) and optimized infiltration values (INFIL_2).

For the whole building, the discrepancy in the heating demand is strongly decreased and reduced at 1%. A slight difference between monitoring and simulation still remains due to the fact that in the simulation model:

- occupancy is not monitored, but assumed [36];
- thermostat set-points temperature have been deduced from monitored internal temperature;
- infiltration rate value has been defined to be constant for the whole day during the year, but in the reality it varies according to several factors.

As a consequence, higher or lower heating demand with respect to the monitored consumption might occur in the apartments.

2.2.3. Simulation Boundary conditions

Monitored data have been used as several boundary conditions. In particular, external temperature, relative humidity and solar radiation, electrical and thermal energy consumption and supply air velocity have been collected for a whole year.

In the following, boundary conditions used in the simulations are presented.

- **Weather**: some data during the summer miss and they have been substituted with the last days available. File format is a *.epw (Energy Plus format) and it is read by Type 15. This component serves the purpose of reading data at regular time intervals from an external weather data file, interpolating the data at time-steps of less than one hour and making it available to other TRNSYS components. It also processes and calculates radiation falling on tilted surfaces.
- **Infiltration**: a yearly fixed value for each apartment have been defined, according to Par. 2.2.2.2. This value takes into account wind direction, internal and external temperature, users' behavior. For apartments 3, 4 and 7, an infiltration rate of 0.33 h^{-1} has been individuated, while 0.43 h^{-1} has been taken for apartments 1, 2, 5, 6 and 8. For the staircase, in correspondence of basement, ground floor and third floor, a value of 0.35 h^{-1} [46] has been fixed in order to taking into account the opening of external doors and the presence of an air intake.
- **Ventilation**: supply air flow rate has been defined for each apartment, as already explained in Par. 2.2.2.1. According to the external conditions, air velocity slightly varies; for this reason, supply air flow rate is not defined with a fixed value. An Air Handling Unit (AHU) is used to condition the supply air. An air-to-air heat exchanger and two fans, one for supply air, another for exhaust air, are included in a case. The cross-counter flow heat exchanger has a nominal sensible efficiency of 85%. A nominal flow rate of 1400 m^3/h is blown by the two fans with controlled frequency motors. A bypass damper is installed in order to allow free cooling.
- **Internal gains**: monitored data of electrical consumption are used to model internal gains due to electrical devices, lighting and cooking. The measured value is split into radiative (40%) and convective (60%) part. They have been measured for each apartment during a whole year with a time step of 1 hour. Monitored data for user occupancy are not available, so a schedule based on standard EN ISO 7730 [47] has been used. Presence of persons is assumed to be in accordance with power consumption; different user activities during the day are also taken into account. The occupancy profile has been defined as the combination of persons assumed to be present in the building and their metabolic rate [36].
- **Heating**: an indoor air set-point of 21°C is defined; the heating season is fixed from October to April;
- **Cooling**: an indoor air set-point of 26°C is defined; the cooling season is fixed from May to September.

All the simulations have been run for one year (8760 hours) with a time step of 5 minutes. For calculating building energy balance, building preconditioning has been taken into account.

Simulations have been run with a Intel® Core ™ Duo CPU T9400 @2.53GHz; System type 32-bit Operating System.

2.3. Radiation mode

In TRNBuild, direct and diffuse short-wave radiation and long-wave radiation distribution within a zone can be modeled with standard or detailed radiation mode.

2.3.1. Standard Radiation mode

For the standard mode, the incoming (primary) direct solar radiation is distributed among zone surfaces according to a user-defined distribution coefficients, known as GEOSURF. The value of GEOSURF represents the fraction of the total entering direct solar radiation that hits the surface. GEOSURF values can be defined for each zone (not airnode).

The incoming diffuse solar radiation and reflected primary direct solar radiation is distributed according to absorptance-weighted area ratios, where the solar absorption of the surface and the reflectance for diffuse solar radiation of the surface are taken into account.

To calculate the long-wave radiation in a zone, the standard mode uses the "Star network" approach [48] which is referred to a single air-node. This approach approximates the long-wave radiation exchanges between the surfaces within the air-node and the convective heat flux from the inside surfaces to the air-node (Fig. 2.16).

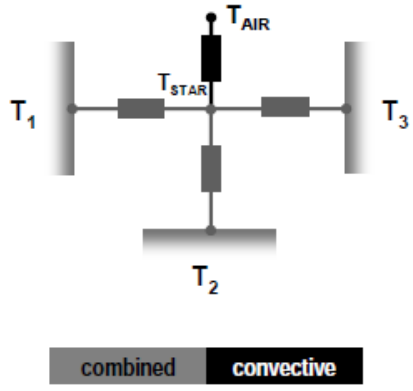

Fig. 2.16 Model of the distribution of standard radiation mode for a zone with three surfaces.

For internal surfaces, the radiation heat flux absorbed at the inside surface can include both solar radiative and long-wave radiation generated from internal objects such as people or furniture. Radiation heat flux absorbed at the outside surface consists of solar radiation only.

2.3.1. Detailed Radiation mode

The primary short-wave solar radiation entering the zone is distributed using shading and insolation matrices, created by an auxiliary program called TRNSHD [49].

For a detailed treatment of short-wave beam radiation shading and distribution, the multi-zone building model reads in the sunlit factor matrices. For each time step, the current sunlit fraction of surfaces is determined by a bilinear interpolation of the four nearest center points with respect to the sun's actual position. The matrices are used for distributing primary beam radiation entering a zone through external windows only. For direct radiation entering a zone through adjacent windows, the standard model based on user defined GEOSURF values is used.

Detailed long-wave radiation heat transfer is based on the following assumptions:

1. Radiation absorbed at outside surface is indicated by a negative sign of the corresponding heat flux, whereas net emission means a positive heat flux;
2. all surfaces are isothermal;
3. all surfaces are perfect opaque for long-wave radiation;
4. all surfaces are ideal grey surface, that is emissivity and absorptivity do depend neither on wavelength nor on direction.

In comparison to the standard model, there is no artificial star node; the long-wave radiation heat transfer model follows the scheme shown in Fig. 2.17.

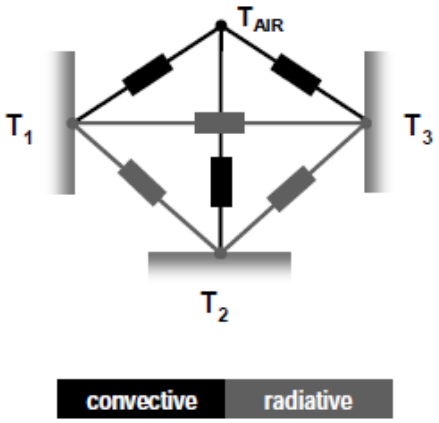

Fig. 2.17 Model of the distribution of detailed radiation mode for a zone with three surfaces.

In the Detailed mode, long-wave exchange and convection is described by the Gebhart Method [50]. The so-called Gebhart-Factor $G_{ir,j\rightarrow k}$ is defined as the fraction of the emission from surface A_j that reaches surface A_k and is absorbed. $G_{ir,j\rightarrow k}$ includes all the paths for reaching A_k,, that is the direct path and the path of one or multiple reflections. The Gebhart-Factor considers also the infrared, that is the long-wave range of the radiation spectrum. The Gebhart-Factor is a function of view factors which are defined as the fraction of diffusely radiated energy leaving surface A that is incident on surface B. The view factor matrix is generated by the auxiliary program called TRNVFM.

For the diffuse radiation, all surfaces are assumed to be transparent, meaning that the solar radiation enters the zone from outside. The surfaces are not emitting radiation, they are assumed to be "passive" because they are only reflecting, absorbing and/or transmitting solar radiation originating from outside of the zone. Based on this idea, a solar Gebhart matrix can be created. For opaque surfaces (walls), the transmitted diffuse solar radiation is zero.

The Detailed Radiation mode can be selected only if the geometry mode is set to "3D data" and zones have convex and closed volumes.

2.3.2. Comments and results

The influence of the use of standard or detailed radiation mode on the building model has been studied considering for each zone, the incoming (+) and the out-coming (-) energy fluxes. Energy losses and gains have been then calculated for the whole building (see Fig. 2.18).

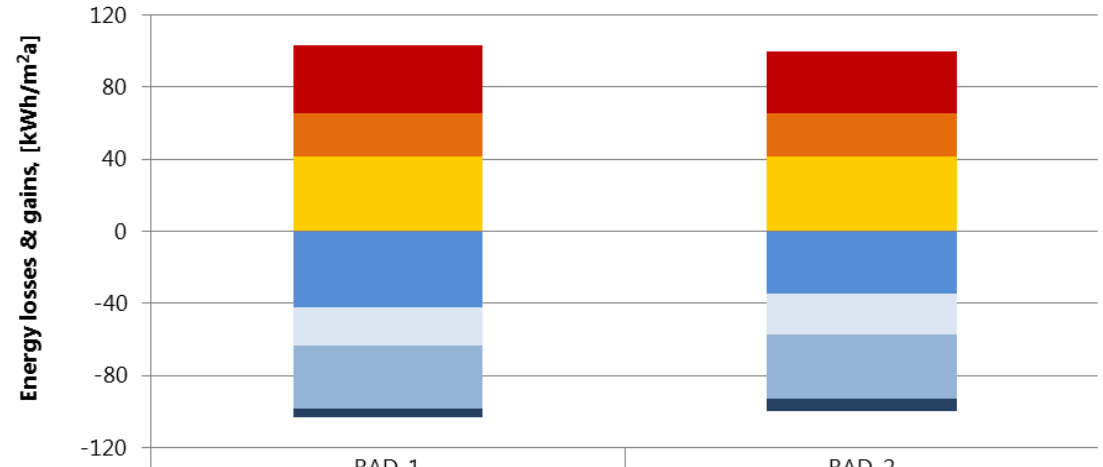

	RAD_1	RAD_2
QHEAT	37.63	34.13
QSOL	23.80	23.68
QGINT	41.88	41.88
QCOOL	-4.73	-6.86
QINF	-35.00	-35.42
QVENT	-21.83	-22.60
QTRANS	-41.76	-34.81

Fig. 2.18. Yearly energy gains and losses for the whole building in RAD_1 and RAD_2 cases.

Looking at the yearly energy gains and losses for the whole building, internal gains (q_{GINT}) are equal for all cases because fixed as boundary conditions. Infiltration (q_{INF}), ventilation gains (Q_{VENT}), transmission losses (q_{TRANS}), heating demand (q_{HEAT}) and cooling demand (q_{COOL}) depend on solar gains and internal temperature, so they are influenced by the different radiation distribution within the zone. Between the two cases, heating differs of 9%. In order to figure out the reason of this discrepancy, the radiation absorbed by all the apartments' walls has been further analyzed. Table 2.5 shows the total radiation absorbed (and transmitted) at all inside (Q_{ABSI}) and outside (Q_{ABSO}) surfaces. For the sake of clarity, the term "inside" is referred to the radiation coming from the zone, while the term "outside" concerns the radiation coming from outside the zone. Labels "EXT", "BND", "ADJ" are referred to the surface's boundary conditions, external, boundary or adjacent respectively. The radiation mode is referred to the inner radiation distribution, in fact the total external radiation absorbed at external surfaces (Q_{ABSO_EXT}) is the same in both cases. As already specified for the detailed mode, negative values indicate the absorption of radiation on a surface, whereas positive heat flux means a net emission. The main difference between standard and detailed mode has been highlighted by adjacent surfaces. In fact, all apartments border with a no conditioned multi air-node zone (the staircase and the lift), that influences the external absorbed radiation for adjacent walls. In particular, lower apartments are more affected by the exchange with "stair zone" than higher ones

Table 2.5 Absorbed radiation on internal and external walls.

CASE		Q_{ABSI}				Q_{ABSO}			
		TOT [kWh]	EXT [kWh]	BND [kWh]	ADJ [kWh]	**TOT** [kWh]	EXT [kWh]	BND [kWh]	ADJ [kWh]
AP_1	RAD_1	**2654**	620	948	1086	**42495**	42927	0	-432
	RAD_2	**2638**	647	948	1043	**44004**	42927	0	1077
AP_2	RAD_1	**2091**	471	742	878	**31353**	32098	0	-745
	RAD_2	**2096**	467	790	840	**33164**	32098	0	1066
AP_3	RAD_1	**2467**	366	-	2102	**21297**	21990	-	-693
	RAD_2	**2474**	380	-	2094	**23691**	21990	-	1701
AP_4	RAD_1	**1493**	629	-	864	**27831**	27505	-	326
	RAD_2	**1483**	679	-	805	**28497**	27505	-	993
AP_5	RAD_1	**2368**	442	-	1926	**24763**	25098	-	-335
	RAD_2	**2353**	463	-	1890	**26902**	25098	-	1804
AP_6	RAD_1	**2135**	831	-	1304	**79724**	79693	-	32
	RAD_2	**2142**	787	-	1356	**80535**	79693	-	843
AP_7	RAD_1	**1693**	665	-	1028	**61442**	61261	-	181
	RAD_2	**1685**	667	-	1017	**61865**	61261	-	604
AP_8	RAD_1	**2303**	1140	-	1164	**113303**	113091	-	213
	RAD_2	**2289**	1129	-	1160	**114060**	113091	-	969
Stair_0	RAD_1	**25**	0	25	-	**0**	0	0	-
	RAD_2	**177**	0	177	-	**205**	0	205	-
Stair_1	RAD_1	**27**	2	-	25	**4757**	2786	-	1971
	RAD_2	**0**	0	-	0	**476**	80	-	396
Stair_2	RAD_1	**73**	0	-	73	**1348**	0	-	1348
	RAD_2	**29**	0	-	29	**45**	0	-	45
Stair_3	RAD_1	**201**	19	-	182	**17982**	16824	-	1158
	RAD_2	**3044**	15	-	3029	**17239**	16824	-	415

Maintaining all the boundary conditions unvaried and changing only the distribution of the radiation, the effect of the different heat transfer with multi air-node zones can be observed with the Mean Radiant Temperature (T_{MR}) within the zone. The T_{MR} of a zone is the area weighted mean temperature of all the walls of the zone [53], so a variation on the T_{MR} might come out analyzing the different T_{MR}. The cumulative frequency of the Mean Radiant Temperature for apartments 2 (situated in the GF) and 8 (situated in the F2) is shown in Fig. 2.19. The graphs represent the yearly frequency distribution of the T_{MR} in the zones for cases RAD_1 and RAD_2. In the apartment 2, the T_{MR} differs of about 0.7°C for the 40% of the year, while in the apartment 8, there is a good overlapping of the two curves.

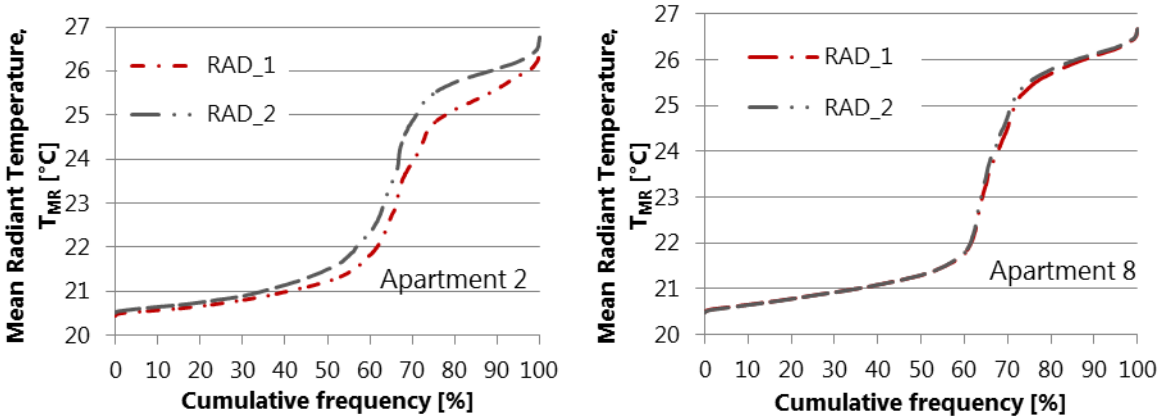

Fig. 2.19 Cumulative distribution during a year of the Mean Radiant Temperature in apartment 2 (left) and 8 (right)

A different distribution of the radiation within the zone influences the ventilation load, the heating and cooling supply energy and the infiltration load. In particular, a discrepancy of about the 9% is observed on the whole building heating load (Fig. 2.18).

The radiation mode does not influences only internal air temperature within the zones, but also the simulation runtime. In fact, computational effort are strongly affected and a reduction of the 86% of runtime passing from the detailed to the standard radiation mode is observed.

In light of this, the choice of the radiation mode is very important for the reduction of computational effort, but attention should be paid when multi air-node zones are adjacent to single air-node zones.

2.4. Shading devices

External or internal shading devices may be defined for any transparent surface of a zone. Building's shadings consist of an overhang from the roof and balconies which drop shadows on the windows. Because of thick insulation of the exterior walls, there is also shading on the windows caused by this framing. To implement these shadings in the SketchUp building model, several shading groups have been set up. Furthermore, the house is surrounded by two other buildings which partially shades the south-east and the north-west facades. To model the shading of these buildings, the walls of the buildings next to the passive house have been drawn in SketchUp with a shading group as well.

At the beginning of the simulation, TRNBuild generates a shading matrix which takes into account the presence of external shaders and self-shading of the building. For generating shading/insolation matrices, TRNbuild calls an auxiliary tool based on TRNSHD. TRNSHD subdivides the sky vault into patches, based on the so-called Tregenza model [51]. For each center point of a patch, the sunlit fraction of external windows, with three dimensional data, is calculated and saved into the shading matrix file, called *.shm. In addition, a diffuse radiation sunlit factor is calculated, assuming an isotropic sky, and written to the file. If no external windows are shaded, no *.shm is generated. In addition to sunlit fractions of external windows, TRNSHD calculates the beam sunlit

fractions of the window that strikes each inside surface of the zone. During the simulation, Type 56 determines the actual sunlit fraction of surfaces thanks to the use of the shading matrix file with respect to the sun's current position for each time step.

In TRNBuild, windows can be defined as Adjacent or External. For an adjacent window, an internal shading device can be defined at the FRONT side only. For an external window, the user can select an internal and/or external shading device and must specify its shading factor. The shading factor can be a constant, an input or a schedule. The External Shading Factor is named ESHADE, while the Internal Shading Factor is named ISHADE. Shading factor indicates the opaque fraction of the device and it is expressed in %/100. Shading factor reduces the amount of solar radiation that passes through the general window by multiplying the incident total radiation by the shading factor. The factor affects beam and diffuse radiation the same. For external shading factors, the incident radiation is reduced before passing through the windows. For internal devices, the energy balance is different and the reflectance of the shading device toward and from the zone comes into play.

2.4.1. Shading coefficient of external shadings

In TRNSYS, energy balances are automatically calculated [51]. Balance outputs can be chosen like a normal output in Type56. The values are hourly integrated and printed in an external file. Balance 3 is the Solar Balance for External Window (NTYPE 903) and it shows the amount of blocked and entering solar radiation within the zone through an external window. If NTYPE 903 is selected in the output manager, this balance will be printed for all selected external windows. This balance shows the performance of a window and its shading devices; only the solar radiation entering an external window is taken into account and no reflected radiation from room or solar radiation entering through other windows is excluded.

$$Q_{BAL} = Q_{SEXT} + \\ -Q_{BESHD} - Q_{BFRM} - Q_{BREFG} - Q_{BABSG} - Q_{BRISHD} - Q_{BLWISHD} - Q_{SHFPR} - Q_{STRNS} \quad \text{Eq. 2.12}$$

For each external window, Balance 3 should be always zero. Solar balance (Q_{BAL}), measured in [kJ/h], is the sum of maximum possible gains, blocked gains and gains of the zone. The total amount of solar gains, Q_{SEXT}, is the total external solar radiation on the external windows including frame. Blocked gains include solar radiation blocked due to:

1. external shading devices of external window (Q_{BESHD}),
2. frame of external window of a zone (Q_{BFRM}),
3. reflection of glazing external window (Q_{BREFG}),
4. absorption on glazing of external window (Q_{BABSG})
5. reflection on internal shading device, including both short-wave radiation (Q_{BRISHD}) and part which is absorbed and then going out ($Q_{BLWISHD}$).

Gains of the zone are referred to the secondary heat flux of external window including only primary solar not reflected radiation or radiation through other windows (Q_{SHFPR}) and short-wave transmission through external window to zone (Q_{STRNS}).

Balance 3 outputs also include the g-value of external window (g_{tot}). It might be calculated as the ratio of the gains of the zone and the total external radiation or as the total g-values of internal and external shadings, frame and glass. This second relation is expressed as:

$$g_{tot} = fc_{Eshade} * g_{frame} * g_{glass} * fc_{ishade} \quad \text{Eq. 2.13}$$

Where g_{frame} and g_{glass} are the g-values referred respectively to the frame and to the glass of the window, while fc_{Eshade} and fc_{Ishade} are the shading coefficient of external and internal shading. In particular, fc_{Eshade} is the ratio between Q_{BESHD} and Q_{SEXT}, that is the shaded portion area of the window. The complementary of fc_{Eshade} is used as external shading factor in Type 56 to approximate shading effects on windows.

2.4.2. Overhangs and wing walls type

In TRNSYS standard library, Type 34 models "Overhang and wing wall shading" [43]. Type 34 characterizes overhangs and wing-walls size and their position with respect to a receiver. The receiver corresponds to the entire external surface, as the shading (balcony or overhang's roof) is extended all along the surface. In this case, no wing-walls are present, but only overhangs. Type 34 performs its own calculation of incident diffuse radiation assuming an isotropic sky model.

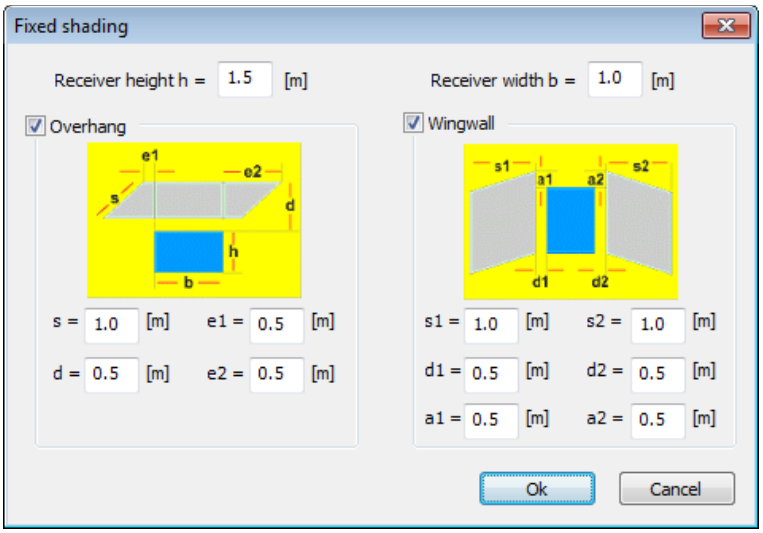

Fig. 2.20 Type 34's wizard for the definition of overhangs and wing-walls characteristics

A wizard interface (Fig. 2.20) allows to easily define the overhang and wing-wall's characteristics as well as receiver height and width. For each orientation and shading (balcony or roof overhang) a shading model has been defined. The Type 34 outputs "Incident receiver radiation", "Beam radiation on receiver" and "Angle of incidence" have been linked to the correspondent building type inputs. In Type 56, new orientations have been created for each shaded surface. In Type 56, the "orientation" for the external walls is changed according to the new shaded orientations. Type 34's output "Fraction of solar shading" (FSS) computes the shading factor as follows:

$$FSS = 1 - \frac{I_{SH}}{I_{tot}} \qquad \textit{Eq. 2.14}$$

Where I_{SH} is the total specific radiation shaded by the modeled shading and Q_{tot} is the total specific radiation on the receiver plane.

The FSS has a value of 0 for a no-shaded surface and 1 for a completely shaded surface. This output is used as external shading factor in Type 56, to approximate shading effects on windows [52].

2.4.3. Comments and results

In cases SHD_1 and SHD_2 a building with no shading devices has been modeled and shadings' effect has been reproduced by External Shading Factors. An external file (SHD_1) and a TRNSYS component, Type 34 (SHD_2) have been used to determine the External Shading Factor inputs.

The use of both shading factors and Type 34 produces a difference of the yearly heating demand of the whole building, Q_{HEAT}, of 1% with the case of shading groups (case RAD_2). The use of Type 34 increases the cooling demand of the building, Q_{COOL}, of around the 8% (see Fig. 2.21).

	RAD_2	SHD_1	SHD_2
QHEAT	34.13	34.28	33.86
QSOL	23.68	23.11	23.25
QGINT	41.88	41.88	41.88
QCOOL	-6.86	-6.71	-6.28
QINF	-35.42	-35.40	-34.78
QVENT	-22.60	-22.56	-22.49
QTRANS	-34.81	-34.60	-35.44

Fig. 2.21. Yearly energy gains and losses for the whole building in cases RAD_1, SHD_1 and SHD_2

In order to understand the different cooling demand needed in the two cases, single apartments have been analyzed. As already seen in Par.2.3, in the detailed radiation mode, matrices are used for distributing primary beam radiation entering a zone through external windows only. For these reasons the incident radiation on windows only will be taken into account.

Case SHD_1 has been considered to find out the difference of the simulation runtime when an external file with the sunlit portion area is used. Regarding the energy building balance, as the external file here used corresponds to the external shading factor of the RAD_2 case, no difference is shown.

The accuracy of the shadings modeled with Type 34 influences the agreement between cases SHD_2 and RAD_2. In Table 2.6 the incident radiation on all apartments' windows for cases RAD_2 and SHD_2 is reported. The third column indicates the difference, in percentage, of incident radiation between the two cases.

Table 2.6 Incident radiation on windows in the Shading group case (RAD_2), in the case with Type 34 (SHD_2)

	RAD_2	**SHD_2**	**$\Delta_{RAD\_2-SHD\_2}$**
	[MWh/y]	**[MWh/y]**	**[MWh/y]**
APART_1	6.2	6.2	-0.3%
APART_2	5.9	6.7	-12.8%
APART_3	7.2	6.7	7.6%
APART_4	3.6	4.9	-30.8%
APART_5	5.9	5.7	4.7%
APART_6	8.5	7.4	13.2%
APART_7	4.0	3.6	10.2%
APART_8	6.0	6.2	-3.6%

Type 34 has been set to model roof's overhangs and balconies, while surrounding contribution and building's shadings (wall thickness, balconies in the adjacent sides) have not been reproduced. A high effect of this modeling is shown in some apartments like apartment 4, where the difference with case RAD_2 is 31%, or in that apartments oriented to South-East, where the difference amounts to the 8-13%.

Regarding the simulation runtime, the use of external file for the external shading factor (case SHD_1) reduces the simulation runtime of 6%, while the use of Type 34 (SHD_2) increases it of about 4%. The result of case SHD_2 also depends on the number of Type 34 units used into the model.

2.5. Geometry mode

For each zone, TRNBuild [39] supports different levels of geometric surface information, known as "Manual" and "3D data" mode. In the manual mode, the geometry of the building is individuated according to the definition of walls and floors and their boundary conditions. The advantage to model directly in TRNBuild is that no detailed shape definition is requested. Defining the area and the boundary conditions for each surface, the software automatically calculates the interactions between the surfaces and the zone. The walls' categories used in this case are external, boundary and adjacent. External is referred to exterior walls, boundary is a wall with boundary conditions of the first type [39] and adjacent is a wall which borders another air-node.

The "3D data" mode provides, for all surfaces of the zone, three dimensional coordinates. Geometry model is designed in Google SketchUp [37] with the Trnsys3D plugin [38] and then an *.idf file is imported to the TRNBuild environment. Zone volume and surface area, which are automatically calculated entities, are derived from the 3D coordinates. In Trnsys 3D plugin, it is possible to define surface type: name, type (ceiling, roof, floor…), category and outside boundary conditions. If the detailed radiation mode (see Par. 2.3.1) is used, radiative zones must be convex polyhedrons. The advantage in using the 3D geometry drawn in Google Sketchup is a user friendly interface in

defining the geometric characteristics. This helps to avoid mistakes, but in some cases, it might be time consuming. In case of changes in the geometric characteristics, the 3D geometry asks to re-edit the *.idf file, while the manual geometry allows modifications in the TRNBuild environment itself. Moreover, the 3D geometry model, if coupled with detailed radiation mode, has to have convex volumes (see also Par. 2.3.1), instead, the model in the manual geometry mode is not strictly connected to the building shape, but it only takes into account area and boundary conditions of each zone.

2.5.1. Comments and results

The last step of Table 2.1 consists on the analysis of the effect in using the 3D data or manual geometry mode. As well as in the previous cases, yearly energy gains and losses on the whole building model have been calculated (see in Fig. 2.22).

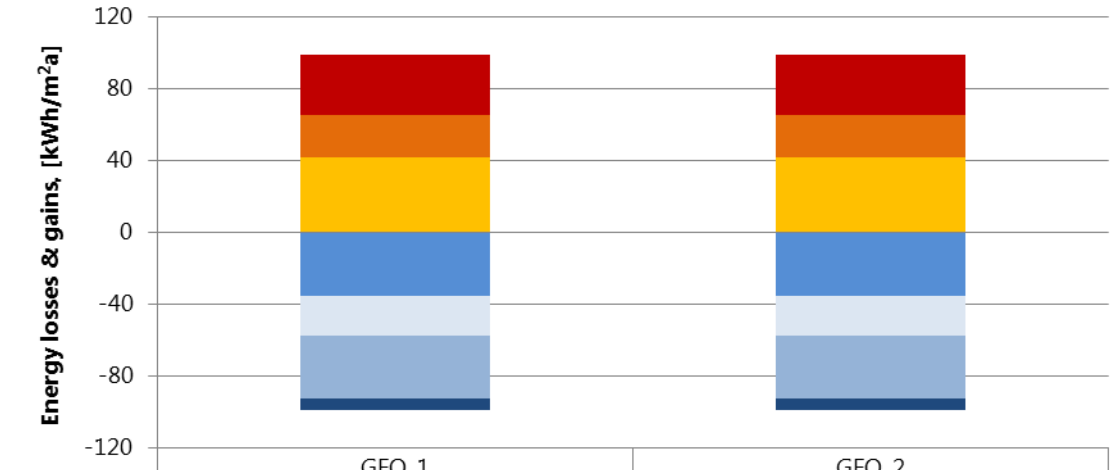

	GEO_1	GEO_2
QHEAT	33.86	33.86
QSOL	23.25	23.25
QGINT	41.88	41.88
QCOOL	-6.28	-6.28
QINF	-34.78	-34.78
QVENT	-22.49	-22.49
QTRANS	-35.44	-35.44

Fig. 2.22. Yearly energy gains and losses for the whole building in cases GEO_1 and GEO_2

Looking at Fig. 2.22, no differences in yearly energy gains and losses have been observed. For both cases, the simulation runtime is also unvaried.

For the calculation of shadings effect, the manual geometry mode does not use shadings matrix. In fact, even if shading devices are inserted in the building model, the manual calculation mode does not use that information. For this reason, if this mode is used, external inputs for modeling the shadings are requested.

2.6. Simplified building model

The steps analyzed above have been used as a guide for the definition of a simplified model. This new model has been realized following the criteria of the reduction of time consuming during the design phase and computational effort during the numerical calculation. The 8 zones model has been created with the manual geometry mode in order to create zones in a flexible way and not directly related to their geometry shape; the model has been run with the standard mode, in order to reduce the simulation runtime; the use of Type 34 has allowed to simulate shading devices without any previous calculation or model. Finally, building energy gains and losses have been compared with the Reference case in order to verify the accuracy of the results.

2.6.1. Building description

In the 8 zones case, walls have been defined with the same area and boundary conditions used in the detailed model. Thanks to the fact that no correlation with the shape of the zone exists, one zone for each apartment has been created. For the staircase, a unique zone with 4 air-nodes, one for each floor, has been created; as in the detailed model, the staircase zone is not conditioned.

For the external walls, same orientations and thermal characteristics of the detailed case have been set. In TRNBuild, the thermal capacitance of each zone has been set automatically as the capacitance of the air in the zone, without considering any furnishings or zone contents. In simplified models, it is commonly used to multiply the capacitance 5-10 times in order to consider the internal mass too. In this case, as the model has been compared with the Reference case, the capacitance has been defined as in that model [36]. In particular, the internal wall capacitance has been calculated and added to the air capacitance. This calculation has been made according to a spread-sheet program considering the guidelines of the standard EN ISO 13786 [55].

Windows geometry characteristics have been not defined as in the detailed case, but the total amount of glazed surface for each external wall has been taken into account.

Infiltration rate, ventilation flow rate, temperature and relative humidity, heating, cooling and internal gains have been defined as in the detailed case [see Par. 2.1.3.5]. For the external walls, new orientations have been created and the FSS output has been connected to the "External Shading Factor" input in the Type 56. One shading for each orientation and each floor has been modelled.

2.6.2. Comments and results

The 8 zones model has been simulated using the same boundary conditions used in Par.2.2.3. The results have been compared with the Reference case.

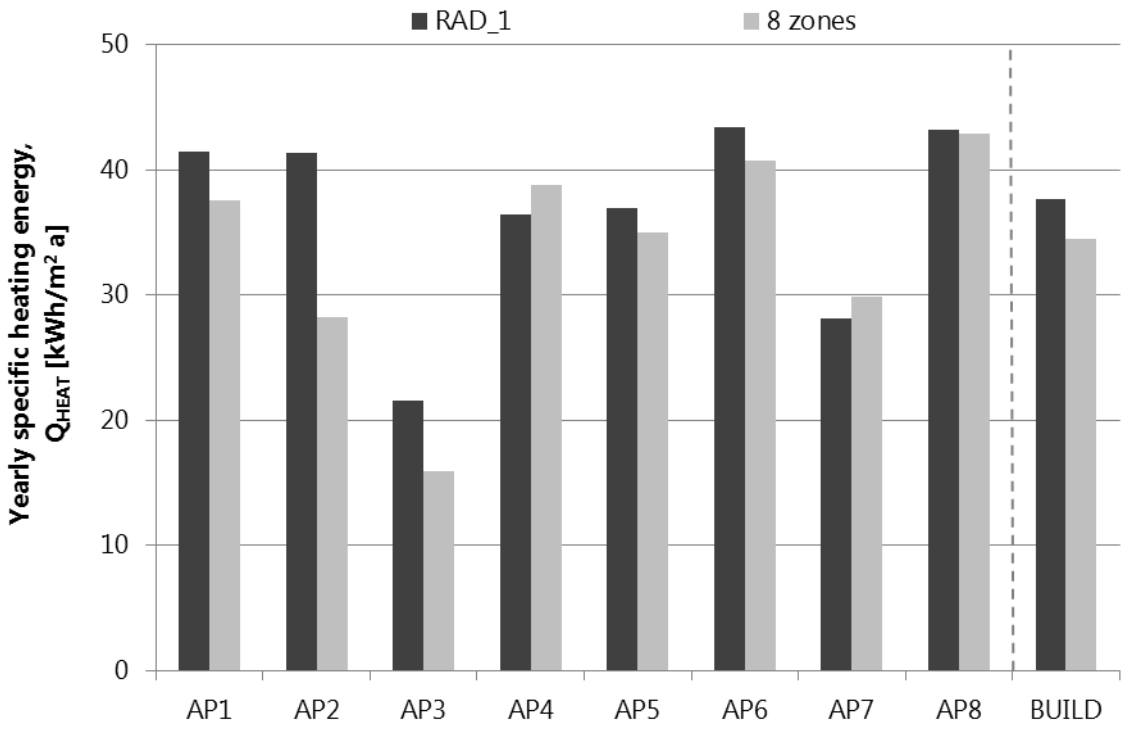

Fig. 2.23. Yearly specific heating energy in the Reference case (RAD_1) and in the 8 zones case (8 zones)

The difference of heating demand of the whole building between Reference case and 8 zone is around 8% (see Fig. 2.23). Higher differences are observed in those apartments in which the constant infiltration value approximates with lower accuracy the real infiltration rate or in which the incident solar radiation differs more from the reference case. In particular in apartments 2 and 3, this difference is around 25-30%, due to the fact that Type 34 does not take into account the building on the sides. As a consequence, higher solar radiation hits the apartment in the simulations and lower heating demand is requested. Similar situation, but with minor impact, is also observed for apartment 6, because it is located on the same side, but on the third floor, where the influence of shading from the surrounding is lower.

Comparing the simulation runtime in the two cases, a strong reduction of the 89% is observed. This result is due to the fact that the standard radiation mode has been used and 9 zones (apartments zones + staircase zone) versus 15 of the Reference case have been modeled.

2.6.3. Conclusions

The use of the manual or 3D data geometry mode, does not produce changes in both simulation runtime and building energy response. The geometry mode selected influences the use of specific radiation mode, the definition of building geometry characteristics, the number of zones or the shadings modeling. An important reduction of computational effort is observed moving from detailed radiation mode to standard mode (around 85%). This difference is due to the use of matrices by the detailed mode for the sunlit surfaces calculation, rather than GEOSURF values and fixed absorption coefficients, as in the standard mode. This simplification does not affect solar

gains, but leads to a change in the air-node temperature when conditioned single air-node zones borders with non-conditioned multi air-node zones; in particular in the standard radiation mode, the Mean Radiant Temperature is higher than in the detailed mode. As a consequence, when the standard mode is used, the building heating and cooling demand differs of about the 9% with respect to the detailed mode. The use of external input for the External Shading Factor does not reduce significantly the simulation runtime: it might vary of around ± 5%. The use of Shading Factors obtained from the Reference case, does not influence energy gains and losses, while in the case with Type 34 there are some changes, depending on the apartment orientation. This last case does not consider the shading effect of the surrounding shadings, but it takes into account only the overhangs or wing walls of the building.

The modeling of External Shading Factor with external inputs does not reduce significantly the simulation runtime, which might varies of around ± 5%. The influence on energy gains and losses using Type 34 depends on the apartment's orientation. Type 34 models the shadings taking into account only the overhangs or wing-walls of the building and not the shading effect of the surrounding.

In general, the use of the standard radiation mode leads a significant reduction of simulation runtime maintaining the same solar radiation arriving on walls and windows, but the effect of multi-reflection within the zone is neglected. Attention has to be paid in that cases in which conditioned zones border with non-conditioned multi air-node zones. If detailed radiation mode is used and the shadings shape is not complex to be modeled, there are not advantages in using external inputs for the definition of the sunlit portion area. Indeed, if the geometry characteristics of the building are defined directly on TRNBuild and the manual geometry mode is set, the use of inputs for the External Shading Factor is requested. In particular, better results can be achieved with an external file which defines the sunlit portion area considering all the shadings effects (for example obtained by a shader program [54]). If these information are not available a good approximation of shading effect on windows can be made by Type 34.

A unique solution for the reduction of computational effort does not exist because it is strictly correlated to the aim of the simulation and the parameters which have to be analyzed. The main aim of the work here presented, is the definition of a building model which reproduces as reliably as possible the real building behavior, reducing the computational effort.

For this purpose, the standard radiation mode has been selected, as it is the aspect which strongly reduces the simulation runtime. Moreover with the standard radiation mode, there are no specific conditions for the zones shape. Manual geometry mode has been set to allow the definition of building geometry characteristics directly in the TRNBuild environment and one zone for each apartment has been so created. Shading devices have been modeled with one Type 34 for each external wall; in this way, no external files obtained with previous calculations or modeling need.

The final simplified building model runs with a reduction of the simulation runtime of the 89% and a discrepancy of the heating demand of around 9%. This numerical model has been used for the analysis presented in the next chapters.

Bibliography

[31] IBPSA-USA. Building Energy Modelling. IBPSA-USA, Rocky Mountain Institute, ASHRAE. http://bembook.ibpsa.us/

[32] Energy Modeling of Buildings. IBPSA_US. http://energymodeling.pbworks.com

[33] IPES. La casa passiva Bronzolo. Istituto per l'edilizia sociale della Provincia Autonoma di Bolzano, Bolzano (2006).

[34] Direttiva tecnica Casaclima, (2011)

[35] Castagna M. Studio di una Casa Passiva con un programma di simulazione dinamica. Tesi, Universitá di Trento, Trento (2009)

[36] Ecker M. E. Modelling and Parametric Analysis for a Small-Scale Solar Heating and Cooling System. Master thesis, Fachhochschule Technikum, Wien (2011)

[37] Google SketchUp, ---

[38] Trnsys 3D plugin. http://www.trnsys.de/docs/trnsys3d/trnsys3d_uebersicht_en.htm

[39] A.V. Bitsadze. Equations of mathematical physics. MIR publisher, Moscow (1980)

[40] Incropera F., Dewitt David., Bergman T. & Lavine A. Fundamentals of heat and mass transfer. John Wiley & sons, United States of America (2007)

[41] J.M. Ortega & W.C. Rheinboldt. Iterative Solution of Nonlinear Equations in Several Variables. Academic Press, New York (1970).

[42] TRNSYS 17- A Transient Simulation Program. University of Wisconsin, Madison, USA (2010)

[43] TRNSYS 17 Documentation, 04. Component Mathematical Reference. Solar Energy Laboratory, University of Wisconsin, Madison, USA (2010)

[44] EN13829:2001, Thermal performance of building. Determination of air permeability of buildings. Fan pressurization method. (2001)

[45] Sherman, M. Estimation of infiltration from leakage and climate indicators". Energy and Buildings vol. 10 (1987).

[46] Diamond R. C., Feustel H. E. & Dickerhoff D. J.. Ventilation and Infiltration in High-Rise Apartment Buildings. Technical report, Lawrence Berkley Laboratory, University of California, Berkley, California (1996)

[47] ISO 7730:2005. Ergonomics of the thermal environment – Analytical determination and interpretation on thermal comfort using calculation of the PMV and PPD indices and local thermal comfort criteria. (2001)

[48] Seem, J.E., "Modeling of Heat in Buildings," Ph. D. thesis, Solar Energy Laboratory, University of Wisconsin Madison (1987)

[49] Hiller, M. D.E., Beckman, W.A & Mitchell, J.W. TRNSHD – a program for shading and insolation calculations, Building and Environment vol.35 (2000).

[50] Gebhart, B., Heat Transfer, McGraw-Hill, New York (1971).

[51] Tregenza, P., Subdivision of the Sky Hemisphere for Luminance Measurements, Lighting Research and Technology, Vol 19 (1987)

[52] TRNSYS 17 Documentation. 05 Multizone Building. Solar Energy Laboratory, University of

Wisconsin, Madison, USA (2010)

[53] Gulyás A., Unger J. & Matzarakis, A. Assessment of the microclimatic and human comfort conditions in a complex urban environment: Modelling and measurements. Building and environment, Vol.41 (2006)

[54] Jones N. & Greenberg D. Hardware accelerated computation of direct solar radiation through transparent shades and screens. Program of Computer Graphics, Cornell University, Ithaca, New York, USA (2012)

[55] EN ISO 13786:2007 Thermal performance of building components – Dynamic thermal characteristics – Calculation methods. International Organization for Standardization (2007)

3. Supply Energy System

3.1. Introduction

Solar Heating and Cooling (SHC) systems use heat from solar thermal collectors to provide space heating in winter, space cooling in summer and Domestic Hot Water (DHW) during all the year.

The annual collector yield of all water-based solar thermal systems in operation by the end of 2010 was 162,125 GWh (= 583,649 TJ). An estimated 85% were used for domestic hot water preparation in single family houses and 10% were attached to larger domestic hot water consumers such as multifamily houses, hotels, hospitals, schools, etc. The remaining 5% of the worldwide installed capacity supplied heat for both domestic hot water and space heating (solar combi systems) and for other applications, such as solar supported district heating networks, industrial processes and solar air conditioning applications. The market for solar combi systems is well established in some mature European markets such as in Germany and Austria accounting for more than 40% in these local markets and for 4% in a worldwide context (see Fig. 3.1) [56].
Other applications such as solar supported district heating networks, solar process heat and solar air conditioning systems are at a very early stage of market penetration in a worldwide context amounting for less than 1% of the total installed capacity.

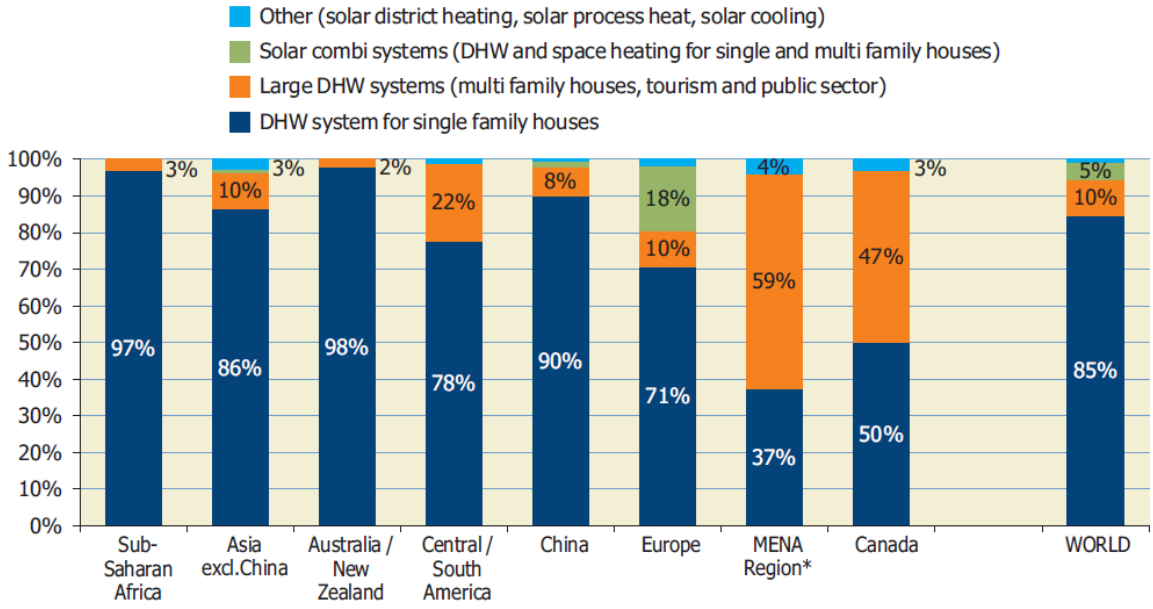

Fig. 3.1 Distribution of solar thermal systems by application for the total installed glazed water collector capacity in operation by the end of 2010 [56]

By the end of 2011 approximately 750 solar cooling systems were installed worldwide and the major markets were in Spain, Germany and Italy [57]. The market still can be categorized as a niche market under development, but nevertheless the annual growth rates are high as can be seen in the following Fig. 3.2.

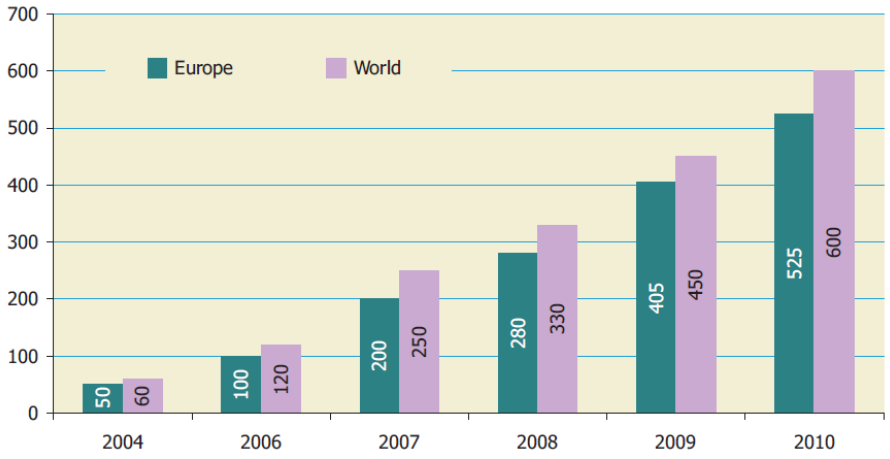

Fig. 3.2 Market development of small to large-scale solar air conditioning and cooling systems worldwide as well as in Europe [56]

A SHC installation consists of a typical solar thermal system made up of solar collectors, storage tank, control unit, pipes and pumps and a thermal driven cooling machine. Commonly, solar cooling systems have also a heat backup to feed the thermally driven chiller with a fossil fuel driven heat support when solar heat is not available. A cold backup, consisting of an electrically driven compression chiller, is not common in small scale application. SHC systems are very suitable for cooling and air conditioning because of [58]:

- coincidence of solar gains and cooling loads;
- reduction of electric peak load created by air conditioning;
- high use of solar gains during the entire year;
- reduction of summer surplus of solar gains in solar systems designed for heating applications.

The case study here treated presents some differences in the main components of the system. No heat backup nor cold backup are installed in the plant. A heat backup is considered to be in the sorption chiller itself, while a compressor chiller has been not included for economic reasons even if, from the point of view of primary energy efficiency, a compression chiller would be most feasible.

3.2. Case study layout

The SHC here presented has been developed within the 7th Framework Programme (FP7), as a case study of the project ALONE (smAll scaLe sOlar cooliNg devicE) [68]. The main aim of the ALONE project has been to overcome the lack of small scale units, developing fully automated and autonomous package-solutions for residential and small commercial or industrial solar cooling applications. The objective has also included the developing and improvement of new components of small capacity cooling systems (small size systems, 5-13 kW of cooling capacity), collectors and control systems, as well as plants characterized by pre-engineered solutions. The project has foreseen two test sites, situated both in Italy, one at Misericordia Hospital in Florence and one in Bronzolo, close to Bolzano. The considerations made in this work are referred to the Bronzolo's site.

In this project, efforts have been concentrated on the DHW, space heating and cooling distribution. The control system, in fact, is a weak point of solar cooling till now because there are no standards or guidelines to be followed. The project also helped in the definition of control strategies for design a unique control system for solar field and chiller in order to improve the overall system performance, make the units fully automated and independent assuring the system security.

The control strategy presented in this work has been applied to the test side and it has been defined according to the following criteria:

- improvement of the energy management control strategy for the different operation states over the whole year: cooling with sorption unit, heating directly with collectors, heating with sorption unit;
- improvement of the utilization of low temperature solar contribution and the best coordination of collector and chiller temperature control;
- the definition of optimal strategies for different utilization of the types (sorption machine, heat rejection circuit).

The supply energy plant under investigation has been installed in the building described in Par. 2.2.1. The system has been designed and implemented in two different moments. The previous system only covered the production of space heating and DHW; after some years of monitoring, an integration for the cooling space too has been done. An Air Handling Unit (AHU) is located in the utility room in the cellar. Fresh air coming from the north-façade is cleaned up and filtered by the AHU. With the cross-flow heat exchanger, up to 85% of the exhaust thermal energy is recovered by heating up the fresh air. In addition to that and also to avoid freezing condensation water, the fresh air is heated up in advance by horizontal geothermal probes. Through the living rooms, the delivery of fresh air is performed, whereas the discharged air is take away from the bathroom and the corridor. So the exhaust air is detracted from humid rooms and from rooms with a built up of odours. The distribution of fresh air within the flats is carried out via slots above the doors. The flat heating is mainly done via post heating of the fresh air through a heat battery. These heat batteries, with a capacity between 2.1 and 2.4 kW, are driven by a pellet boiler (for heating and DHW supply) which is coupled with a storage buffer of 800 L. In addition to that, a common radiator is used in the bathroom. To regulate the energy consumption, different thermostats are installed in the dwellings. The DHW is provided by a 3000 L stratified storage fed by solar energy; the pellet boiler and the 800 L puffer work as heat back up. Using the different weight of cold/hot water the storage stratifies and the hottest water rises on the top of the tank. On the other side of the tank the water goes to two heat exchangers to get heat the tap water up to a fixed temperature (T44). After that, the warm water flows to the puffer in which the temperature is maintained around 70°C, for hygienic reasons, by a pellet boiler.

For different reasons, the new system has been added to the previous, maintaining the independency of the first in case of maintenance, installation of components or not appropriate functioning of the new system. One main point for the decision to install a SHC system in Bronzolo has been the high indoor temperatures during the summer time. The preceding measurements on this passive house have carried out that temperatures up to 30 °C prevail in the dwellings so that an air-cooling system would have been necessary. A second point has been the relatively easy way to combine the existing system with the SHC. The needful area for the new components has been

distributed between the cellar, for the chiller and the 3000 L tank, and the roof, for the solar field. A third point has been the possible interconnection with the existing geothermal probes which have been used as a heat sink. Fig. 3.3 shows the layout of the energy supply system; into the red dotted line, the previous system is represented.

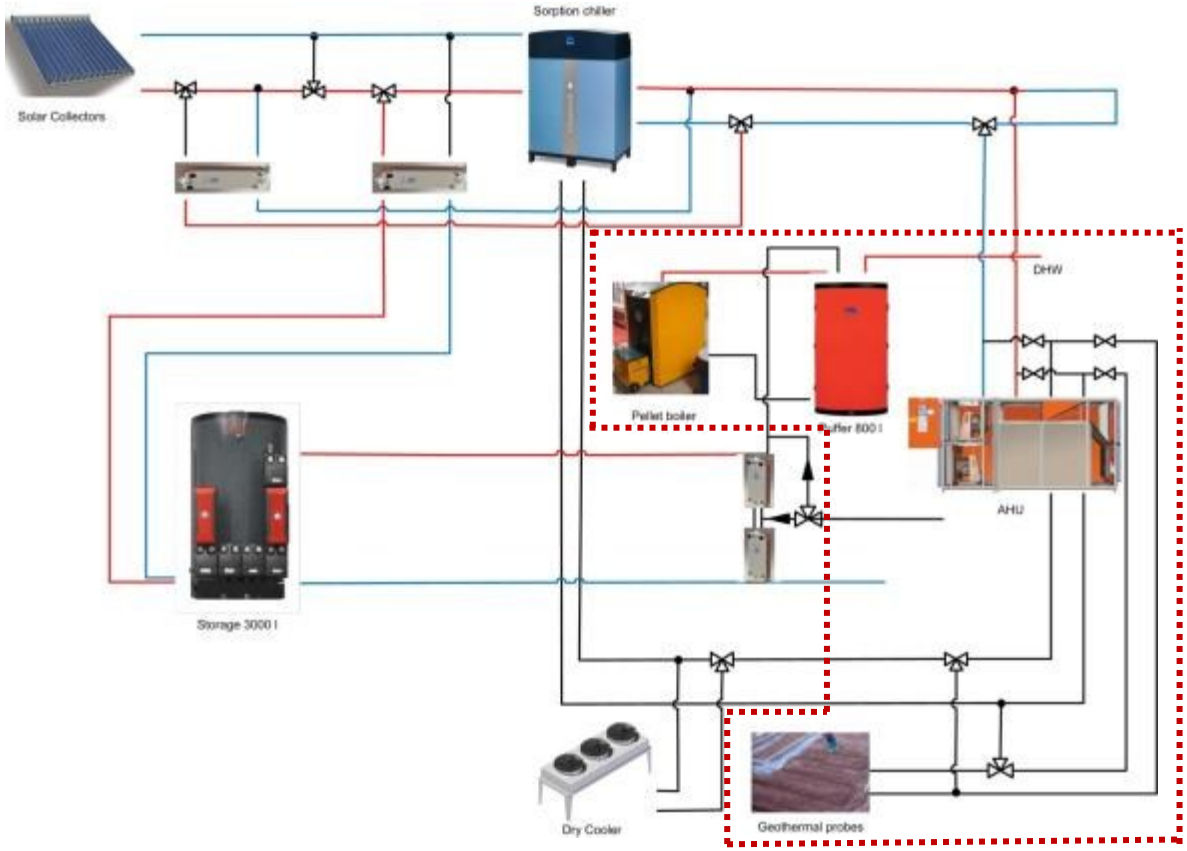

Fig. 3.3 Layout of the energy supply system; in red dotted line, the previous system is shown

A special effort in the design phase has been spent for the heat rejection loop where the dry cooler utilization should be reduced as an aim of the project. Instead of that, two different solutions have been considered. Firstly, an air heat exchanger battery, at the exhaust side, has been thought to cool down the condenser/absorber of the thermally heat driven chiller; then, the already existing geothermal probes may be switched on till the ground will be capable to acquire the heat; finally, just in case that the two previous components will not be enough, the dry air cooler will be turned on.

3.3. Supply energy system modelling

In order to find the best configuration and control strategy, a model of the whole plant layout has been developed; several simulations have been carried out and results have been evaluated.
The model of the supply energy plant has been created in TRNSYS 17 [64]. Characteristics of the devices have been reproduced with the TRNSYS' types, according to rated performances. Fig. 3.4 shows all components included in the system: valves, pumps, heat exchangers, solar collectors,

geothermal probes, dry cooler and storage. Building, AHU and sorption chiller have been modeled in three macros because they consist of several types. Two more macro have been added in the deck, one includes the entire control, while the other all external files and plotters. Monitored data have been used for the DHW demand. In this chapter, no building model has been considered and all the considerations on building behavior are neglected. For the system control, the only supply air is taken into account.

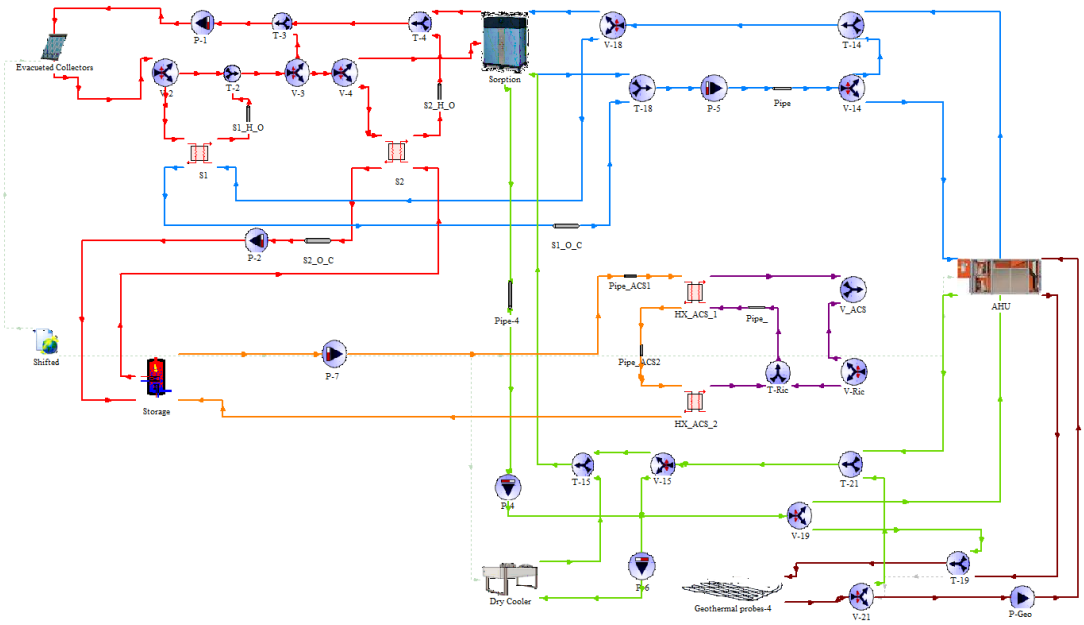

Fig. 3.4 Model of the energy plant in TRNSYS (TRNSYS deck)

3.3.1. Solar field

The installation in Bronzolo regards a building in a residential zone in the periphery of the town; it is surrounded by buildings in the south-east and north-west side (Fig. 3.5).

Fig. 3.5 top view of the building and its surrounding

The amount of installed solar collectors depends on the capacity of the storage for the DHW, on the power of sorption chiller [58] and on availability of free surface. The best site for that is the flat roof (Fig. 3.6). The solar field has been sized according to the rule of thumb of 50 – 75 l/m^2 of storage capacity [58]. For a 3000 liter storage, 40 m^2 of evacuated solar collectors have been installed.

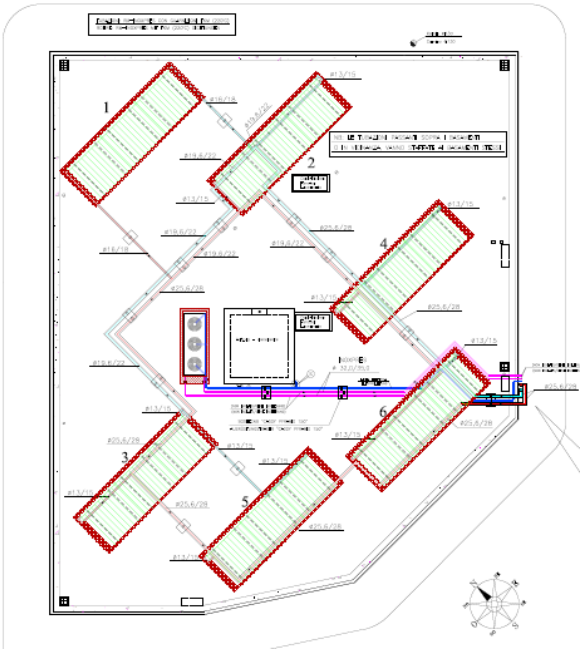

Fig. 3.6 Plant of the solar field on the roof

The collectors installed are the CSV 25 model provided by Riello (Fig. 3.7). The evacuated solar collector CSV25 is constituted by 14 evacuated pipes to double wall of glass, each of which contains a copper pipe folded up to "U" and a fluid composed by water + glycol in order to avoid the freezing in the winter season. Inside the pipe the vacuum has been created to reach more

insulation. In such a way collectors are able to produce useful solar energy also during winter or warm seasons.

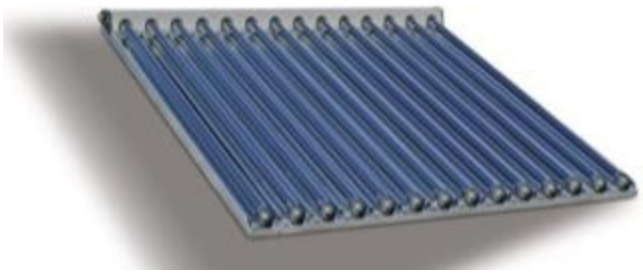

Fig. 3.7 Evacuated solar collectors CSV 25

Solar field has been modelled with the Type 71 of the standard library. Intercept efficiency (a_0), negative of first order efficiency coefficient (a_1) and negative of second order efficiency coefficient (a_2) have been set as rated values (see Table 3.1). Type 71 reads the biaxial incidence angle modifier (IAM) data from an external data file. These data are read and interpolated by subroutine and consists of 7 values of incidence angles (in both directions) and modifiers. In the Table 3.2 there are the IAM for the specific collectors.

Table 3.1 Efficieny of evacuated solar collectors – CSV 25

Intercept efficiency	Negative efficiency coefficient	
(a_o)	a_1 (W/m^{2}K)	a_2 (W/m^{2}K)
0,641	1,059	0,0045

Table 3.2 Longitudinal and transversal angle of evacuated solar collectors

Angle	**0°**	**30°**	**45°**	**50°**	**60°**	**65°**	**80°**
Longitudinal (IAM_{Long})	1	1	0.97	0.96	0.87	0.8	0.5
Transversal (IAM_{Trans})	1	1	1.05	1.08	1.15	1.18	0.72

3.3.2. Storage

The storage has been dimensioned in order to satisfy the demand of DHW of all apartments. The storage is a OSKAR – Ratiotherm stratified storage with a volume of 3000 liter.

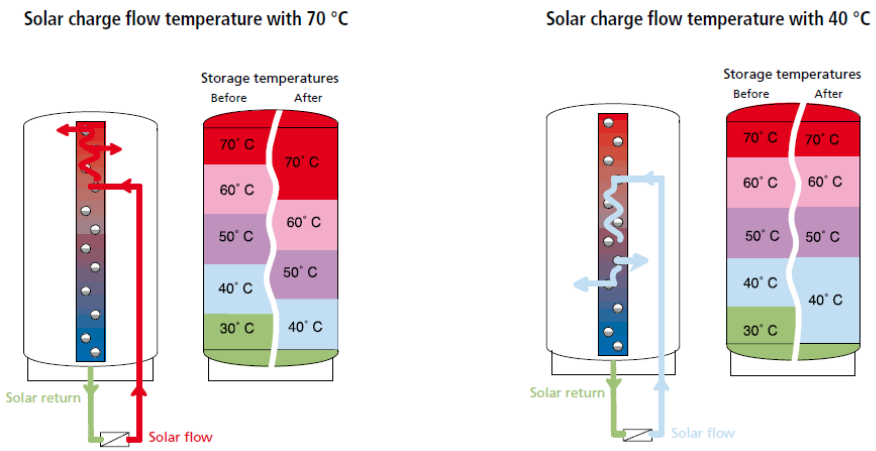

Fig. 3.8 Functioning of the stratified storage [60]

For the stratification process, this storage exploits the effect of a calm positive or negative lift according to the physical law of gravity (warm water is lighter than cold water). All connections are introduced into the tank from underneath through the bottom and emerge in the corresponding temperature zone of the multi-chamber system. The water into the lift takes place sorted according to temperatures. As an example, water with a temperature of 40 degrees from the sun collectors is layered into the 40 degree zone without getting mixed with the 70 degree warm layer from the sunny previous day and without cooling the same down, that is, to dissipate energy with high temperature again (Fig. 3.8).

The storage has been modelled with the Type 340 [66]. The fluid in the store is assumed to consist of N_{max} completely mixed equal volume segments (nodes). The store can be charged and discharged directly by ten double ports. A double port is a pair of two pipes that belong to the same circuit. The schematic of the Type 340 store model is shown in Fig. 3.9. The relative position of ports and heat loss capacity rate have been set with rated values.

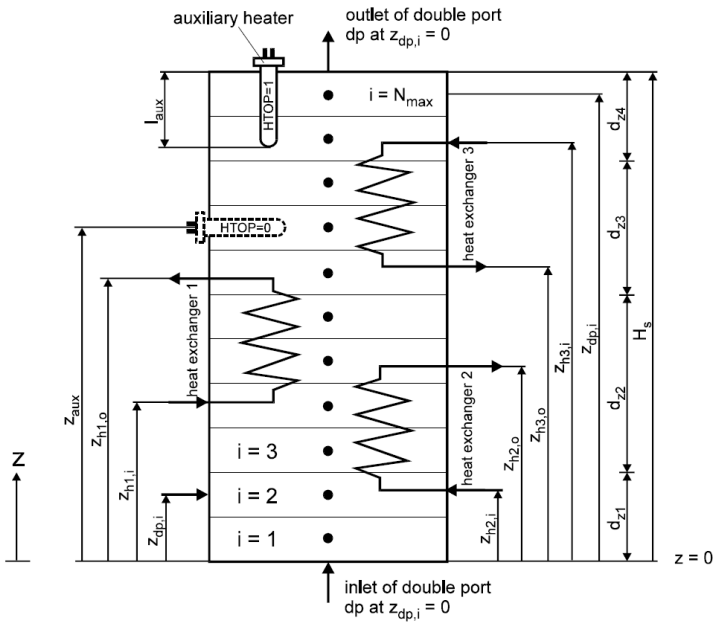

p = number of a double port [1…10]

x = number of a heat exchanger [1…4]

d_{zk} = relative height of a zone with $(UA)_{s,ak}$ = const [k=1…4]

Fig. 3.9 Scheme of the storage model in TRNSYS

One double port is used for the charging of the storage, the other for the user. Through a heat exchanger, the primary circuit transfers heat to the secondary circuit up to a set temperature of the water in the storage. The other double port is connected to two heat exchangers for the production of DHW.

3.3.3. Sorption chiller

The ClimateWell solar chiller consists of two twin barrels where the absorption process takes place, a connection kit with valves and fittings and a control system that manages the valves and calculates power and energy [61]. The chiller has two separate bowls in a closed environment. One is filled with salt (reactor) and one with water (evaporator) (Fig. 3.10). The water molecules are more strongly bound to the salt than to liquid water at the same temperature. The salt will thus begin to absorb the water.

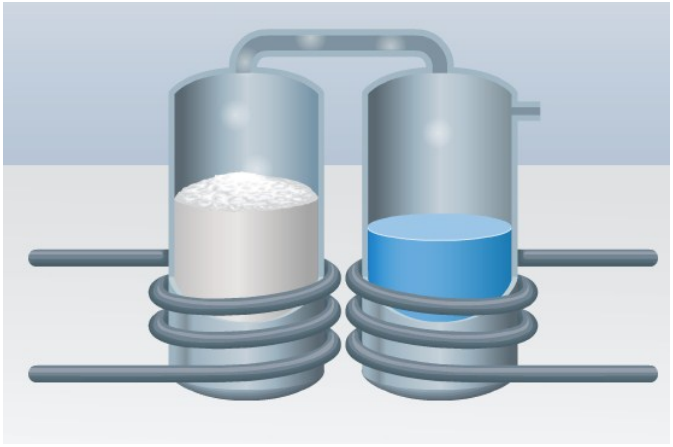

Fig. 3.10 Image of the reactor and evaporator barrels inside the chiller

When the salt cannot absorb more water, it has to be dried (through warming) to regain its hygroscopic ability. In this way, the water returns to the water bowl. To improve the process, air can be extracted to produce a vacuum, in order to increase the speed and the water starts to boil and produce vapour at the same speed it is absorbed by the salt. This process requires energy. In a closed system, the energy is taken from the water itself. As a result, the water gets colder. In the salt, the energy is released and heated. The difference in temperature will increase until a maximum is reached, which is defined by the properties of the applied salt. In this way, a heat pump has been created. A coiled tube connects both bowls to two different objects outside the system. Water can be circulated to transport energy (hot or cold) out of the system. When connected to the indoor heat exchanger, the house is conditioned. The waste heat is rejected or it could be used for warming a swimming pool. To store energy in the system, the salt bowl is connected to a source of thermal energy, like solar thermal collectors. The necessary temperature in the energy for the charging of the system is usually between 85-120 °C. The impulsion temperature lie between 10 and 18 °C, whereupon the minimum temperature is about 10 °C. The power supply lies around 6 to 7 kW depending on the impulsion temperature and the heat sink circuit.

In the deck, the sorption machine is contained in a macro, since two different components are used. The types have been developed by ClimateWell, one for the barrel (Type 825) and one for the switching unit and internal controller (Type 26). The combination of a controller and two barrels types makes the sorption chiller model (Fig. 3.11).

The model of the barrel (unit with reactor and condenser/evaporator) is a grey box model based on the physical properties of the standard equations for heat transfer, mass and energy balances. The heat transfer coefficients are identified from measurements.

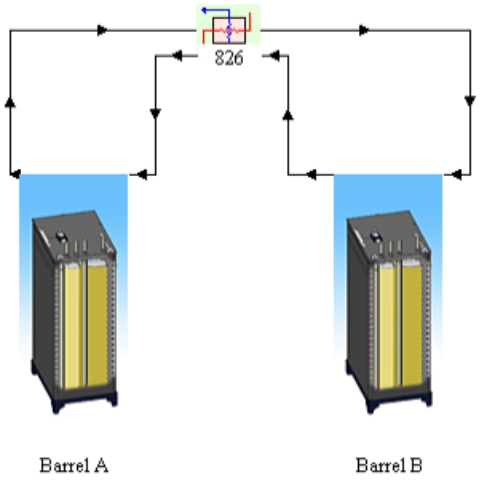

Fig. 3.11 Subsystem model of a complete ClimateWell machine in TRNSYS studio (top), comprising two units (Type 825) and a switching/controller unit (Type 826)

The barrel model calculates losses from the switching unit to the ambient at both outlet and inlet, as shown in the equivalent resistance network for the unit in Fig. 3.12. There are also losses from the reactor and condenser parts of the unit to ambient as well as internal (radiative) losses between reactor and condenser.

The concentration of the solution is calculated using a mass balance for the water and the total mass of LiCl in the unit. The temperature difference between the inlet fluid to the reactor and the inlet fluid to the condenser is dependent on the theoretical properties of the working pair (LiCl-water). For the solution, equations published by Conde [67] are used and for the region with solid salt, correlations derived by ClimateWell and SERC are applied. The model calculates the heat transfer for the input flows and temperatures from the connected circuits, and all the temperature control has to be implemented externally the model of the machine, just as is in the real systems.

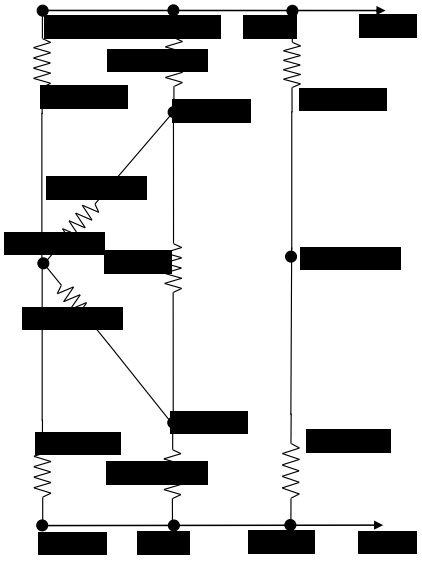

Fig. 3.12 Equivalent resistance network for the unit model (Type 825)

The model for the controller and switching unit (Type 826) determines whether a unit is fully charged and also when discharge is complete. The algorithm works with the same principles as that used in the commercial machine.

3.3.4. Air Handling Unit

The installed air handling unit (AHU) is the type "Trisolair 52.11.01", brand "MENERGA" [61]. It consists of a cross-counter flow heat exchanger with a nominal temperature efficiency greater than 80%. The nominal recuperation power is 5 kW at 8°C fresh air and 22°C exhaust air or 9.9 kW at -12°C fresh air temperature. The two fans have frequency controlled motors which can force an air flow rate of nominal 1440 m³/h. An optional bypass damper is installed to allow free cooling (Fig. 3.13).

Fig. 3.13 internal view of the AHU case [61]

In the new plant, two additional heat exchanger coils have been installed on the primary AHU – one in the supply duct and one for the exhaust air. The first battery is used for the direct heating during the winter or the cooling during the summer. The other coil is a heating battery used during the summer as heat rejection of the dissipation circuit.

In the TRNSYS deck, the model of the AHU includes not only the components of the AHU itself (air-to-air heat exchanger and fans) but also the other components that act for the conditioning of supply air (Fig. 3.14). Each component is further presented.

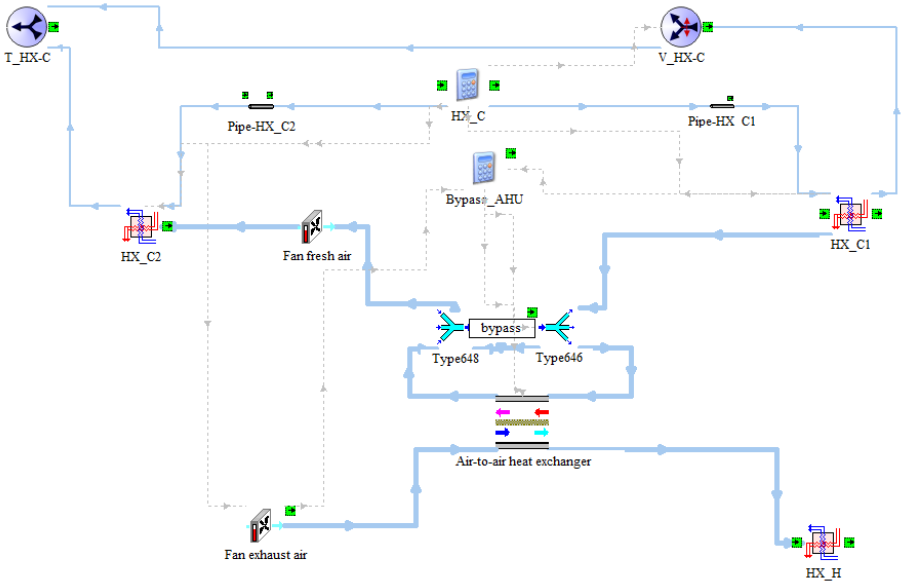

Fig. 3.14 View of the AHU macro

Air-to-air heat exchanger: Type 667 models a heat recovery device using a "constant effectiveness – minimum capacitance" method [65]. In the case here presented, Type 667 is used as a counter flow heat exchanger with only energy transfer. The schematic diagram of the heat recovery is shown in Fig. 3.15. The two air streams are separated by an impermeable membrane that allows only energy to transfer from one stream to the other. No moisture transfer is foreseen. "Fresh air" is referred to external air, while "exhaust air" is the air withdrawn from the building.

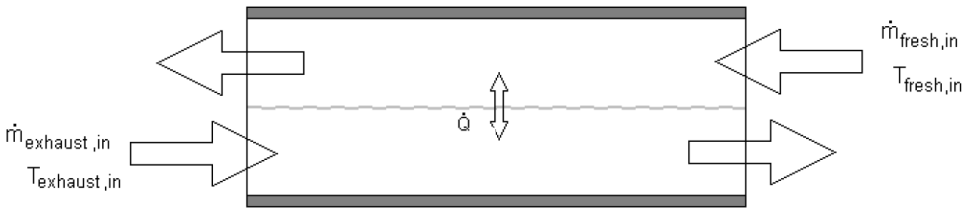

Fig. 3.15 Air to air heat recovery device schematic

Fan: Type 744 models a fan that sets its outlet mass flow rate equal to a user specified inlet mass flow rate. The inlet mass flow rate can be fixed or it can change, depending if the fan is a constant or variable speed fan. The fresh air flow rate is defined according to the calibration of the ventilation already presented in Par. 2.2.2.1. The exhaust air flow has been supposed to be the 80% of the fresh air for maintaining a overpressure inside the building and reducing the losses.

Coil: the coils installed in the AHU are modeled with Type 5, as a heat exchangers water to air. The water+glycol is considered to be in the source side, instead the air in the load side.

As for the water-to-water heat exchangers, the UA value has been calculated according to

$$UA_{hx} = \frac{\dot{Q}_{hx}}{LMTD} \qquad \textit{Eq. 3.2.}$$

Two different UA values have been considered, one for summer working condition (condensation

might happen) and one for winter working conditions.

Calculator: the equations within the box "Control signals" control the opening and closing of the bypass. According to the external and exhaust air, boolean operations regulates the opening of the by-pass in the AHU. When fresh air temperature is lower than 14°C or the exhaust air is at least 2°C colder than fresh air, the by-pass damper is positioned in order to allow the heat transfer between fresh and exhaust air.

Other equations have been used to simulate the split of the chilled water flow in the two cooling coils, in order to perform a pre-cooling and cooling of the fresh air during the summer season.

3.3.5. Geothermal probes

Eight geothermal probes are installed at 50 cm beneath the house, with a length of 80 m and a diameter of 5 cm (Fig. 3.16). A fluid of water+glycol is used for reducing the size of the system and avoiding the icing of the fluid with low external temperatures. These probes are used as a preheater in winter season, for the ventilation system to achieve a better efficiency factor for the heating system and to avoid freezing condensation in the cross-flow heat exchanger. In summer, these probes are used as a heat sink for the solar cooling system. As the probes have been designed not for this purpose, they are not able to reject the 30 kW oh heat required by the system. As already specified, a air heat exchanger has been included into the heat sink system together with a dray air cooler. The installation of the probes was realized before the construction of the building (Fig. 3.17).

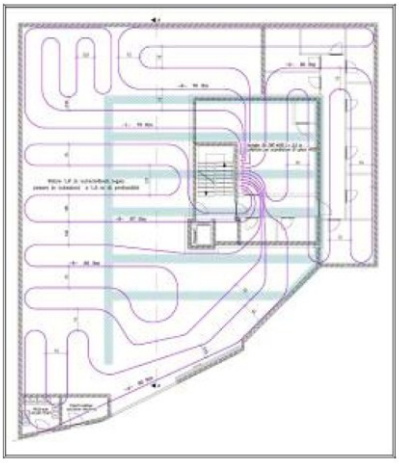

Fig. 3.16 Scheme of the path of geothermal probes

Fig. 3.17 Installation of geothermal probes

Ground heat exchangers have been modelled with Type 952 from TESS Library. This routine models the energy transfer from a liquid-filled cylindrical pipe to the soil surrounding it. The energy transfer between the pipe and surrounding ground is assumed to be conductive only and moisture effects within the soil are not accounted in the model. The model relies on a 3-dimensional finite difference model of the soil and solves the resulting inter-dependent differential equations using a simple, but effective, iterative method.

3.3.6. Dry Cooler

The dry cooler (or air-cooled heat exchanger), consists of a finned tube heat exchanger bundle arranged above or below a fan plenum chamber. Forced or induced draft fans, respectively, blow or draw air across the finned tube bundles.

The Dry Cooler used in Bronzolo is a "Thermics Dry Cooler CTH25" and it has been designed to satisfy absorbing technology plants like the case study here presented. This dry cooler is completely aluminum made, with increased exchange surface, being a "plate and fins" type. The kind of fans used grants low noise levels and energy efficiency. The dry cooler is installed on the roof as shown in Fig. 3.18.

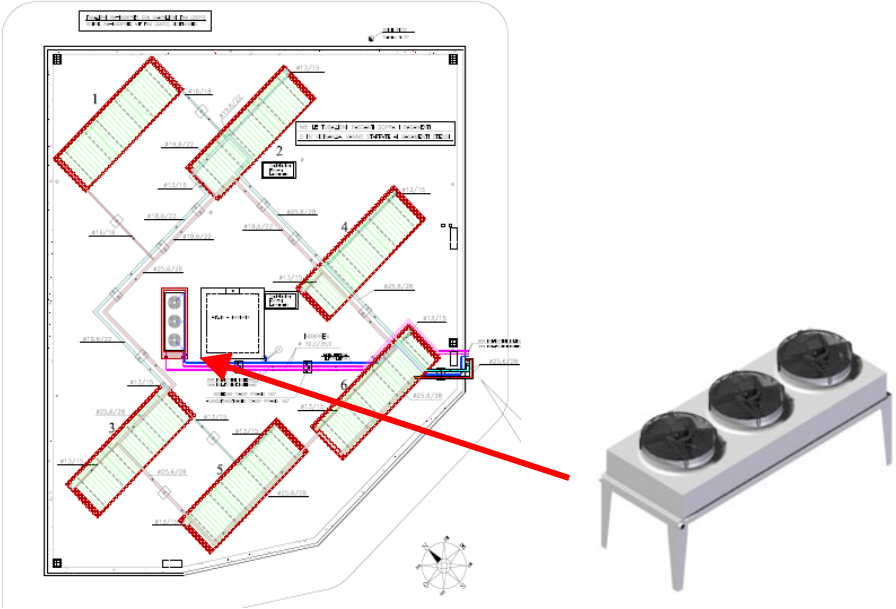

Fig. 3.18 Picture of the dry cooler and its position on the roof

Dry Cooler

At the moment in standard library of TRNSYS, a complete and specific dry cooler model is not available. Usually it could be used Type 52b like a cooling coil which models a cross-flow heat exchanger. In this case, a specific type for dry coolers, Type 879, has been modeled by Eurac and set with real operating characteristics.

Type 879 has been modeled by following an iterative procedure where the energy and draft equation must be satisfied simultaneously.

As already specified, for the heat transfer rate in heat exchanger, it is commonly used the Log Mean Temperature Difference (LMTD seen above) method. When only the inlet temperatures are known, instead of a iterative procedure for the definition of LMTD, the *effectiveness*-NTU method is preferable [65]. The NTU value is calculated as follows:

$$NTU = \frac{UA_{drycooler}}{C_{\min}} \qquad \textit{Eq. 3.1}$$

Draft equation for an air-cooled heat exchanger is obtained by matching only the fan performance curve and the flow characteristics through the heat exchanger bundles.

3.3.7. Heat Exchangers

Primary solar circuit and DHW exchangers have been modelled with the Type 5, a zero capacitance sensible heat exchanger, modelled in the counter flow configuration and based on the

effectiveness minimum capacitance approach [65]. The overall heat transfer coefficient UA_{xh} of each heat exchanger, has been derived by design values of temperatures, flow rates and powers. In the following, the relations used for the calculation are highlighted:

$$UA_{hx} = \frac{\dot{Q}_{hx}}{LMTD} \qquad \textit{Eq. 3.2}$$

where:

$$\dot{Q}_{hx} = \dot{m}_w c_{p,w} \left(T_{in} - T_{out}\right) \qquad \textit{Eq. 3.3}$$

The subscripts "h" and "c" are referred to heat or cold side, depending on each heat exchanger considered.

$$LMTD = \frac{\left(T_{h,o} - T_{c,i}\right) - \left(T_{h,i} - T_{c,o}\right)}{\ln \frac{T_{h,o} - T_{c,i}}{T_{h,i} - T_{c,o}}} \qquad \textit{Eq. 3.4}$$

The model calculates the capacitance in both, the cold (load) and the hot (source) side, the minimum capacitance, C_{min}, is individuated and the effectiveness is elaborated in accordance with

$$\varepsilon = \frac{1 - \exp\left(-\frac{UA}{C_{\min}}\left(1 - \frac{C_{\min}}{C_{\max}}\right)\right)}{1 - \left(\frac{C_{\min}}{C_{\max}}\right)\exp\left(-\frac{UA}{C_{\min}}\left(1 - \frac{C_{\min}}{C_{\max}}\right)\right)} \qquad \textit{Eq. 3.5.}$$

$$T_{ho} = T_{hi} - \varepsilon\left(\frac{C_{\min}}{C_h}\right)\left(T_{hi} - T_{ci}\right)$$

The heat exchanger outlet conditions are so computed using Eq. 3.6 and $Q_{tot} = \varepsilon \cdot C_{\min} \cdot \left(T_{hi} - T_{ci}\right)$ Eq. 3.7.

$$\varepsilon = \frac{1 - \exp\left(-\frac{UA}{C_{\min}}\left(1 - \frac{C_{\min}}{C_{\max}}\right)\right)}{1 - \left(\frac{C_{\min}}{C_{\max}}\right)\exp\left(-\frac{UA}{C_{\min}}\left(1 - \frac{C_{\min}}{C_{\max}}\right)\right)} \qquad \textit{Eq. 3.5}$$

$$T_{ho} = T_{hi} - \varepsilon\left(\frac{C_{\min}}{C_h}\right)\left(T_{hi} - T_{ci}\right) \qquad \textit{Eq. 3.6}$$

$$Q_{tot} = \varepsilon \cdot C_{\min} \cdot \left(T_{hi} - T_{ci}\right) \qquad \textit{Eq. 3.7}$$

3.4. Control strategy

The complexity of the plant and the different uses of the solar energy (DHW production, space heating and cooling), have required a strategy control systems for the managing of all components.

The control has been based on three main steps:

1 temperatures and mass flows are read by the Enegy Box (see also Par. 3.5) which verifies some conditions, called "Hysteresis";
2 the combination of more than one hysteresis individuates a "Scheme" which represents an operating condition;
3 each component (pumps, valves, dry cooler, sorption chiller) receives a control signal which determinates the functioning of the device.

At the same time, more than one scheme which acts in different circuits, may work. In fact, the solar circuit runs independently of the distribution system, while heat rejection system can work with both circuits (solar and distribution). The production of DHW represents the priority of the system, so during the charging of the storage, no other schemes run; exception is made for the dissipation of the surplus heat.

3.4.1. Hysteresis

In solar energy system control, the use of the differential temperature controller (DTC) is common. This is simply a fixed temperature difference (ΔT) thermostat with hysteresis. The differential temperature controller is a comparing controller with at two temperature sensors that control one or more devices.

The differential temperature controller monitors the temperature difference between two points. When the temperature difference exceeds a certain fixed value, the control system gives a signal "1". When the temperature difference drops under the lower extreme of the range, the signal becomes "0". The optimum differential on set point is difficult to calculate, because of the changing variables and conditions.

Initially, values from literature or best practice have been set, then a optimization of these parameters has been carried out.

The list of hysteresis defined in the control is presented in Table 3.3.

Table 3.3 List of hysteresis used in the control

HYSTERESIS

Summer / winter season		A	NOT(A)	Storage charging		H	NOT(H)
				(T2-T28)	>ΔH_up	1	0
2880<time<6550		1	0	(T2-T28)	<ΔH_low	0	1
Enough solar radiation		B	NOT(B)	Direct heating starting		I	NOT(I)
(R1-R1_B)	>ΔR1_B	1	X	(T2-T48)	>ΔI_up	1	X
(R1-R1_B)	<0	0	X	(T2-T48)	<ΔI_low	0	X
Stagnation		C	NOT(C)	Cooling starting		M	NOT(M)
(T2-T2_C)	>ΔT2_C	x	0	(T18-T18_M)	>ΔT18_M	1	0
(T2-T2_C)	<0	x	1	(T18-T18_M)	<0	0	1
Generator charging		T	NOT(T)	Geothermal probes starting		N	NOT(N)
(T2-T2_T)	>ΔT2_T	1	0	(T15-T31)	>ΔN_up	1	0
(T2-T2_T)	<0	0	1	(T15-T31)	<DN_low	0	1
Heating Demand		D	NOT(D)	Dry cooler starting		O	NOT(O)
(Tamb-Tamb_D)	>Δtamb_D	x	0	(T14-T14_O)	>ΔT14_O	1	0
(Tamb-Tamb_D)	<0	x	1	(T14-T14_O)	<0	0	1
Cooling Demand		E	NOT(E)	Heat Rejection starting		U	NOT(U)
(Tamb-Tamb_E)	>ΔTamb_E	1	X	(T15-T15_U)	>ΔT15_U	1	0
(Tamb-Tamb_E)	<0	0	X	(T15-T15_U)	<0	0	1
DHW Demand Winter		F	NOT(F)	DHW tempering		P	NOT(P)
(T27-T27_F)	>ΔT27_G	1	0	(T46-T46_P)	>ΔT46_P	1	X
(T27-T27_F)	<0	0	1	(T46-T46_P)	<0	0	X
DHW Demand Summer		G	NOT(G)	DHW return circuit		R	NOT(R)
(T27-T27_G)	>ΔT27_G	1	x	(T43-T43_R)	>ΔT43_R	1	x
(T27-T27_G)	<0	0	x	(T43-T43_R)	<0	0	x

The first column of Table 3.3 represents the difference temperature between measure and set point or between two measurements. In the second column there are the upper and lower values of the hysteresis' width. The third and fourth columns represents the equivalent signal.

Sensors labels are reported in Fig. 3.19. Within the red dashed line, the components included in the Energy Box are reported. The red labels indicates the sensors used in the control.

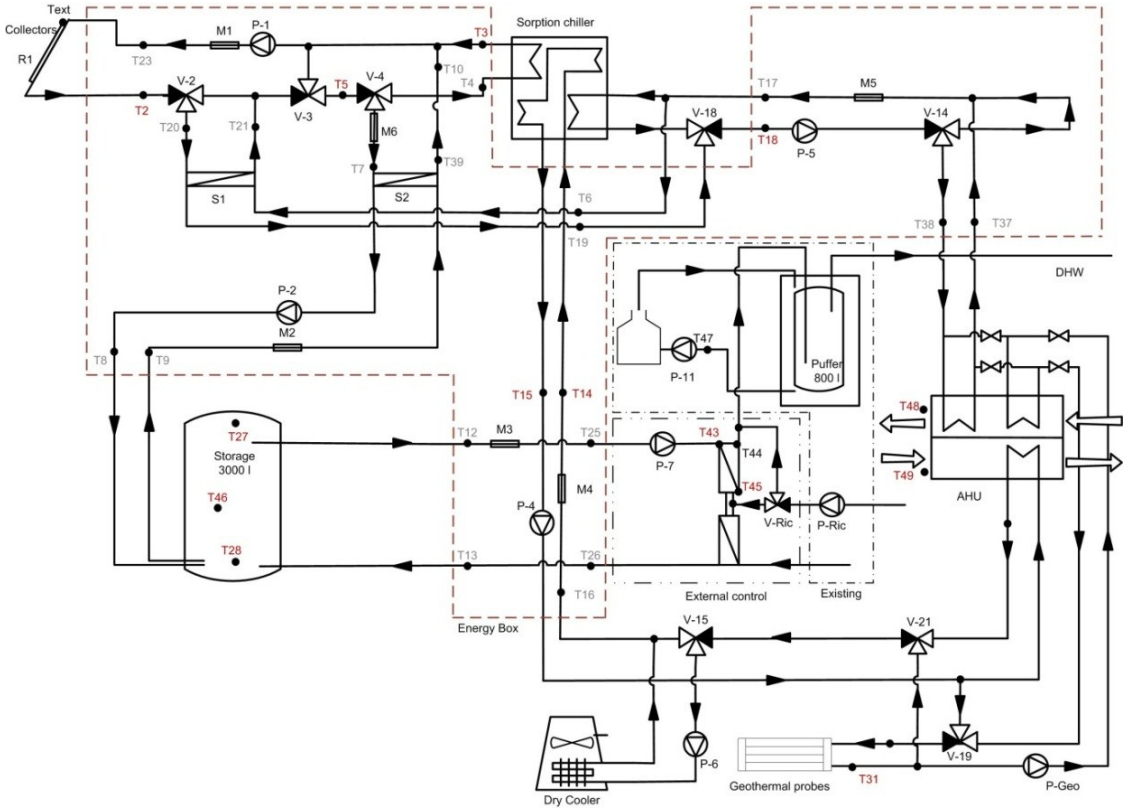

Fig. 3.19 Layout of supply energy plant

3.4.2. Operating modes

Sc 1 – Starting of the primary circuit

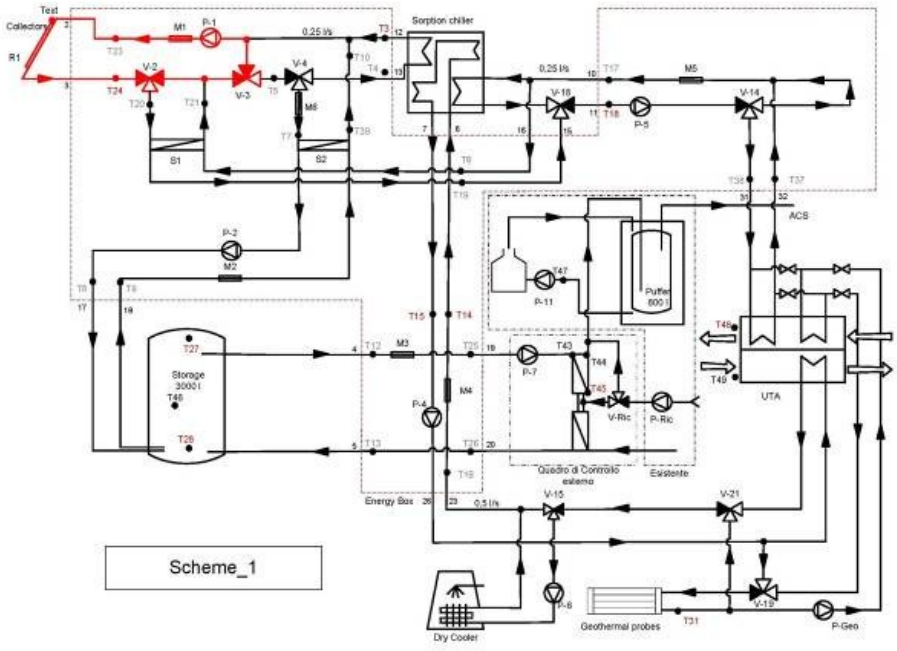

Fig. 3.20 Sc1 – Starting of the primary circuit

Sc 1 represents the starting of the solar system (Fig. 3.20). It occurs when a minimum value of solar radiation is achieved and a minimum thermal power is assured (about 3 kW). This scheme determines the switching on of the pump P1 whose speed is proportional to the solar radiation. When a minimum solar radiation of 150 W/m^2 is read through the weather station, the pump runs with the 40% of the total speed; the maximum speed is achieved with a solar radiation of 700 W/m^2 (Mod_1). With 40 m^2 of evacuated solar collectors, considering an efficiency near 50%, a minimum thermal power may be achieved with a radiation of 150 W/m^2 (40 [m^2] *0.5*150 [W/m^2]= 3kW). The pump P1 is stopped whenever the temperature of the fluid inside the circuit is higher than 110°C, in order to avoid damage of the component at high temperatures. This scheme is activated both in summer and in winter.

Sc 2 - Charging of the storage tank

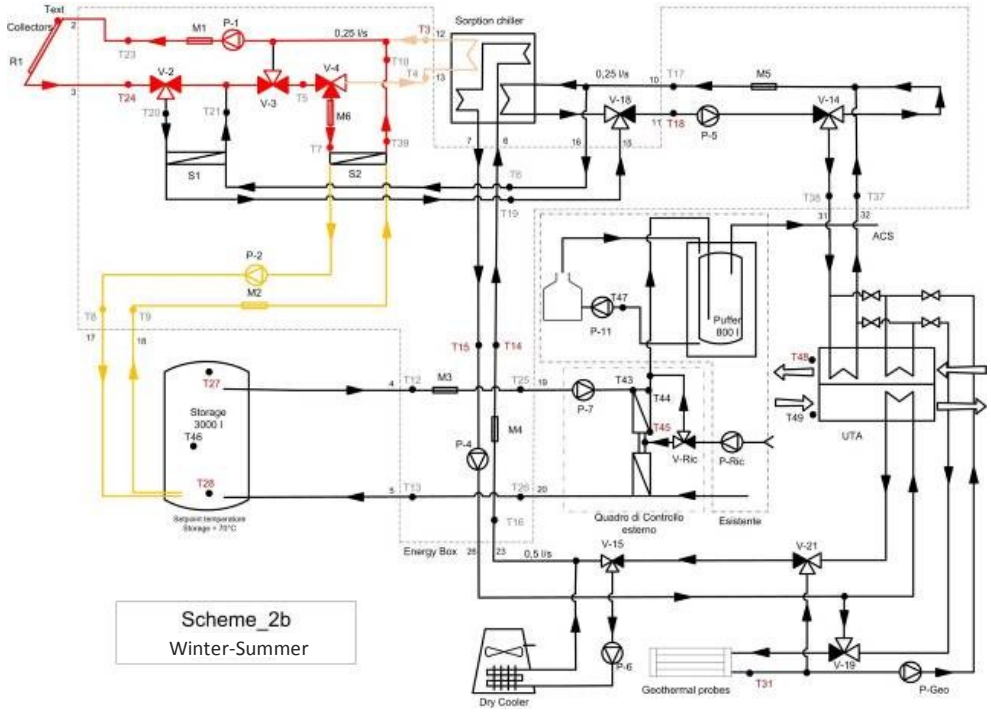

Fig. 3.21 Sc 2 – Charging of the storage tank

Sc 2 indicates that conditions for charging the stratified storage up to a set point temperature (different for winter and summer) (Fig. 3.21).

Scheme 2 starts when there is a minimum thermal power in the primary circuit; the temperature out of the solar collectors (T2) is higher than the temperature in the bottom of the storage (T28) (hysteresis H); the storage has not reached its set temperature (T27) (hysteresis F for winter and G for summer) and the temperature in the primary circuit is less than 110°C (T2_C).

The flow rate of the pump P2 (P2n) is equal to P1's (P1n); both flow rates therefore depend on the radiation. Valves V-2 and V-3 are in direct way, whereas V-4 is oriented toward the heat exchanger S2.

When the storage is charged or there is no availability of thermal energy from the sun and neither there is demand of heat from the tank, a security condition is used on valve V-4 in order to avoid stagnation problem. Valve V4 is modulated is partially opened through the chiller (Mod_6).

Sc 3 - Direct Heating

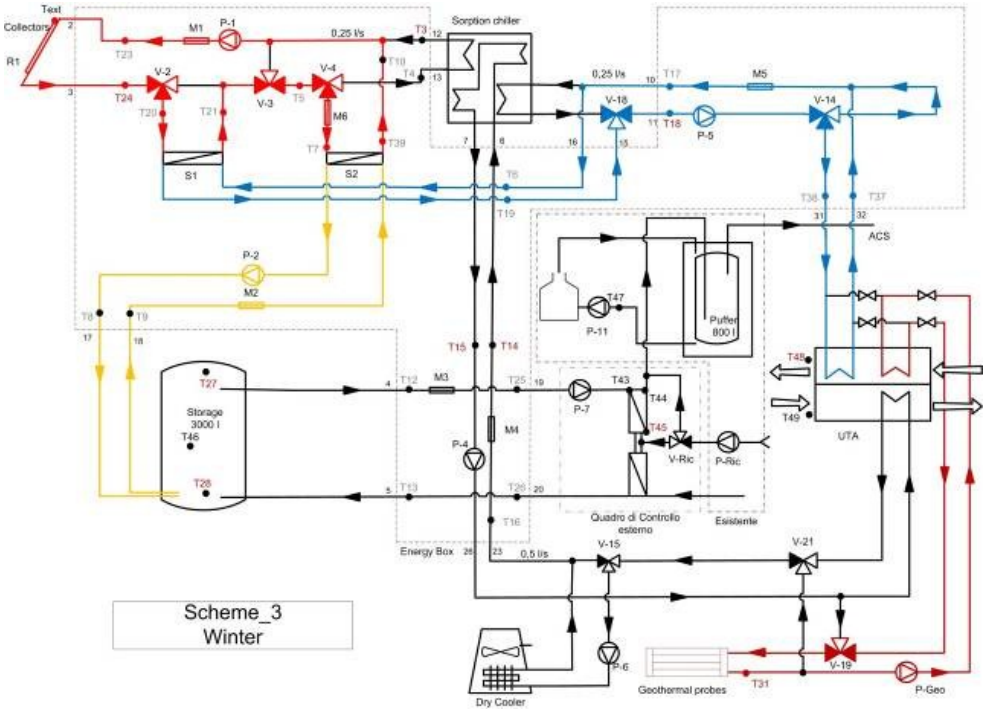

Fig. 3.22 Sc 3 – Direct heating

Sc 3 is activated only during the winter and concerns the direct heating from solar collectors to the user (Fig. 3.22).

This scheme is active when there is a minimum thermal power in the primary circuit (B), there is heating demand from the apartments (NOT(D)), the storage is already charged (F), that is, the temperature on the top of the tank (T27) is in a range around the set temperature and T2 is higher than the inlet temperature of the air in the building (T48) (hysteresis I).

From the collectors, water flows into the coil beyond the AHU and warm up the external air. If the temperature of the water in T5 is higher than T28 (Mod_5), the pump P2 is switched on and the surplus heat is delivered to the storage; if not the pump P2 is off and there will not be heat exchange.

Also in this case, the flow rate of the pump P1 is regulated through the radiation; whereas the valve V-2 is oriented toward the heat exchanger S1, the valve V-3 toward the valve V-4 and the latter to S2. Under the modulation Mod_5, the speed of P2 is equal to P1. The valve V-18 is positioned in order to receive the fluid coming from the heat exchanger S1 and to send it to the valve V-14; the positioning of valve V-14 is regulated by a PID in order to reach a set temperature of the air coming out from apartments around 21°C.

Sc 4 – Chiller charge

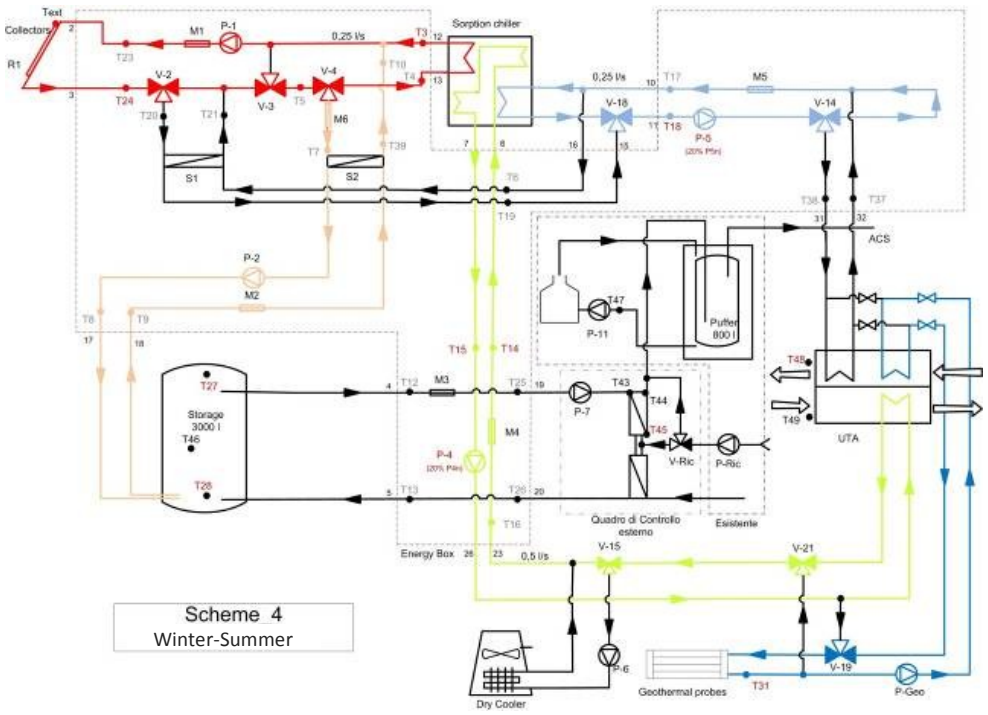

Fig. 3.23 Sc4 – Charge chiller

Sc 4 is used for charging the sorption chiller and it works both in winter and in summer (Fig. 3.23).

In Sc 4, a radiation for a minimum thermal power in the primary circuit (B) is reached and the temperature in the circuit is less than 110°C (NOT(C)); the temperature on the top of the storage (T27) has reached the set value (F) or T2 is less than the temperature on the bottom of the storage (T28) (hysteresis NOT(H)); T2 is higher than the temperature inside the generator (T3) (L) and, in any case, is higher than 75°C in summer (T) and 50°C in winter (V).

In these conditions, P1 is switched on and P4 and P5 go with 40% of the speed; valves V-2, V-3 and V-4 are in direct way, oriented toward the sorption chiller.

In Sc 4, the distribution circuit works in a closed loop up to the chiller is ready to deliver chilled or warm water. For this reason, V-14 is oriented in direct way closing the flux toward the building.

When temperature at generator circuit increases above 105°C, a security condition is utilized to prevent the stagnation (Mod_7); valve V-4 is modulated in order to deliver part of the heat to the storage. In this case the pump P2 is switched on and the speed is regulated according to P1's speed and V4 modulation.

Sc 5 – Chilling start

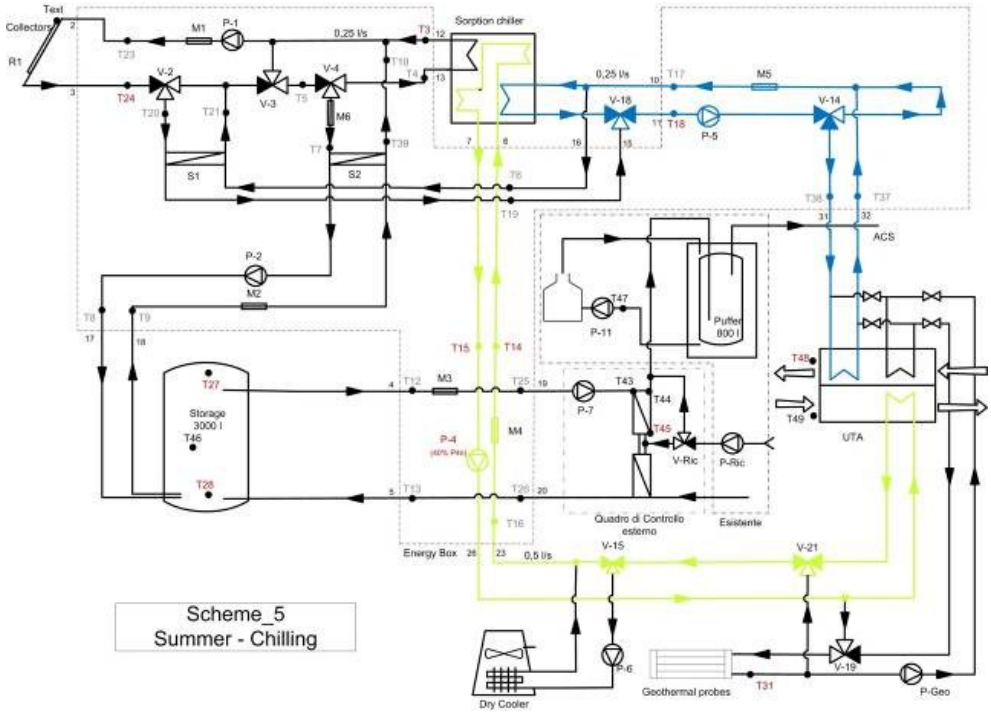

Fig. 3.24 Sc 5 – Start chilling

Sc5 is active when the sorption chiller is charged and there is heating (hysteresis NOT(D)) or cooling (hysteresis E) demand. During the summer, the machine works as a chiller when the fluid in the distribution circuit is cold (T18<11°C) (hysteresis NOT(M)); during the winter, it works as a heat pump when the fluid is warm (hysteresis Y).

In both cases, the pump P5 is switched on to the maximum speed; the valve V-18 is in direct way toward the pump P5 and the valve V-14 is regulated by a PID in order to guarantee a set temperature of the air coming out from the AHU of 21°C in winter and 26°C in summer (Fig. 3.24).

During the summer, the dissipation circuit is also active and P4 works with a speed equal to 40%; in this way the heat extracted from the building is rejected using one of the heat rejection modes. Depending on the inlet temperature to the sorption chiller (hysteresis O) and the cooling power of geothermal probes (hysteresis N), the dissipation can be made with waste air, geothermal probes or dry cooler.

Sc 6 – Heat Rejection through waste air

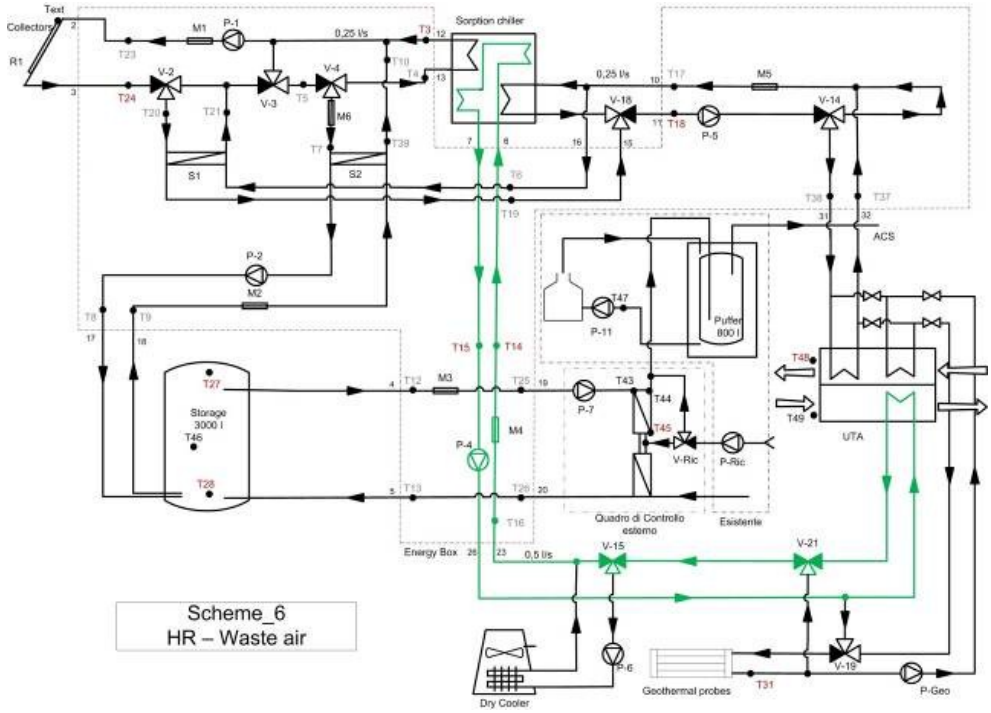

Fig. 3.25 Sc 6 – Heat rejection by waste air

Sc 6 is on when solar circuit or distribution circuit are active. In these schemes, pump P4 is on with 40% of its speed in order to guarantee a flux in the circuit and allow measuring the water temperature.

When the outlet temperature from the chiller (T15) is higher than 35°C (hysteresis U); the temperature difference between T15 and T31 is lower than 5°C (hysteresis NOT(N)), so the dissipation by the geothermal probes is not allowed; T14 is lower than 35°C and the dissipation by waste air is enough to dissipate the surplus heat (hysteresis NOT(O)), Sc 6 is active and the pump P4 is regulated by a PID with a set point of T14 equal to 27°C. The heat rejection mode used in Sc 6 exploits the heat transfer between the cool water from the chiller and the waste air from the building, whose temperature is supposed to be around 26°C (Fig. 3.25).

In Sc 6, valves V-15, V-19 and V-21 are in direct way oriented towards the AHU.

Sc 7 – Heat Rejection through geothermal probes

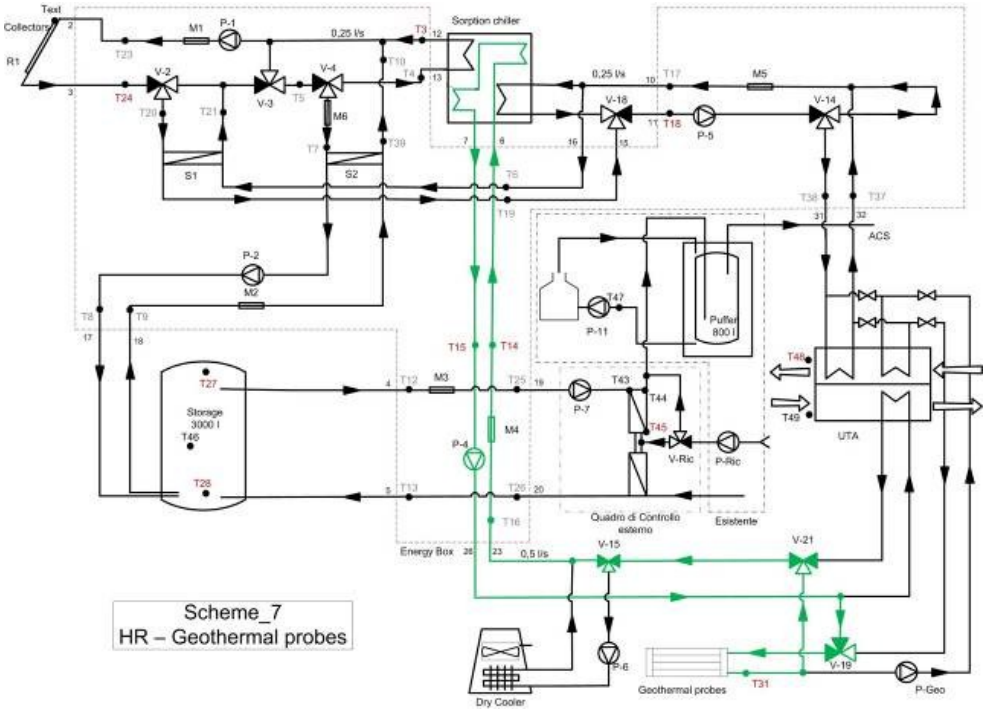

Fig. 3.26 Sc7 – Heat rejection by geothermal probes

In Sc 7, the dissipation circuit exchanges heat with the ground thanks to geothermal probes.

Sc7 works when T15 is higher than 35°C (hysteresis U), so there is surplus heat to dissipate in the circuit; the temperature difference between T15 and T31 is higher than 5°C and the dissipation by geothermal probes is allowed (hysteresis N); T14 is lower than 35°C (hysteresis NOT(O)) so geothermal probes are enough for dissipating the surplus heat.

In Sc7, the pump P4 is regulated by a PID with a set point of T14 up to 27°C; the valve V-15 is in direct way toward the valve V-21 and the valves V-21 and V-19 are oriented toward geothermal probes (Fig. 3.26).

The advantage of this mode is to exploit the lower temperature of the ground and its high thermal capacity.

Scheme 8 – Heat Rejection through geothermal probes + dry cooler

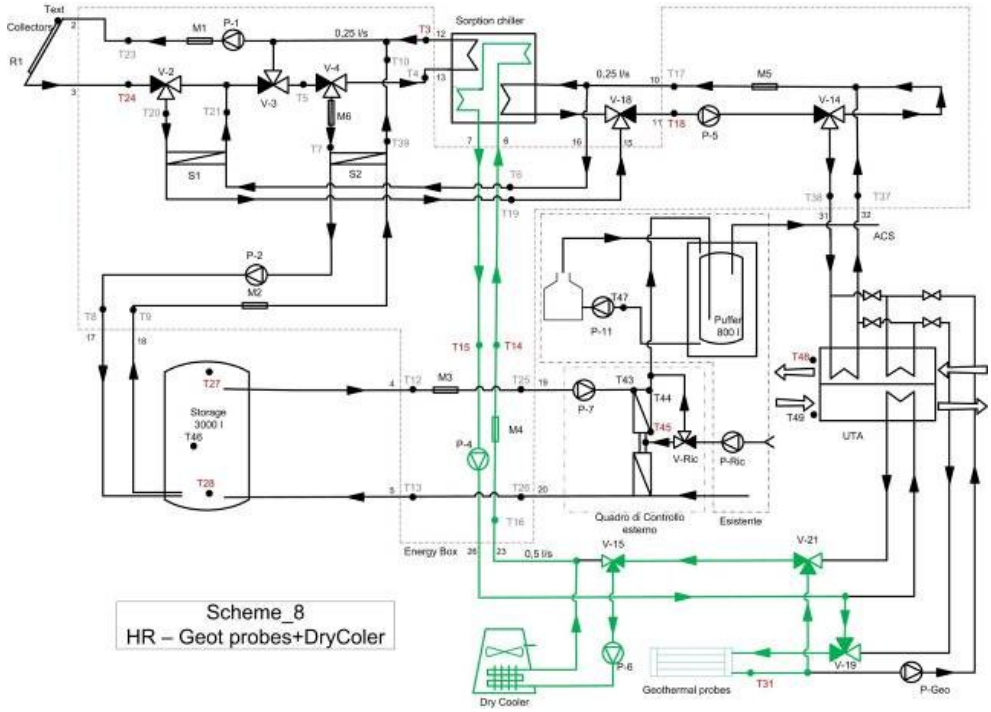

Fig. 3.27 Sc 8 – Heat rejection by geothermal probes + dry cooler

Sc 8 is activated when the surplus heat (hysteresis U) exceeds the capacity of geothermal probes (hysteresis N), so the temperature of the fluid returning from them (T14) is higher than 35°C (hysteresis O). In this case the dissipation circuit uses both geothermal probes and dry cooler in series (Fig. 3.27).

In Sc 8, the speed of pump P4 is regulated by a PID which reaches a set value of T14 up to 27°C; the fluid flows towards the geothermal probes and then goes to the dry cooler to dissipate the exceeding heat. Valves V-21 and V-19 are oriented toward the geothermal probes; the valve V-15 is oriented toward the dry cooler and the pump P6 is switched on. Pump P6 speed is regulated by a PID in order to obtain a set value of T14 up to 30°C.

Scheme 9 – Heat Rejection by dry cooler

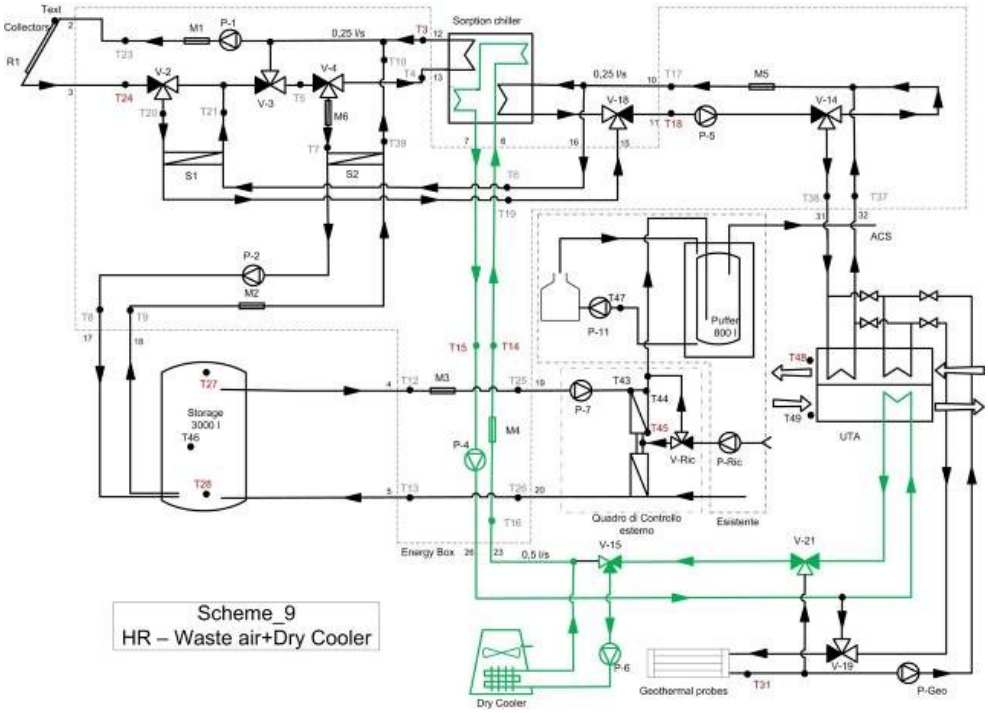

Fig. 3.28 Sc 9 – Heat rejection with dry cooler

Sc 9 is activated when previous schemes are not able to dissipate the waste heat of the system (hysteresis U). This means that the temperature of the fluid entering into the chiller is higher than 35°C (hysteresis O) and the temperature difference between T15 and T31 is lower than 5°C (hysteresis NOT(N)); this means that geothermal probes are saturated.

In this scheme, the pump P4 works with a PID control which reaches a set temperature of T14 up to 27°C; the valve V21 is positioned in direct way toward the AHU; the valve V15 is positioned toward the dry cooler; the pump P6 is switched on and is regulated by a PID which reaches a set value of T14 up to 30°C.

In Sc 9, the surplus heat is rejected by using in series the coil of the exhaust air and the dry cooler. At first, the fluid crosses the coil to exchange heat with the exhaust air coming from the building, which temperature is around 26°C. Then the fluid is cooled crossing the dry cooler. The fans speed depends on the quantity of heat to be dissipated. Higher speeds mean higher electricity consumption. In case of high T15, the dry cooler cools down the fluid temperature up to 3°C above the outside air.

3.5. Monitoring and control unit

Many components took place into the Energy Box: valves, pumps, heat exchangers, sensors. The EB is essentially divided in three main parts: the hydraulic circuit, the electrical circuit and the electronic circuit.

The main purpose of the Energy Box's development has been to achieve a flexible device that could be fitted into different and generic SHC applications and could be able to manage its thermo-vector fluids and energy. For this reason, the system is developed as an unique device, capable of managing thermal energy coming from different kinds of solar field toward various users (chiller, DHW, AHU) and auxiliaries (Storage, Dissipation) (Fig. 3.29).

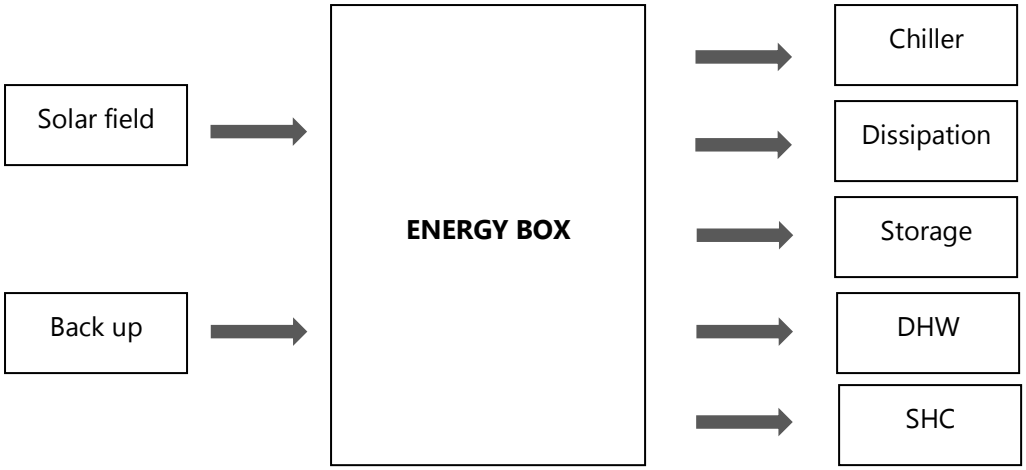

Fig. 3.29 The Energy Box concept

The three components have been conceptually grouped together, but they have been collocated in different cases, all positioned on the basement. The Energy Box is able to monitor the defined parameters, save data and make the collected data available via web.

The functioning of the monitoring system is schematized in Fig. 3.30. Measured data coming from all meters (temperature sensors, flow meters, energy meters) have been collected by the Energy Box and by the existing monitoring system. Using an Ethernet connection, these data have been sent to a switch and then to a umts modem. After that, data have been download via internet and saved in a server. Monitored data have been so elaborated and used for the system calibration and optimization.

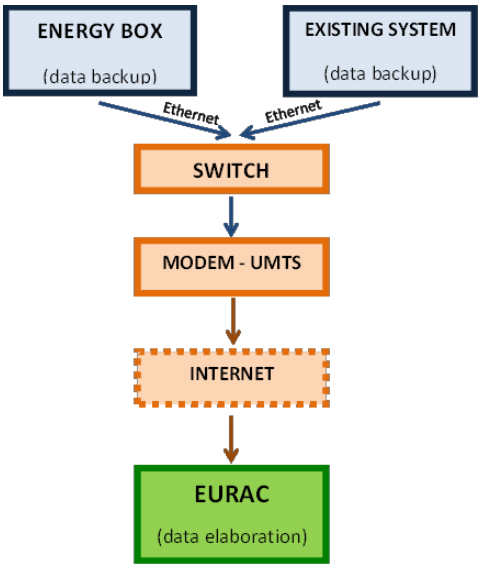

Fig. 3.30 Bronzolo's monitoring system

Monitoring and control systems have been managed by Labview [69]. A graphical interface reproduces the same layout already explained in Par. 3.2 where all data from weather station, temperature and flow rate sensors are plotted in real time on screen (Fig. 3.31).

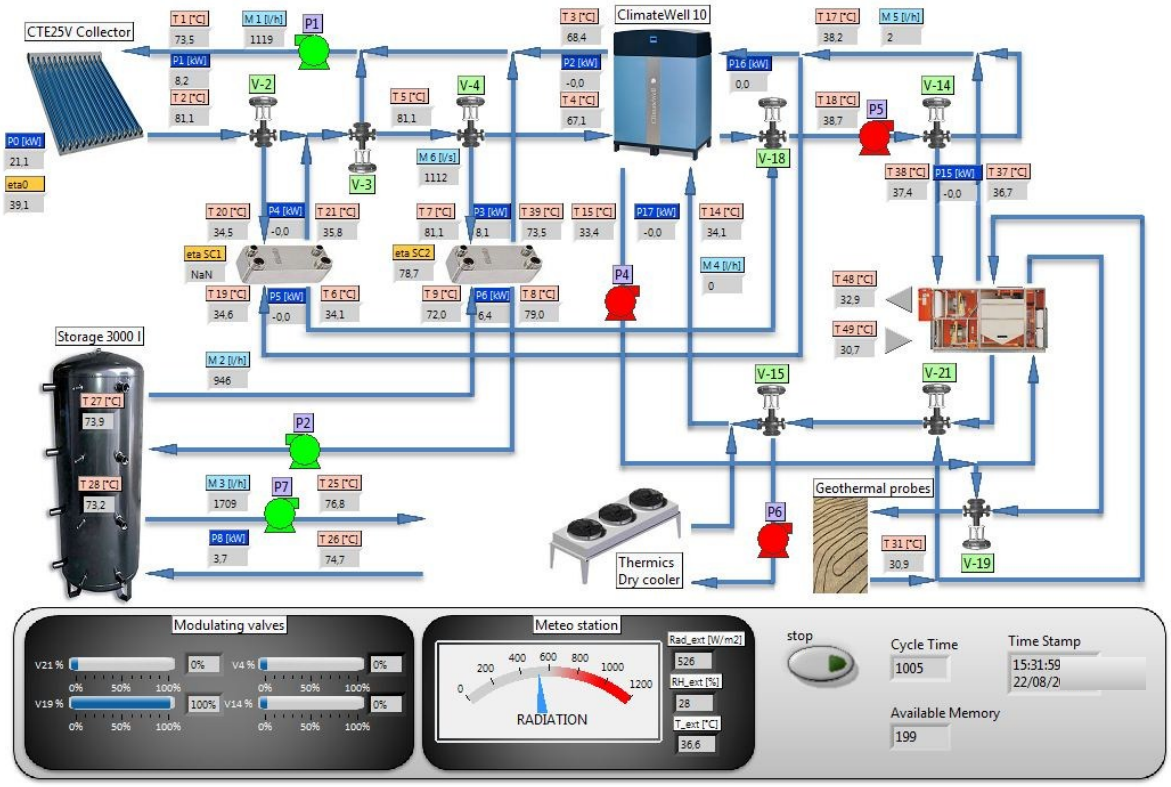

Fig. 3.31 Graphical interface of the monitoring software

3.6. Model optimization

3.6.1. Component validation

Comparing simulated and monitored system' performance, common limitations of standard Trnsys models have been underlined: thermal inertia of the components itself (collectors, pipes, chillers, etc.) is usually not taken into account by the models. External validation is so required and it is an integral part of the process of simulation model development. Many methods for external validation of continuous system simulation models have been proposed; the approach selected in any given application is highly dependent upon the purpose of the model and the associated accuracy requirements. An iterative validation method has been here applied for the validating of the system components [70]. This method is applicable for generic validation energy system when monitoring data and simulation outputs are available. It is an extension of usual V&V methods [72], obtained by integrating new techniques for a more effective and consistent validation result (see Fig. 3.32).

As first step, all the necessary information of the monitoring system set-up (e.g. temperature sensor, flow-meter position, acquisition time step) have been gathered. This phase, defined as "Numerical Model Definition" (see Fig. 3.32), is essential for defining the outputs and the requirements that the numerical model has to fulfill.
When a large amount of raw monitoring data are collected, it is important to manage them properly from statistical/mathematical point of view. Bin Method Analysis (BMA) [73] has been used as the main technique for data reduction. This technique consists in time-averaging instantaneous monitoring data, with the aim of reducing the influence of unsteady conditions and deriving a clear understanding of the system component behavior. For the application here investigated, a period of 5 minutes has been considered to be sufficient. The so-arranged data can be further averaged in bins and typical component performance curves (e.g. efficiency curve, heat transfer coefficient, …) can be derived. This analysis can be carried out on raw or post-processed monitoring data, according to the case or the needs.

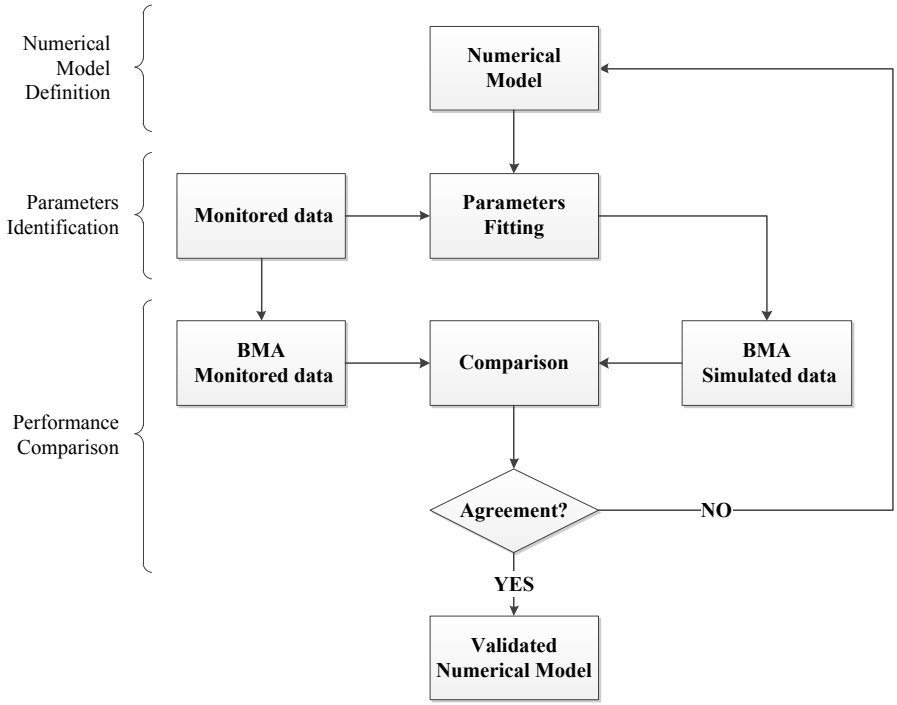

Fig. 3.32 Iterative validation procedure [71]

In order to test the adherence of simulations to reality, a phase of "Parameter Identification" (PI) (see Fig. 3.32) follows, where monitoring data (temperatures and mass flow rates) are used as boundary conditions to the simulation models, while simulated and monitored outlets quantities are compared. During the PI, minor component parameters have been varied within realistic bounds, in order to minimize the objective function. The historical data period on which carrying out the PI should represent typical working conditions of the system component [74].

For the present work, a specific objective function, OBJ, has been developed ($OBJ = 1 - PCC + TIC$ *Eq. 3.8*). It is a combination of two correlation coefficients based on the simulated (x) and monitored (y) heat transfer power: the first is known as Pearson product-moment Correlation Coefficient (PCC) [74] (

$$PCC = \frac{n\left(\sum_{i=1}^{n} xy\right) - \left(\sum_{i=1}^{n} x\right)\left(\sum_{i=1}^{n} y\right)}{\sqrt{n\left(\sum_{i=1}^{n} x^2\right) - \left(\sum_{i=1}^{n} x\right)^2}\sqrt{n\left(\sum_{i=1}^{n} y^2\right) - \left(\sum_{i=1}^{n} y\right)^2}} \qquad \textit{Eq. 3.9}$$

and the second is known as Theil Inequality Coefficient (TIC) [72][75][76] (

$$TIC = \frac{\sqrt{\sum_{i=1}^{n} (x - y)^2}}{\sqrt{\sum_{i=1}^{n} x^2} + \sqrt{\sum_{i=1}^{n} y^2}} \qquad \textit{Eq. 3.10}$$

).

The objective function OBJ is defined in a way that the optimum value has to tend to 0, when PCC and TIC tend to 1 and 0 respectively.

$$OBJ = 1 - PCC + TIC \qquad \textit{Eq. 3.8}$$

$$\mathrm{PCC} = \frac{\mathrm{n}\left(\sum_{i=1}^{n} \mathrm{xy}\right) - \left(\sum_{i=1}^{n} \mathrm{x}\right)\left(\sum_{i=1}^{n} \mathrm{y}\right)}{\sqrt{\mathrm{n}\left(\sum_{i=1}^{n} \mathrm{x}^2\right) - \left(\sum_{i=1}^{n} \mathrm{x}\right)^2}\sqrt{\mathrm{n}\left(\sum_{i=1}^{n} \mathrm{y}^2\right) - \left(\sum_{i=1}^{n} \mathrm{y}\right)^2}} \qquad \textit{Eq. 3.9}$$

$$\mathrm{TIC} = \frac{\sqrt{\sum_{i=1}^{n} (\mathrm{x} - \mathrm{y})^2}}{\sqrt{\sum_{i=1}^{n} \mathrm{x}^2} + \sqrt{\sum_{i=1}^{n} \mathrm{y}^2}} \qquad \textit{Eq. 3.10}$$

When the PI converges towards the minimum, the maximum agreement has been found. This however, does not say anything on the accuracy of the model. A comparison of the numerical results with the monitoring data, in fact, has to be performed on the basis of quantitative performance figures. To this purpose, a further BMA is made on the simulation outputs. A quantitative comparison among the monitoring and simulated BMA curves is then performed ("Performance Comparison", see Fig. 3.32). If the Root Mean Square Error (RMSE) value of the curves is within the acceptance criterion defined by the user, then the validation is accomplished, otherwise the numerical model has to be revised or upgraded. This process is repeated until an adequate level of agreement is found.

The validation presented above has been applied to all that components in which a performance curve could have been individuated, that is solar collectors, solar heat exchanger, sorption chiller and dry cooler. Following, the procedure applied to solar collectors only is presented.

Monitored data have been collected by temperature sensors and flow meters installed in the EB. The efficiency curve of collectors has been obtained according to the EN 12975:

$$\eta = a_0 - a_1 \cdot \frac{T_{coll,i} - T_{amb}}{I} - a_2 \cdot \left(\frac{T_{coll,i} - T_{amb}}{I}\right)^2 \qquad \textit{Eq. 3.11}$$

As already specified in Par. 3.3.1, the solar field has been modeled in TRNSYS 17 with Type 71. Monitored data (from September 2011 to March 2012) have been elaborated with the BMA to evaluate the real efficiency curve of the collectors' field. The comparison between the rated efficiency curve for the single collector and the monitored performance of the entire field showed a difference around 10% for the operating conditions and up to 30% transient conditions. For this reason, a Parameter Identification procedure has been performed using the optimization tool GenOpt [77] to reduce the gap and the Theil coefficient defined on the basis of the energy collected from the solar field, *Q*.

$$TIC = \frac{\sqrt{\Sigma_i^n \left(Q_{i,sim} - Q_{i,real}\right)^2}}{\sqrt{\Sigma_i^n Q_{i,sim}^2} + \sqrt{\Sigma_i^n Q_{i,sim}^2}} \qquad \textit{Eq. 3.12}$$

The TIC value obtained with this process has been 0.22, lower than the suggested 0.3. For this reason, a good agreement between the real and simulated behavior has been supposed, but the comparison of the monitored efficiency and the optimized collector performance shows again a quite large difference for the solar field performance at transient conditions. Low values of T^*_m correspond to a lower working temperature differences, that typically arises during transient conditions (starting of the system), both in terms of radiation and mass flow. In order to simulate the inertia of the system, a moving average, Type 84, has been used upward the solar collectors type. The moving average approximates the effective thermal capacity of the solar collectors and pipes with sufficient accuracy. Thanks to the parameter fitting procedure, the optimal number of time steps for the moving average has been calculated. The minimum optimal value of 14 time steps (time step duration 1 minute) has been found out. A good agreement between monitored and simulated data is shown in Fig. 3.33. Efficiency curves for monitored and simulated data have been compared and a RMSE between the two curves of around 3% has been observed.

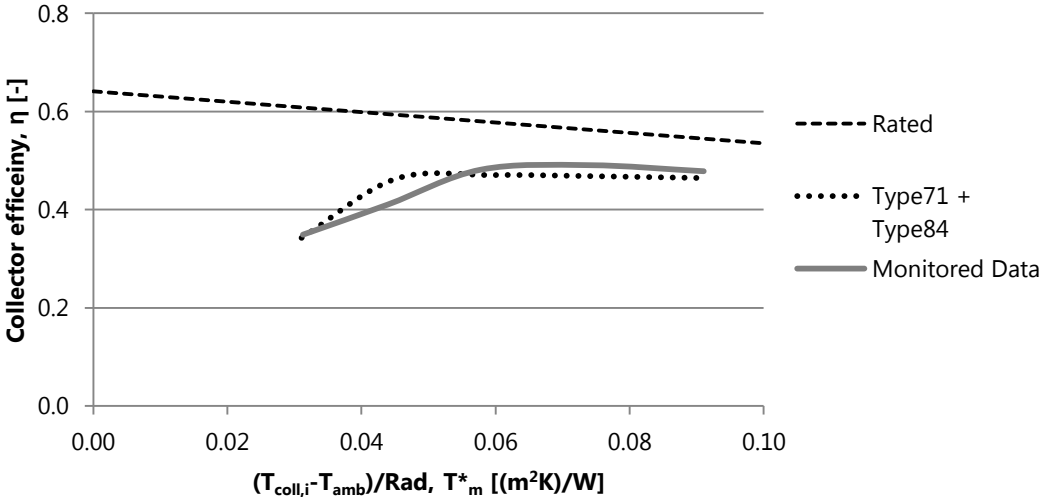

Fig. 3.33 Comparison between monitored and simulated data (using Type 71+Type 84) elaborated with BMA

Same procedure has been applied to the other components in which a performance curve could have been individuated.

From monitoring, losses around 1 kW have been observed in the solar heat exchanger. For this reason the definition of the heat exchanger efficiency has been individuated with the BMA. A pipe (Type 31) has been coupled to the Type 5.

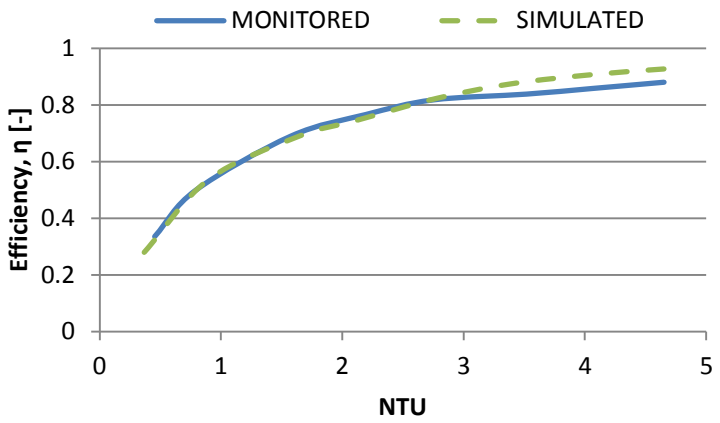

Fig. 3.34 Comparison between monitored and simulated heat exchanger (Type 5 + Type 31) efficiency

Pipes have been used to simulate system losses, so length and losses have been optimized. To this end, pipes have been considered as heat exchangers and the heat loss coefficient has been compared between simulated and monitored values.

Fixing values of 108.75 kJ/(h m² K) and 793.75 kJ/(h m² K) for pipes in solar circuit and in the cold circuit respectively, a good agreement between simulated and monitored values has been individuated Fig. 3.35.

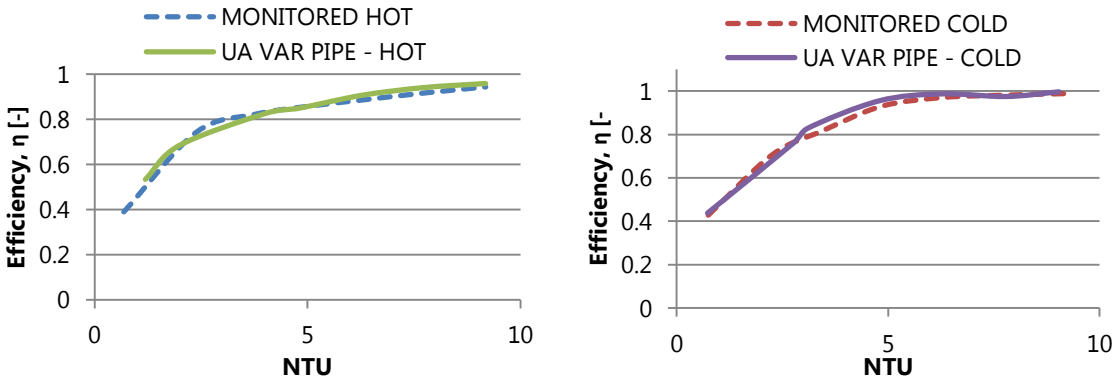

Fig. 3.35 Comparison between monitored and simulated heat losses for the pipes in the solar and cold circuits

The individuation of the heat losses in the sorption chiller type has been made comparing monitored and simulated values of the available power on the hot side of the chiller. Powers for different inlet fluid temperature in the heat rejection circuit are considered Fig. 3.36.

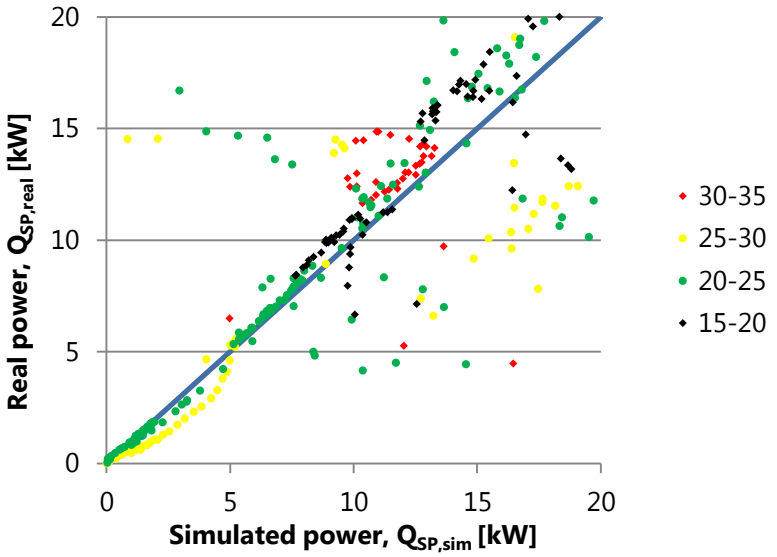

Fig. 3.36 Comparison between simulated and real power on the chiller hot side (solar panel circuit)

For geothermal probes and the storage, no performance curves can be individuated, so only a Parameter Fitting has been applied.

Several parameters are involved in the geothermal probes type as characteristics of probes and soil. Initially data from soil tests before the installation have been used; after the Parameter Fitting, new values for thermal conductivity of the soil, density of the soil, specific heat of the soil, average surface temperature and amplitude of surface temperature have been found out. One year of monitored data has been used for the optimization. Fig. 3.37 shows a screenshot of the scheme used for the Parameter Fitting. Simulated input values are connected to the type and output values are compared to the monitored ones. Inputs and parameters to be optimized are defined as strings, the GenOpt tool minimizes a cost function ($OBJ = 1 - PCC + TIC$ *Eq. 3.8*), and new parameters are found out. Table 3.4 shows the optimized parameters before and after the Parameter fitting.

Table 3.4 Geothermal probes characteristics before and after Parameter Fitting

		Before validation	After validation
Thermal conductivity of the soil	[kJ/(h m K)]	3.55	3.24
Density of the soil	[kg/m^3]	2000	1787.5
Specific heat of the soil	[kJ/(kg K)]	0.80	0.60
Average surface temperature	[°C]	23.0	21.1
Amplitude of surface temperature	[°C]	10	8

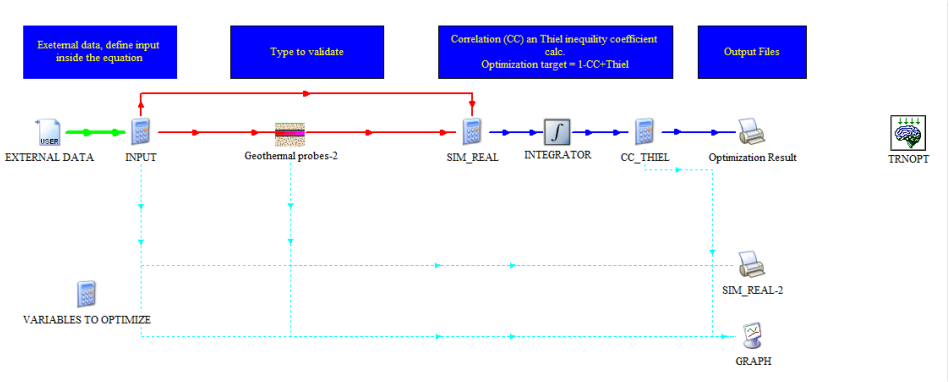

Fig. 3.37 Screenshot of the TRNSYS deck for the Parameter Fitting (geothermal probes example)

In the storage type, heat losses have been optimized comparing output temperatures from simulation and monitoring. Initial values have been defined according to rated values; after the optimization an increase up to 29% of the heat loss capacity rate of the store mantle has been found out.

After the complete V&V procedure, the optimized model has been used within the simulations of the entire supply energy plant model.

Simulations have been run in TRNSYS 17 [64] for a whole year (8760) with a simulation time-step of 1 minute. Monitored data have been used for the weather file and the DHW consumption.

In the not validated model, components' rated values have been used, while values obtained from the validation process have been used in the validated model. In this phase, temperature sets from design or user manual have been used. For the sake of clarity, the system's priority has been individuated in the DHW production, so temperature sets and logic control have been defined in order to cover the DHW demand. The use of sorption chiller is subordinated to the storage charging, so not constant energy supply is available. Moreover, the size of the machine is underestimated with respect to the total building cooling demand. For these reasons, the chiller COP is quite low (around 0.3) and the cooling delivered to the user is consequently unsatisfying.

The comparison of system performance before and after the validation procedure is reported in Fig. 3.38. After the validation, the PER shows a decrease of 3% from no validated to validated system, while The yearly solar collectors efficiency drops from 54% to 46%.

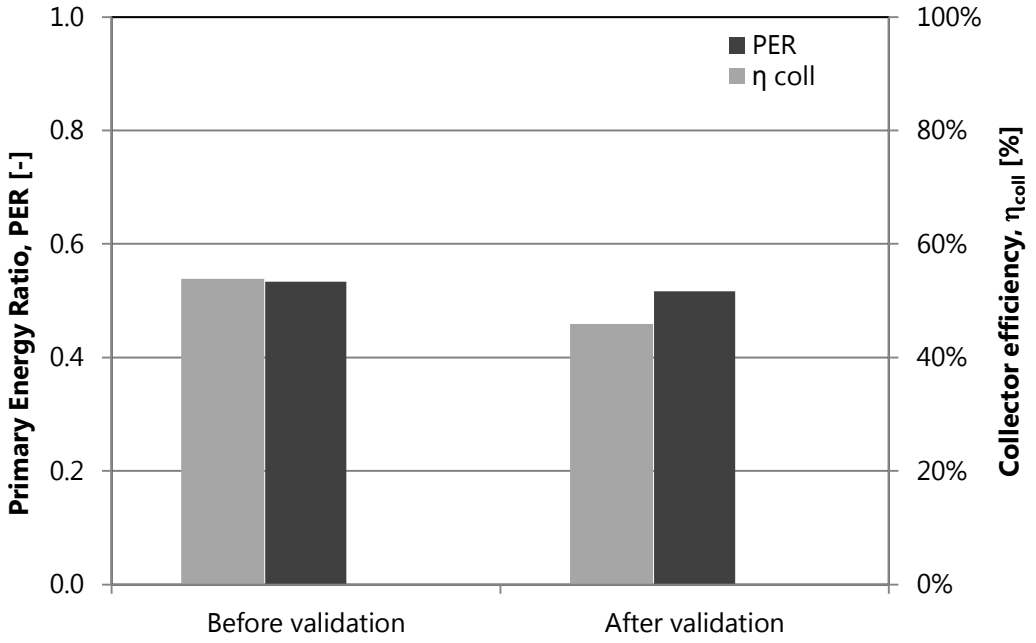

Fig. 3.38 System performance before and after solar collectors model validation

Looking at the heating, cooling and DHW production, a strong decrease of solar fractions in shown. The apparent improvement on the PER is due to the fact that in the validated case a minor cooling production occur, so lower primary energy is also used. In the not validated model, the 8% of the assessed cooling demand is provided by solar system, while in the validated model only the 0.3%, because the chiller works with a lower COP and less solar thermal power is available. The DHW solar fraction, much higher than the heating and cooling ones, has a reduction around 12%.

A reduction of 15% of GSY in the validated case means lower available energy in the system. Moreover the use of pipes for the system losses, the increase of thermal losses in the storage, in the sorption chiller and in the heat exchanger contributes to a reduction of system performance.

Bibliography

[56] Weiss W., Mauthner F. Solar Heat worldwide, markets and contribution to the Energy Supply. Solar Heating and Cooling Programme, International Energy Agency (2012)

[57] Mugnier D., Jacob U. Keeping cool with the sun. International Sustainable Energy Review, Vol. 6, Issue 1 (2012)

[58] Fedrizzi, R., Nienborg, B., Franchini, G. Identification of Standard System Configurations. Solar Combi+ project, v 4.0, Eurac, Bolzano (2010)

[59] Wiemken, E., Nienborg, B., Koch, L. Report on the methodology of the virtual case study. Solar Combi+ project, Fraunhofer Insitut Solare Energiesysteme, Freiburg, Germany (2009)

[60] OSKAR catalog. Ratiotherm, Wärme intelligent genutzt (2010)

[61] Climatewell. Design guidelines for Solar Cooling (2010)

[62] Type 52- Trisolair solvent. Menerga, Air conditioning Technology (2008)

[63] Riello. Istruzioni per l'installatore (2011)

[64] Klein S.A. et al. Trnsys 17. A transient simulation program. Solar Energy Laboratory, Univeristy of Wisconsin, Madison, 2006.

[65] Incropera, F., Dewitt David., Bergman T. & Lavine A. Fundamentals of heat and mass transfer. John Wiley & sons, United States of America (2007)

[66] Drück H. Trnsys Type 340. Multiport Store- Model, version 1.99F. ITW Stuttgart University, Germany (2006)

[67] Conde, M.R. Properties of aqueous solutions of lithium and calcium chlorides: formulations for use in air conditioning equipment design. International Journal of Thermal Sciences, (2004)

[68] Alone project, 7th Framework Programme (FP7). www.aloneproject.eu

[69] LabView, National Instruments ---

[70] Ferruzzi G., D'Antoni M., Fedrizzi R., Dipasquale C. Experimental validation of the numerical model of a solar heating and cooling system within the FP7 project Alone. Ises – Europe Solar Conference, EUROSUN, Rijeka, Croatia (2012)

[71] D'Antoni M., Ferruzzi G., Bettoni D., Fedrizzi R. Validation of the numerical model of a turnkey Solar Combi+ system. International conference on Solar Heating and Cooling for buildings and industry, San Francisco, California (2012)

[72] Murray-Smith D.J. Methods for the external validation of continuous system simulation models: a review. Mathematical and computer modeling of dynamical systems, Vol.4, (1998)

[73] IEC 61400-12-1:2005. Wind turbines – Part 12-1: Power performance measurements of electricity producing wind turbines (2005)

[74] Kleijinen J.P.C. Theory and Methodology. Verification and validation of simulation models. European Journal of Operational Research (1995)

[75] White A.S., Sinclair R. Quantitative validation techniques data base (I). Simple example. Simulation Modeling Practice and Theory (2004)

[76] Theil, H. Economic forecasting and policy. North Holland, Amsterdam, 1970.

[77] GenOpt reference

[78] Morris, M.D. Factorial sampling plans for preliminary computational experiments. Technometrics, Vol.33 (1991)

[79] Nowag J., Boudéhenn F., Le Denn A., Lucas F., Marc O., Raduslescu M., Papillon P. Calculation of performance indicators for solar cooling heating and domestic hot water systems. International conference on Solar Heating and Cooling for buildings and industry, San Francisco, California (2012)

[80] Malenkovic I, Eicher S., Bony J. Definition of main system boundaries and performance figures for reporting on SHP systems- A technical report of Subtask B- Deliverable B1.1. IEA SHC Task 44, HPP Annex 38 (2012)

[81] Campolongo F., Cariboni J., Saltelli A. An effective screening design for sensitivity analysis of large models. Environmental Modeling & Software 22 (2007)

4. Integrated system control

4.1. System model

The analysis of how changes in the input data affect the optimal solution of the problem is often essential for the practical usefulness of optimization models. Improvements on system performances and internal comfort level may be reached with configurations which maximize specific performance factors. The combination of all systems' parameters in a defined range, can require elevate computational effort. For this reason, the selection of parameters which mainly influence the energy consumption and the internal comfort, becomes an important step of the optimization process.

In this chapter, the whole system, building + supply energy plant, has been treated. The model has been developed in the TRNSYS environment [58]. A macro containing the building type (Type 56), external shadings, apartments' coil and an exhaust air mixing valve, has been added to the deck of the supply energy system (Fig. 4.1).

The connection between the two systems is mainly made by the ventilation system. Supply air temperature, relative humidity and flow rate comes from the AHU macro. As in the reality, external air is pre-treated in the AHU, warmed up or cooled in the battery following the heat recovery and blown in the apartments. In the model, the post heating has been considered as "ideal heating" and the internal set-point has been investigated with regard to the heating energy consumption.

The exhaust air coming from all apartments is mixed and the temperature is read beyond the mixing valve. As in the reality, a supply air control specified for each apartment is not allowed.

The sizing of the system has been based has started from the storage volume definition in order to cover the majority of the DHW demand; consequently, the surface of solar collectors to be installed has been calculated according to the rule of thumb of 50 – 75 l/m^2 of storage capacity [83]. Finally the sorption chiller has been added to the layout. As the priority of the system has been defined to be the DHW production, the sorption chiller can work only when the storage is already charged. This fact let the chiller works, but not constantly and usually optimal working conditions are not verified.

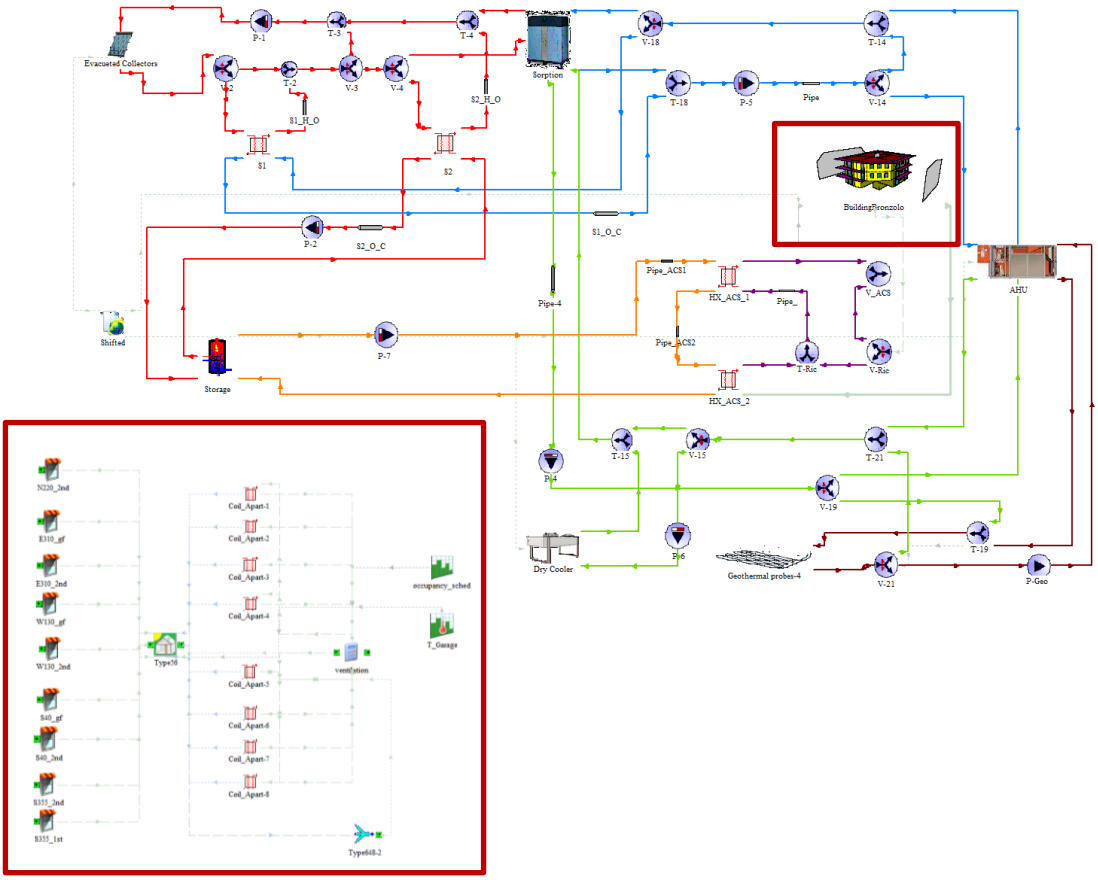

Fig. 4.1 Screenshot of the system modeled with TRNSYS and detail of the building macro

The regulation of supply heating and cooling made by solar system has been held by the V14 valve. The modulation of this valve has been regulated by a PID which follows an optimal temperature. The difficulty in defining this set is related to the fact that apartments have different loads and a unique supply air temperature only can be controlled. Studying the level of internal comfort (PMV) in each apartment with regard to the temperature of the mixed exhaust air (T_{exh}), a linear relation has been found. In particular, a mean PMV value of all apartments around 0 (optimal comfort condition, see also Par. 1.4) corresponds to a value of T_{exh} around 25 °C for summer and 21° for winter[2].

For further simulations, same boundary conditions explained in Par. 2.2.1 have been used, only exception is the ventilation air that is treated as specified above. Simulations have been run with TRNSYS 17 [58] for a whole year plus a period of preconditioning, with a time-step of 5 minutes.

[2] For the PMV calculation, conditions of activity, clothes and air speed have been assumed to be 1.2 met, 1.1 clo for winter and 0.5 clo for summer and 0.1 m/s respectively, as specified in [29] for residential buildings.

4.2. Sensitivity analysis on control system parameters

Several temperature sets and pump modulations play a role in the system management. The influence of each input parameter on the system behaviour is not the same. To individuate the weight of each parameter, a sensitivity analysis has been carried out. The parameters to be compared are many and different in terms of range in which they operate. A sensitivity measure method which fits with this kind of systems (wide and numerous parameters), is the Morris method [85].

The Morris method is a qualitative method and only ranks parameters by its influence on the target function. However, it also allows to determine whether the parameters have (a) negligible, (b) linear and additive, or (c) non-linear or involved in interactions with other parameters. In this case, a global performance indicator [85] and an indicator for the thermal comfort have been used as target functions, the Primary Energy Ratio (PER) [80] and the Predictive Percentage of Dissatisfied (PPD) (see also Par. 1.4).

The Morris method varies one factor (x_i) of the model *y* at time across a certain number of levels (r) selected in the space of the *i* input factors. For each variation, a factor's Elementary Effect (EE) is computed, which is an incremental ratio for that factor:

$$EE_i = \frac{[y(x_i + \Delta_i) - y(x_i)]}{\Delta_i} \qquad \textit{Eq. 4.1}$$

where the Δ represents the increment per step of the factor. Based on this number of elementary effects calculated for each input factor, two sensitivity measures are proposed by Morris: (1) the mean of the elementary effects, μ, which estimates the overall effect of the parameter on a given output; (2) the standard deviation of the effects, σ, which estimates the higher-order characteristics of the parameter (such as curvatures and interactions).

$$\mu_i = \frac{1}{r_i} \sum_{t=1}^{r_i} EE_{i,t} \qquad \textit{Eq. 4.2}$$

$$\sigma_i = \sqrt{\frac{1}{r_i - 1} \sum_{t=1}^{r_i} (EE_{i,t} - \mu_i)^2} \qquad \textit{Eq. 4.3}$$

A high value of μ_i flags a high linear effect for a given factor, while a high value of σ_i flags either nonlinear or non-additive factor behavior. For the computation of the average distribution, the modulus of the $|EE_i|$ has been considered, μ_i^* [81]. The importance of factors influence on the system's performance is assessed plotting factors on the (μi^*, σi) axes. The factors closest to the origin are less influential.
The sensitivity analysis has been applied on the parameters reported in Table 4.1 (see also Par. 3.4.1 for labeling.

Table 4.1 Parameters investigated and range of variation

Parameter	[-]	REF	MIN	MAX	STEP	Parameter	[-]	REF	MIN	MAX	STEP
R1_B	[kJ/hm^2]	360	180	720	180						
Δ R1_B	[kJ/hm^2]	180	180	720	180	T14_O	[°C]	30	30	45	5
T2 _C	[°C]	110	95	110	5	Δ T14_O	[°C]	3	0	10	3
T2_T	[°C]	70	70	85	5	T15_U	[°C]	30	30	45	5
Δ T2_T	[°C]	3	3	21	6	Δ T15_U	[°C]	3	0	10	3
T_{amb}_D	[°C]	15	12	21	3	P1n	[kg/h]	1200	800	2000	400
Δ T_{amb}_D	[°C]	4	1	10	3	P2n	[kg/h]	1200	800	2000	400
T_{amb}_E	[°C]	17	14	23	3	P4n	[kg/h]	1600	800	2000	400
Δ T_{amb}_E	[°C]	4	1	10	3	P5n	[kg/h]	1200	800	2000	400
T27_F	[°C]	55	40	85	15	P6n	[kg/h]	1600	800	2000	400
T27_G	[°C]	55	45	75	10	P7n	[kg/h]	1600	800	2000	400
Δ T27_G	[°C]	15	10	25	5	T_V4_{max}	[°C]	100	100	115	5
ΔH _up	[°C]	3	3	15	4	T_V4_{min}	[°C]	95	90	105	5
ΔH_low	[°C]	0	0	8	3	T46_P	[°C]	100	100	115	5
ΔI_up	[°C]	6	3	12	3	Δ T46_P	[°C]	95	90	105	5
ΔI_low	[°C]	3	0	9	3	T43_R	[°C]	30	30	60	10
T18_M	[°C]	12	8	20	4	Δ T43_R	[°C]	10	5	20	5
Δ T18	[°C]	4	1	10	3	T_{DHW}	[°C]	45	40	55	5
ΔN_up	[°C]	6	3	12	3	$T49_{summ}$	[°C]	25	25	28	1
ΔN_low	[°C]	3	0	9	3	$T49_{wint}$	[°C]	21	19	22	1

A parameter each time has been varied in the range expressed in the Table 4.1. Mean distribution (μ_i*) and standard deviation (σ_i) of EE_i distribution have been calculated for each parameter and for both target functions. Figures Fig. 4.2, and Fig. 4.4 show the distribution of estimated mean and standard deviation of the EEi in the μ*; σ graph.

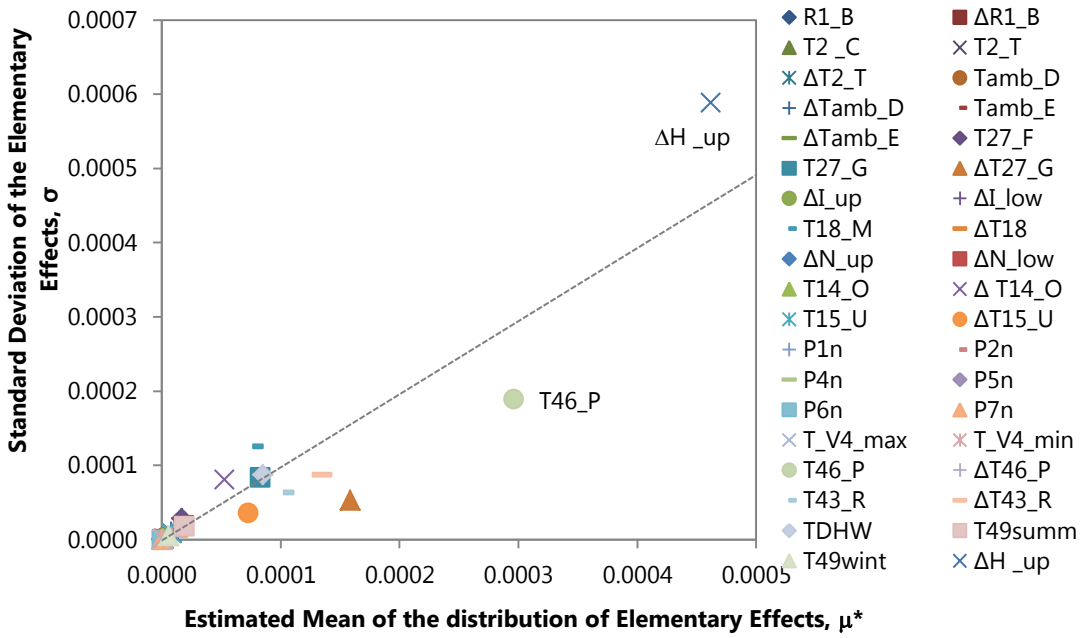

Fig. 4.2 Estimated mean (μ) and standard deviation (σ) for each input factor on Primary Energy Ratio*

The temperature difference between the collectors fluid and the water in the bottom of the storage (ΔH_up) influences not linearly the system more than the other parameters. For a better understanding of which parameters have to be taken into account for the analysis of the system performances, the same graph shown in Fig. 4.2 is further presented, but a focus on the parameters (excepted ΔH_up) is presented Fig. 4.3.

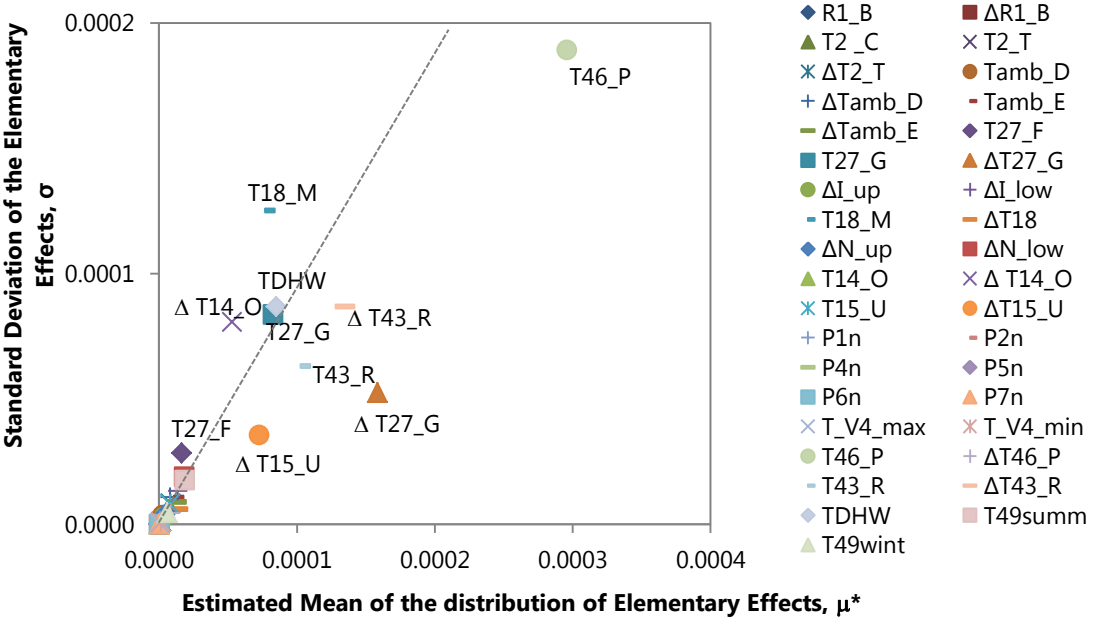

Fig. 4.3 Estimated mean (μ) and standard deviation (σ) for each input factor on Primary Energy Ratio. Focus on the more influenced parameters, except the ΔH_up*

The high influence of ΔH_up is due to the fact that this parameter regulates the charging of the storage when a minimum power is in the solar circuit. This temperature difference defines this power, so the higher the temperature difference, the higher the power in the solar circuit. When the temperature difference is not verified, other circuits can work and the chiller charging or the direct heating is allowed. For this reason, the standard deviation of the EEi related to this parameter is higher than its estimated mean distribution.

Another parameter with a high influence on the PER is the minimum temperature for the DHW production by the solar system. After this, other parameters follow. The parameters with a higher linear influence on the PER are mainly involved in the DHW production; while the ones with higher standard deviation of the EEi are sets referred to the sorption chiller and the dry cooler.

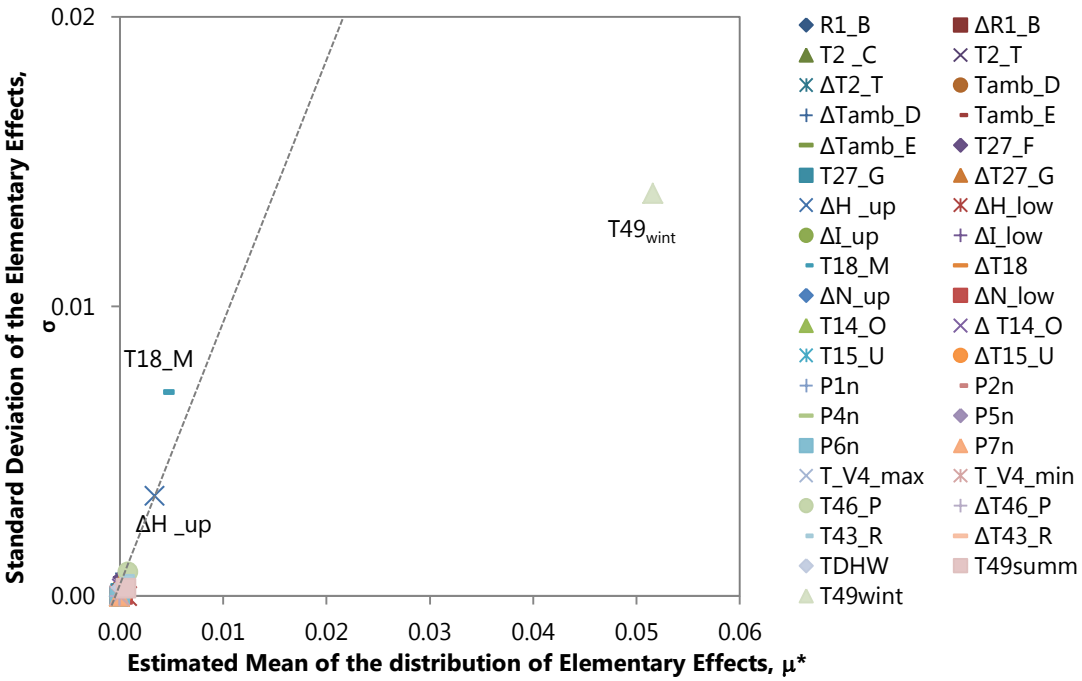

Fig. 4.4 Estimated mean (μ) and standard deviation (σ) for each input factor on PPD*

As expected, Fig. 4.4 shows that the parameter which mainly influences the PPD is the internal set temperature during the winter. The summer set point does not appear because, as already specified above, the cooling system cannot cover the all cooling demand, so usually the $T49_{sum}$ is not achieved. The set of the hysteresis M for the start of the cooling distribution circuit influences the PPD with a not linear effect, because this parameter is related to the state of charging of the chiller and not directly connected to the state of internal comfort. In the system control T18_M has been used as an indicator of the state of charge of the chiller as no output signals from the sorption machine are available. The temperature difference for the start of the storage charging (ΔH_up) influences the PPD value too because this parameter regulates the activation of DHW or cooling and heating production circuits.

4.3. Parametric analysis and best configurations

The selection of some parameters allows a more feasible parameter analysis. For each parameter individuated with the Morris method, two values have been combined and simulations have been run. For each case, performance figures presented in Chapter 1 have been calculated and used as characteristics of the energetic system performances and internal comfort level. In particular, global performance indicators (PER, ΔPE and SPF_{el}) represent the overall system performance and take into account the solar energy use as well as the heating and cooling back-up use; solar performance indicators (GSY, $SF_{cooling}$, $SF_{heating}$ and SF_{DHW}) evaluate the system capacity to use the available solar irradiation; the quality indicator (PPD) evaluates the reliability of the installation and the quality of thermal indoor conditions.

Parameter's range has been established according to reasonable values and taking into account the interaction between the other parameters (Table 4.2). In the parametric analysis, the set T18_M has been neglected because in the control it has been used as an indicator of the state of charge of the chiller.

For the sets not considered in the parametric analysis, rated or design values have been fixed. The set for activating the recirculation circuit (T43_R) and the DHW production by solar energy (T46_P) have been supposed to have the same value.

Parameters here individuated are strictly connected to the layout and operating modes of the system. As already specified, every SHC system has specific features and the control should be established considering the whole system and the interaction between the components.

Table 4.2 Parameters' set for the parametric analysis

Parameter	SET 1	SET 2
ΔH_{up}	7	15
$T49_{wint}$	20	23
ΔT27	15	25
T27_G	55	70
T27_F	30	45
T46_P	40	50
T43_R	40	50
ΔT43_R	5	20
T44	40	60

For each simulation, performance figures described above have been calculated and the best configuration for each performance figures has been taken into account and compared with the others. In Table 4.3, parameters' values of each combination are reported, while in Table 4.4, performance figures' values are shown.

Table 4.3 Best configurations for each considered performance figure

Combination	ΔH_{up}	T49wint	ΔT27	T27_G	T27_F	T46_P	T43_R	ΔT43	T44
	[°C]	[°C]	[°C]	[°C]	[°C]	[°C]	[°C]	[°C]	[°C]
CMB_SF_{heat}	15	23	15	55	45	50	50	5	60
CMB_SF_{DHW}	15	23	25	70	45	40	40	20	60
CMB_SF_{cool}	15	23	25	55	45	40	40	5	60
CMB_SPF_{el}	7	20	15	55	45	40	40	5	40
CMB_PER	15	20	15	70	30	40	40	20	60
CMB_GSY	15	23	15	55	30	50	50	20	60
CMB_ΔPE	15	20	25	70	45	40	40	20	60
CMB_PPD	7	20	15	55	30	50	50	20	40

In SHC systems, the definition of system's priorities plays an important role for the system performance itself. In this case, the storage charging requires large quantity of energy due to the high volume of water. This implies that the activation of space heating and cooling is subordinate to the level of charge of the tank. In this sense, T27_G and T27_F, in accordance to ΔT27, partially determine the priority of the system. The DHW demand is covered by solar energy and auxiliary boiler; the decrease of T43_R and T46_P lead to a higher use of fossil fuel energy, but also a higher available solar energy in the system. Moreover, higher fluid temperature in the hot side of the sorption chiller allows the device to achieve higher performance.

Table 4.4 Performance figures' value for best configurations

Combination	**$SF_{heating}$**	**SF_{DHW}**	**$SF_{cooling}$**	**SPF_{el}**	**PER**	**GSY**	**ΔPE_{tot}**	**PPD**
	[%]	[%]	[%]	[-]	[-]	[kWh/m^2]	[kWh]	[%]
CMB_SF_{heat}	46.1%	7.6%	0.1%	33.2	0.69	761	14751	12.1
CMB_SF_{DHW}	26.8%	58.8%	0.7%	29.7	0.41	742	32928	11.6
CMB_SF_{cool}	26.4%	55.1%	5.9%	29.9	0.45	743	31807	11.5
CMB_SPF_{el}	29.9%	20.7%	0.2%	37.7	0.76	754	17774	11.3
CMB_PER	44.9%	51.0%	0.5%	27.6	0.35	748	31165	11.3
CMB_GSY	45.8%	8.2%	0.0%	32.1	0.67	762	14761	12.0
CMB_ΔPE	26.8%	58.8%	0.7%	29.7	0.41	742	32929	12.0
CMB_PPD	45.5%	5.5%	0.1%	32.3	0.69	760	13642	11.1

Looking at Table 4.1, performance figures values obtained in the best configuration of each performance figure are presented. Depending on the different configurations, smaller variations (less than 10%) occur in the GSY and PPD, while other figures, as the PER and ΔPE, can double. Better PER values are shown for higher SF_{DHW} because no thermal processes occur during the DHW production, but only the gas boiler and electrical pumps consumption are taken into account.

When the maximum value of SPF_{el} is verified, a relevant primary energy saving is shown; this means

that the majority of the useful energy is produced by the gas boiler which consumption is not considered in the SPF_{el}. In this case, a value more than the double of the minimum PER is in fact shown.

Looking at the relation between PER and PPD, good values of PER usually correspond to higher values of PPD (Fig. 4.5). In the best case for PER (CMB_PER), the value of PPD is not so far from its best case. This means that, whilst the winter internal temperature is fixed at 20°C, feasible PPD values may be reached. This result is in contrast with the real case in which higher internal winter temperatures are set and, consequently, higher energy consumption occur.

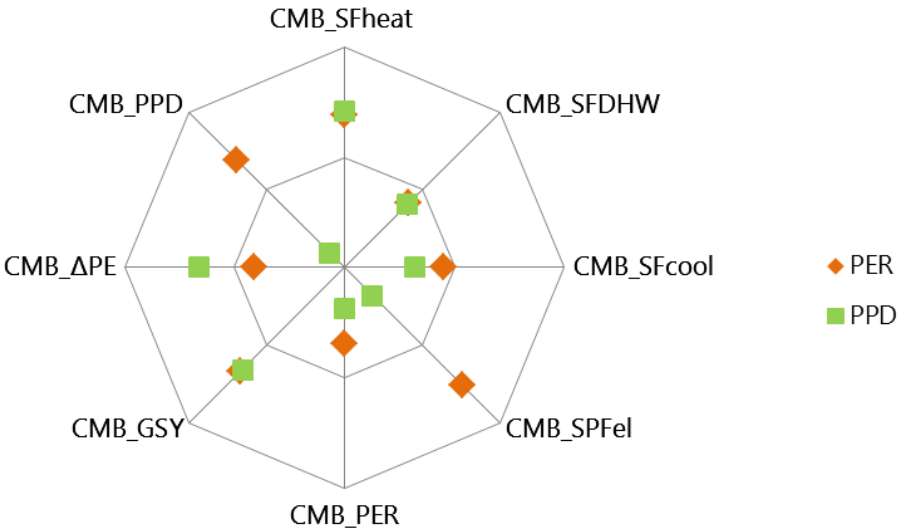

Fig. 4.5 PER and PPD for different configurations

The comparison between the three solar fractions highlights as for high values of $SF_{heating}$ correspond lower values of SF_{DHW}, while the production of cooling has not a relevant effect on the DHW production (Fig. 4.6). This is due to the fact that for the system operating modes, the small quantity of cooling produced has not important effect on the system performances rather than on the electrical consumption (lower values of SPF_{el}).

The best case for the cooling production does not correspond to the best case of PPD; the reason of this is that the PPD here considered is the mean PPD along the year, so also the winter PPD is taken into account. Even if no big improvements on the PPD value are shown along the different configurations, in the CMB_SF_{cool} the lowest value of PPD for summer is achieved and it corresponds to a reduction of 10% of the building PPD without any cooling. For the non-optimal chiller working conditions, the results here obtained can be considered acceptable.

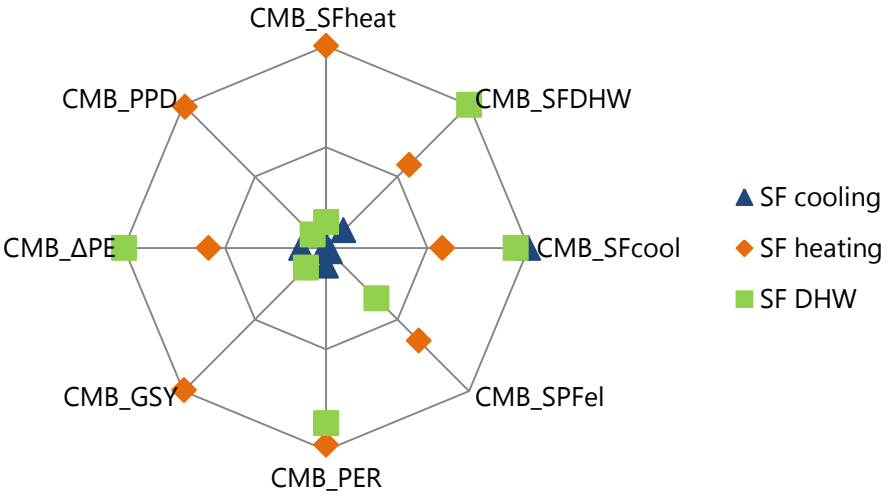

Fig. 4.6 Percentage of solar fractions with respect to the maximum value

For higher improvements, shorter periods can be used in order to maximize different performance figures in accordance with external conditions or system capacity. As an example, as the cooling system is underestimated for covering the total cooling demand, internal comfort can be improved during warm days, while energy savings may be maximized during hot days, when the system capacity at least might lead a very small decrease of internal temperatures. In this sense, systems priorities need to be changed without any modification in the system layout and higher use of solar technologies for the heating and cooling demand might be done.

Bibliography

[82] Klein, S.A., et al.. TRNSYS a Transient System Simulation Program, Version 17.0. Solar Energy Laboratory, University of Wisconsin-Madison, Reference Manual (1996).

[83] Fedrizzi, R., Nienborg, B., Franchini, G. Identification of Standard System Configurations. Solar Combi+ project, v 4.0, Eurac, Bolzano (2010)

[84] ISO 7730. Ergonomics of the thermal environment – Analytical determination and interpretation of thermal comfort using calculation of the PMV and PPD indices and local thermal criteria (2005)

[85] Nowag J., Boudéhenn F., Le Denn A., Lucas F., Marc O., Raduslescu M., Papillon P. Calculation of performance indicators for solar cooling heating and domestic hot water systems. International conference on Solar Heating and Cooling for buildings and industry, San Francisco, California (2012)

[86] Malenkovic I, Eicher S., Bony J. Definition of main system boundaries and performance figures for reporting on SHP systems- A technical report of Subtask B- Deliverable B1.1. IEA SHC Task 44, HPP Annex 38 (2012)

[87] Campolongo F., Cariboni J., Saltelli A. An effective screening design for sensitivity analysis of large models. Environmental Modeling & Software 22 (2007)

[88] Keeney K., Braun J. A simplified method for determining optimal cooling control strategies for thermal storage in building mass. HVAC&R Research, Vol.2, issue 1 (1996)

5. Conclusions

The control of Solar Heating and Cooling (SHC) systems is a crucial issue because the technology is still in an early phase of market development and well established dimensioning standards are still not available. The control of these systems becomes even more important to the end of energy savings, as the 36% of the total electricity consumption is related to residential uses.

SHC systems use energy generated by solar thermal collectors to provide heating in winter, cooling in summer and domestic hot water (DHW) all year round. The advantage of using these systems is the coincidence of cooling demand and cooling production during the summer and space heating and DHW production during the winter.

In a system optimization, two issues have to be dealt with high importance:

- Accuracy of the model
- Individuation of parameters to be optimized.

In this sense, after an introduction in Chapter 1 on SHC systems and performance figures that characterize these systems, the development of accurate energy models of the building and supply energy plant has been described in Chapter 2 and 3. The analysis of parameters involved on the system energy performance and level of thermal comfort has been carried out in Chapter 4. System's model and simulations have been made with the transient simulation tool, TRNSYS 17 [58].

Object of this study has been a case study constituted of a low energy building composed by 8 apartments distributed on 3 levels and a SHC system which provides DHW, space heating and cooling.

The development of a detailed energy building model may imply accuracy in the results, but also elevate computational effort. In Chapter 2, the calibration of a detailed model with monitored data and a process from a detailed energy building model to a simplified one have been described. The real supply air flow has been calculated comparing the monitored heat exchange in the water side of heat batteries with simulated values. A reduction of 22% of the total measured air flow has been found, due to an incorrect position of the air speed sensors in the channels.

The infiltration rate depends on several factors, as building airtightness, building orientation and users' behavior. For these reasons, the characterization of the infiltration rate is a tough issue in the building modeling. The comparison between monitored and simulated internal temperatures has been used for the definition of infiltration rate, equal to 0.33 or 0.43 h^{-1} depending on the apartment.

The influence of shading devices, radiation and geometry calculation modes on building energy balance and simulation runtime have been investigated. The use of standard radiation mode, manual geometry mode and Type 34 for the shadings modeling, has allowed the development of a simplified building energy model with lower number of zones and with a reduction up to 89% of the simulation runtime. The simplified model reproduces with high accuracy the detailed model, in fact a reduction of only 9% of building loads have been calculated.

In Chapter 3, the modeling of the supply energy plant, the definition of the control and the validation of the model has been described. Initially, energy plant components have been set with rated values and the system's working modes have been defined and implemented in the model. Afterwards, thanks to the use of monitored data, components' types have been validated with the BMA (Bin Method Analysis). This method allows to take into account not only the device state conditions, but also transient conditions. The validated model showed a decrease of system performances mainly due to the reduction of 12% of collector efficiency and, consequently, to the total collected energy by the system.

Once developed accurate building and energy plant models, in Chapter 4 the two parts of the system have been unified and a unique model of the whole system has been created.

In systems with a large amount of sets and parameters, the individuation of parameters which have a higher influence on the system's performance and levels of thermal comfort is an important step for the optimization process. The Morris method has been applied to select the sets to be optimized. In particular, set temperatures involved in the DHW circuit have been individuated because the system has been designed mainly for covering the DHW demand. A feasible range for each parameter has been defined and all possible combinations have been run. Global system indicators, solar indicators and quality indicators have been used for characterizing the energetic system performances and thermal comfort level. The best configuration for each performance figure has been selected. Sets related to the internal temperature or sorption chiller working conditions have a less influence on the performance figures or comfort index than DHW circuit sets because the power involved in the space cooling production is much lower than in the DHW production. As the configuration that optimize both energy performances and thermal comfort does not exist, a trade-off between energy savings and suitable internal comfort has been done.

Whilst best configurations are used, the improvement in the cooling production still remains limited, in fact a maximum reduction of 8% of PPD value can be achieved and the maximum solar fraction for cooling can be 6%. These results are due to the system operation modes (priority to the DHW) and system itself characteristics. The installed sorption chiller works with cycles, so non continued cooling can be provided. Moreover in low energy buildings, the ventilation supply system is sized for winter loads and is usually not enough for summer loads.

Further studies will be focused on the control of solar cooling systems on low energy building. The use of predictive or adaptive control may foresee winter seasons overheating or regulate cooling system devices with regard to external conditions and user's behavior.